THE FATTY ACID OLEATE IN THE *C. ELEGANS* INNATE IMMUNE RESPONSE

A Dissertation Presented By:

SARAH MACDONALD ANDERSON

Submitted to the Faculty of the

University of Massachusetts Graduate School of Biomedical Sciences, Worcester

in partial fulfillment of the requirements for the degree of

DOCTOR OF PHILOSOPHY

May 12th, 2021

Program in Immunology and Microbiology

THE FATTY ACID OLEATE IN THE *C. ELEGANS* INNATE IMMUNE RESPONSE

A Dissertation Presented

By

SARAH MACDONALD ANDERSON

This work was undertaken in the Graduate School of Biomedical Sciences

Immunology and Microbiology Program

Under the mentorship of

_____
Read Pukkila-Worley, M.D., Thesis Advisor

_____
Amy Walker, Ph.D., Member of Committee

_____
Neal Silverman, Ph.D., Member of Committee

_____
Megan Orzalli, Ph.D., Member of Committee

_____
Jennifer Watts, Ph.D., External Member of Committee

_____
Javier Irazoqui, Ph.D., Chair of Committee

_____
Mary Ellen Lane, Ph.D.,
Dean of the Graduate School of Biomedical Sciences
May 12, 2021

Acknowledgements

I would like to thank my mentor Read Pukkila-Worley, who has been so supportive and helpful in making me into the scientist I am today. I would also like to thank my TRAC, Javier Irazoqui, Amy Walker, and Neal Silverman for always being supportive while providing great ideas, fresh perspectives, and hearty banter.

I also want to acknowledge my lab mates and collaborators. Nick Peterson and Hilary Cheesman are significant contributors to the work presented here and this would not have been possible without them. My other lab mates Kyle, Sammy, Claire, and Elizabeth made my experience whole and helped me in so many other ways. In addition, the collaboration with James Nhan, Sean Curran, Nandhitha Uma Nuresh, and Cole Haynes made this work possible, and it was fantastic to work with all of them. I want to thank Alex Soukas for collaborating with us so I could work in his lab to learn GC-MS.

I want to thank Melanie Trombly for comments on our manuscripts and for teaching me how much of a difference color coordinating data can make. I must also acknowledge the *Caenorhabditis* Genetics Center, which provided many of the strains used in this work. And finally, I want to thank the *C. elegans* community (WAWM, BAWM, SPAMS, etc.) which made me fall in love with a model system and provided a society that allowed me to thrive.

Dedications

This dissertation is dedicated to my “lab mother” Hilary Cheesman and my First Year Cohort (Sneha Suresh, Debanjan Goswamy, Brent Horowitz, Grant Weaver, Betul Akgol-Oksuz, Nandhitha Uma Nuresh, Melanie Walker, Sunil Guharaja, Salome Funes, Kris Holloway, Christa Park, Serkan Sayin, and all others who worked with me in classes and beyond). My transition into graduate school was less than graceful but all the technical, intellectual, and emotional support I received from these amazing people allowed me to succeed. With all the craziness that encompasses graduate school, I would not have made it here without you all.

Thank you.

Published Works

The work presented in Chapter I of this thesis has been adapted from:

Anderson SM, Pukkila-Worley R (2020) Immunometabolism in *Caenorhabditis elegans*. PLOS Pathogens 16(10): e1008897.

The work presented in Chapter II of this thesis has been adapted from:

Anderson SM, Cheesman HK, Peterson ND, Salisbury JE, Soukas AA, Pukkila-Worley R (2019) The fatty acid oleate is required for innate immune activation and pathogen defense in *Caenorhabditis elegans.* PLOS Pathogens 15(6):e1007893.

The work presented in Chapter III of this thesis has been adapted from:

Nhan JD, Turner CD, Anderson SM, Yen C, Dalton HM, et al. (2019) Redirection of SKN-1 abates the negative metabolic outcomes of a perceived pathogen infection. Proceedings of the National Academy of Sciences 116 (44) 22322-22330.

The work presented in Appendix II of this thesis has been adapted from:

Peterson ND, Cheesman HK, Liu P, Anderson SM, Foster KJ, et al. (2019) The nuclear hormone receptor NHR-86 controls anti-pathogen responses in C. elegans. PLOS Genetics 15(1): e1007935.

Table of Contents

Table of Tables

Table of Figures

List of Online Files

The following tables referenced in Chapter II and III of this dissertation are located on the publisher's website and can be downloaded by following the included links:

Chapter II:

Table 2.1. Relative expression of the 118 genes in the NanoString experiment related to Figure 2.3.

Table 2.2. Sample sizes, mean lifespan, and p values for all trials of the C. elegans pathogenesis assays, related to figures 2.6, 2.7, 2.8, and 2.9.

A. All trials for the pathogenesis assays presented in Fig 2.7. **B.** All trials for the pathogenesis assays presented in Fig 2.6. **C.** All trials for the pathogenesis assays presented in Fig 2.9. **D.** All trials for the pathogenesis assays presented in Fig 2.8.

Chapter III:

Table 3.1: RNA sequencing of *skn-1gf* and wild-type worms at day 2 adulthood

Table 3.2: RNA sequencing of *wdr5lf;skn-1gf*

Table 3.3: RNA sequencing of *skn-1gf* animals treated with paraquat

Table 3.4: Pathogen response genes and *skn-1gf* differentially regulated

Abstract

Host metabolism is profoundly altered during bacterial infection, both as a consequence of immune activation and secondary to virulence strategies of invading pathogens. As a result, the metabolic pathways that regulate nutrient acquisition, energy storage, and resource allocation in host cells must adapt to pathogen stress in order to meet the physiological demands of the host during infection. In this work, we uncover that the synthesis of the monounsaturated fatty acid (MUFA) oleate is necessary for the pathogen-mediated induction of immune defense genes. Accordingly, *C. elegans* deficient in oleate production are hypersusceptible to infection with diverse human pathogens, which can be rescued by the addition of exogenous oleate. However, oleate is not sufficient to drive protective immune activation.

Oleate is also important for proper lipid storage and abundance. We found that exposure to pathogenic bacteria drives rapid somatic depletion of lipid stores in *C. elegans*. Activating the p38/MAPK immune signaling pathway in the absence of pathogens was also sufficient to drive loss of somatic fat. In addition, we found that transcriptional suppression of MUFA synthesis occurs during *P. aeruginosa* infection, in a manner dependent on pathogen virulence. Finally, we showed that the host compensates for the pathogen-induced depletion of fatty acids by promoting the redistribution of oleate from non-intestinal tissues to support immune function in the intestine. Together, these data add to the known health-promoting effects of MUFAs, and suggest an ancient link between nutrient stores, metabolism, and host responses to bacterial infection.

Chapter I: Introduction to Immunometabolism and *C. elegans*

PREFACE

This work is adapted from a review article published in 2020. The original ideas and written draft were done by me with edits by Read Pukkila-Worley. The beginning section on *C. elegans* as a model system was added for completeness of the dissertation. Additionally, some of the work that was originally in the review article but is presented in further chapters of this dissertation was removed.

INTRODUCTION

The *C. elegans* model system

The transparent nematode was first used as a model organism by Sydney Brenner to study neurobiology and development. Since that time *C. elegans* has grown as a model system for almost any biological phenomenon. As these animals are found most abundantly on rotting fruit where they scavenge for bacteria as their food source, they encounter both nutritious and pathogenic bacteria. Thus, they have evolved mechanisms to detect, avoid, and defend against pathogens. Therefore, is not surprising that *C. elegans* is now a strong model for host-pathogen interactions and intestinal immunity.

The *C. elegans* intestine is composed of 20 large polyploid epithelial cells arranged in pairs that form a tube running the length of the animal. This organ, which comprises roughly one third of the total somatic mass, is responsible for food digestion and absorption, stress responses, as well as synthesis and storage of macromolecules. The intestine is the major site of biochemical activity to produce lipids for energy storage

and metabolism. This process begins in the pharynx as bacteria are physically disrupted by the pharyngeal grinder to prevent active replication of bacteria. Highly expressed lysozymes, saposins, and lipases aid in the puncture and degradation of bacterial cell walls providing phospholipids and fatty acids in the intestine for energy and lipid storage. The intestine also includes many peroxisomes, which are a main location for fatty acid oxidation. However, only 7-20% of fatty acids are synthesized from acetyl-CoA, with the remainder synthesized from fatty acids provided by a bacterial diet [1].

Whether from acetyl-CoA or saturated fatty acids, *C. elegans* has the ability to produce all necessary monounsaturated fatty acids (MUFAs) and polyunsaturated fatty acids (PUFAs). This occurs through sequential enzymatic activity of conserved elongase and desaturase proteins (denoted as *elo* and *fat* genes), which increase carbon chain length and introduce double bonds, respectively (Figure 1.1). Therefore, unlike mammals, they do not have any specific dietary requirements for fatty acids allowing the genetic interrogation and deeper understanding of the functions of specific fatty acids.

IMMUNOMETABOLISM IN *C. ELEGANS*

Insulin signaling integrates host metabolism, pathogen resistance, and longevity.

In *C. elegans*, the conserved insulin/insulin-like growth factor signaling pathway has been extensively studied. From its effects on host nutritional status and environmental cues to control of core physiological processes, including metabolism, growth rate, behavior, and stress resistance this pathway has allowed the field to understand the many critical roles of a conserved factor that may have otherwise been

underappreciated in mammalian systems that are perturbed by complexity [2]. Activation of the *C. elegans* insulin/IGF-1 transmembrane receptor (IGFR) ortholog DAF-2 by insulin-like peptides results in the phosphorylation of the Foxo transcription factor DAF-16 causing it to be sequestered in the cytoplasm [3]. Low activity of DAF-2 allows DAF-16 to translocate to the nucleus where it controls the transcriptional output of this pathway [4]. Constitutive activation of DAF-16 in *daf-2* loss-of-function mutants extends nematode lifespan up to three times that of wild-type animals and drives resistance to both abiotic stresses and pathogen infection [5, 6]. In addition, de novo lipogenesis is increased in *daf-2* mutants, which leads to accumulation of somatic fat. The pathogen resistance and lifespan extension phenotype of *daf-2* mutants require the p38 mitogen-activated protein kinase (MAPK) PMK-1 pathway, a critical innate immune pathway in *C. elegans* [7]. However, the transcriptional targets of the DAF-2/DAF-16 and the p38 MAPK PMK-1 pathways during pathogen infection have essentially no overlap, suggesting that these pathways operate in parallel to promote resistance to pathogen infection [7]. Interestingly, infection by the bacterial pathogen *Pseudomonas aeruginosa* activates DAF-2 signaling as an offensive mechanism to suppress host immune defenses by causing DAF-16 to be sequestered in the cytoplasm [8]. Insulin/insulin-like growth factor signaling is strongly conserved across metazoan evolution. Thus, examination of the mechanisms by which the DAF-2/DAF-16 pathway integrates information about host nutrition to control metabolism, pathogen resistance, and lifespan may yield fundamental insights about immunometabolism.

Allocation of lipid resources affect physiological trade-offs between pathogen resistance, lifespan, and reproduction.

Studies of immunometabolism in *C. elegans* have uncovered trade-offs between immune activation and lipid homeostasis that affect pathogen resistance, reproduction, and lifespan. Pathogen and stress resistance programs are suppressed as animals increase resource investment to promote reproductive success. Two conserved homeodomain transcription factors CEH-60/PBX and UNC-62/MEIS function as a heterodimer to promote the synthesis of lipoproteins, which shuttle lipids to the germline to support embryogenesis. In addition, the CEH-60:UNC-62 complex also suppresses genes important for pathogen defense and longevity [9]. Similarly, TCER-1, a transcription elongation and splicing factor, promotes reproductive fitness and lipid synthesis at the expense of pathogen and abiotic stress defenses [10]. Finally, a core host defense pathway in *C. elegans*, the p38 MAP PMK-1 pathway, is activated by nutrient signals independent of canonical mechanisms that sense food availability and accelerates aging when it is hyperactive, providing an example of the deleterious effects of immune activation on longevity [11].

Lipid metabolism is required for immune activation and pathogen defense.

C. elegans pathogenesis assays have defined requirements for specific lipids and lipogenesis enzymes in innate immune regulation and pathogen defense. As mentioned previously, *C. elegans* can synthesize the full range of fatty acid molecules *de novo* and thus does not have a dietary requirement for specific fatty acids. The Δ6-desaturase *fat-3*, which produces the polyunsaturated fatty acids gamma-linoleic acid

and stearidonic acid, is required for basal expression of innate immune genes and resistance to infection by the bacterial pathogen *P. aeruginosa* [12].

Additionally, low levels of s-Adenosylmethionie (SAM), the methyl donor that modifies nucleic acids and histones, and is involved in producing phospholipids, results in a decrease in phosphatidylcholine (PC). Low levels of PC in animals that lack *sams-1*, an enzyme that produces SAM, induces expression of lipogenesis genes resulting in lipid droplet accumulation [13, 14]. Interestingly, low PC increases basal expression of immune genes in *C. elegans* feeding on non-pathogenic food. However, low levels of activating histone methylation in these animals also limits pathogen-responsive transcription and renders animals more susceptible to infection [13]. Together, these studies in *C. elegans* reveal novel connections between nutrient stores, metabolism, and host susceptibility to bacterial infection.

Mitochondria link energy metabolism and immune activation.

Mitochondria are required for multiple aspects of cellular metabolism. Bacteria often target mitochondria during infection as an offensive strategy to promote tissue damage. For example, *P. aeruginosa* secretes phenazine toxins, electron shuttles that disrupt mitochondrial function [15] and *Streptomyces* sp. elaborate antimycin A and oligomycin, inhibitors of mitochondrial respiration that are widely used in the laboratory. Studies in *C. elegans* have characterized several host countermeasures that have evolved to detect mitochondrial dysfunction as a sign of pathogen infection.

The unfolded protein response in mitochondria (UPR^{mt}) is regulated by the transcription factor ATFS-1, a unique transcription factor that contains both a nuclear

localization (NLS) and a mitochondrial targeting (MTS) sequence [16, 17]. Healthy mitochondria import ATFS-1 efficiently, but during mitochondrial dysfunction, protein import is impaired and ATFS-1 accumulates in the cytoplasm, where it can traffic to the nucleus via its NLS. ATFS-1 activates a transcriptional program in the nucleus that promotes both recovery of mitochondrial function and defense against pathogen infection through the induction of secreted innate immune effectors [16, 17]. Interestingly, the pathogen *P. aeruginosa* evolved mechanisms to suppress the UPR^{mt} by exploiting a host pathway that negatively regulates ATFS-1 [15].

In addition, ceramides, a class of host lipids, protect *C. elegans* from mitochondrial dysfunction induced by toxins or pathogen exposure [18]. Likewise, disruption of mitochondrial function activates the nuclear hormone receptor *nhr-45*, which induces detoxification programs that provide protection during pathogen infection [19]. Finally, the iron-binding siderophore pyoverdine, which is produced by *P. aeruginosa*, causes mitochondrial dysfunction during infection, which engages protective destruction of damaged mitochondria (mitophagy) [20]. Together, these studies demonstrate mitochondrial function is closely guarded by host surveillance pathways that function to restore homeostasis and activate protective innate immune defenses.

Transcriptional control of innate immunity and metabolism by conserved nuclear hormone receptors.

The *C. elegans* genome encodes a large number of nuclear hormone receptors (NHRs), unique transcription factors that program adaptive transcriptional responses

following recognition of specific ligands, such as fatty acids, metabolites, hormones, and xenobiotics. NHRs regulate a number of basic biological processes in *C. elegans*, including lipid and cholesterol metabolism, lifespan, development, and anti-pathogen defenses. The marked expansion of NHRs in nematodes — 284 NHRs are present in *C. elegans*, whereas Drosophila and humans have only 21 and 48, respectively — suggests that these proteins may play particularly important roles in nematode physiology, such as the integration of host metabolism with innate immunity to promote resistance to pathogen infection.

Interestingly, 264 of the 284 NHRs in the *C. elegans* genome are orthologous to the alpha isoform of the mammalian nuclear receptor hepatocyte nuclear factor 4 (HNF4α). HNF4α is expressed in the intestinal epithelium and in hepatocytes and has been implicated in the control of intestinal inflammation and the pathogenesis of inflammatory bowel disease and cancer. In *C. elegans,* the HNF4α homolog NHR-86 surveys the chemical environment to activate protective anti-pathogen defenses by binding to the promoters of immune effector genes [21]. These data suggest that the expansion of the HNF4α family in *C. elegans* may have been fueled, at least in part, by the roles of these proteins in the activation of host defense responses. In addition, the *C. elegans* homolog of peroxisome proliferator-activated receptor (PPAR), NHR-49, a central regulator of fat metabolism, is required for resistance to multiple gram-positive bacteria, including *Enterococcus faecalis* [22]. Of note, NHR-49 interacts with a conserved subunit of the Mediator complex MDT-15/MED15 to control the production of fatty acids and a separate study found that MDT-15 also coordinates immune defenses during pathogen infection [23]. Thus, NHR-49 and MDT-15 regulation of fatty acid

metabolism may support immune function in nematodes. In addition, the *C. elegans* homolog of the liver X receptor (LXR), NHR-8, which controls cholesterol and bile acid homeostasis, is required for defense against infection with *P. aeruginosa* [24, 25]. Finally, the nuclear hormone receptor NHR-14 links iron availability with the induction of innate immune defenses that provide protection from pathogen infection [26]. In summary, NHRs are able to mount rapid transcriptional responses to specific intracellular and extracellular cues and are thus poised to integrate host physiology and metabolism to provide protection from pathogens during infection.

FIGURES

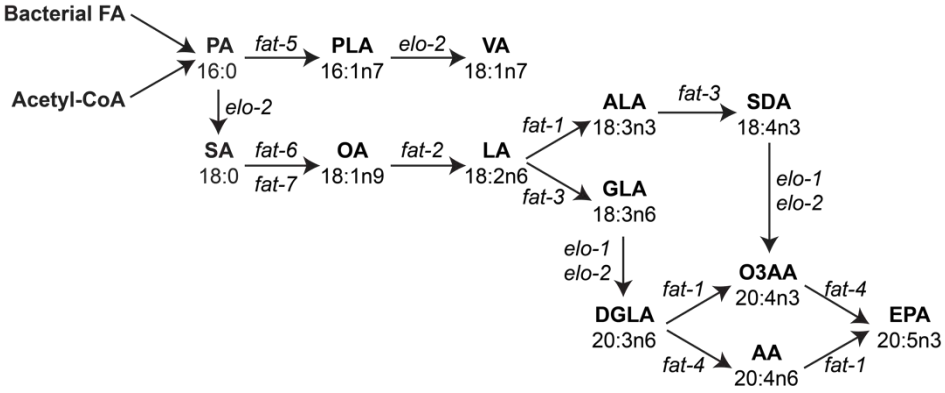

1. Figure 1.1 A schematic of the long-chain fatty acid synthesis pathway in *C. elegans*

Fatty acid nomenclature: X:YnZ, X indicates the number of carbon atoms, Y denotes the number of double bonds, and Z designates the position of the terminal double bond relative to the methyl end of the molecule. Abbreviations: AA, arachidonic acid; ALA, α-linoleic acid; DGLA, di-homo-γ-linoleic acid; EPA, eicosapentaenoic acid; GLA, γ-linoleic acid; LA, linoleic acid; O3AA, v-3 arachidonic acid; OA, oleate; PA, palmitic acid;

PLA, palmitoleic acid; SA, stearic acid; SDA, stearidonic acid; VA, vaccenic acid.

(Adapted from[27, 28]).

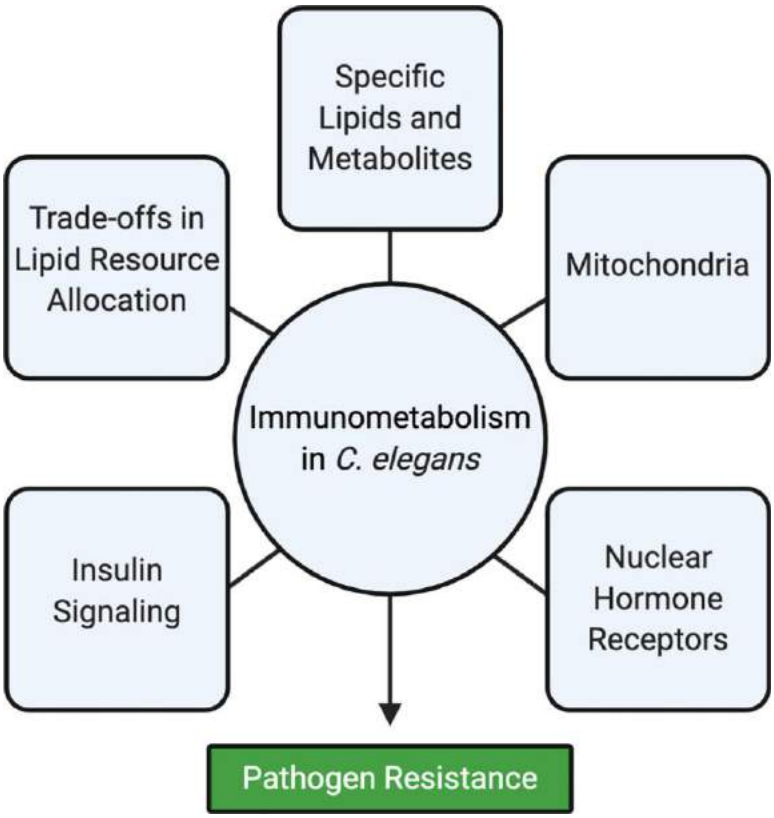

2. Figure 1.2 Immunometabolism in *C. elegans.*

A schematic presents five concepts that have emerged in studies of metabolic and immune interactions in *C. elegans.*

Chapter II: The fatty acid oleate is required for innate immune activation and pathogen defense in *Caenorhabditis elegans*

PREFACE

This chapter is adapted from the publication “The fatty acid oleate is required for innate immune activation and pathogen defense in *Caenorhabditis elegans*” where I am the first author, Hilary Cheesman, Nicholas Peterson, J. Elizabeth Salisbury, and Alexander A. Soukas are the middle authors, and Read Pukkila-Worley is the last author.

ABSTRACT

Fatty acids affect a number of physiological processes, in addition to forming the building blocks of membranes and body fat stores. In this study, we uncover a role for the monounsaturated fatty acid oleate in the innate immune response of the nematode *Caenorhabditis elegans*. From an RNAi screen for regulators of innate immune defense genes, we identified the two stearoyl-coenzyme A desaturases that synthesize oleate in *C. elegans*. We show that the synthesis of oleate is necessary for the pathogen-mediated induction of immune defense genes. Accordingly, *C. elegans* deficient in oleate production are hypersusceptible to infection with diverse human pathogens, which can be rescued by the addition of exogenous oleate. However, oleate is not sufficient to drive protective immune activation. Together, these data add to the known health-promoting effects of monounsaturated fatty acids, and suggest an ancient link between nutrient stores, metabolism, and host susceptibility to bacterial infection.

INTRODUCTION

Fatty acids are the key structural components of phospholipids and triglycerides, and thereby affect nearly every facet of eukaryotic physiology. In addition to forming the building blocks of membranes and functioning as a currency of energy storage, fatty acid molecules promote health in a diverse number of ways. For example, fatty acids act as soluble signals for intracellular communication, affect membrane fluidity, and have been directly linked to lifespan regulation [29-31]. Conversely, excess stores of fatty acids in triglycerides are directly linked to atherosclerosis and type 2 diabetes [32]. Thus, it is important to understand how individual fatty acids affect key physiological processes within a cell.

The nematode *Caenorhabditis elegans* is a valuable model for studying the roles of fatty acids in metazoan biology [33-38]. Through the sequential action of conserved elongase (*elo*) and desaturase (*fat*) genes, nematodes can synthesize the full range of fatty acid molecules found in plants and animals [33-37]. Thus, *C. elegans* does not have a dietary requirement for specific fatty acids, unlike mammals. In nematodes, as in mammals, the majority of fatty acid molecules are synthesized from stearic acid, a saturated, 18-carbon molecule, which is progressively desaturated and elongated to a variety of monounsaturated (MUFA) and polyunsaturated (PUFA) fatty acids (Fig. 2.1A) [33-37]. The contribution of individual fatty acids to specific biological processes can be characterized using genetic approaches in *C. elegans* at the level of an entire organism.

Nematodes rely on inducible host defense mechanisms to provide protection from ingested pathogens [39-42]. Because worms normally eat bacteria for food, their evolution has been shaped by interactions with both pathogenic and nonpathogenic microorganisms. The immune effectors in *C. elegans* include a suite of secreted

proteins, including lysozymes, proteins with CUB-like domains, and ShK toxins, some of which are required for host defense during bacterial infection [7, 21, 28, 43]. *C. elegans* with mutations that abrogate the induction of these immune effectors during infection are hypersusceptible to killing by bacterial pathogens [7, 44, 45]. In this study, we define a requirement for the MUFA oleate in innate immune activation and pathogen defense in *C. elegans*. Previously, Nandakumar et al. showed that two polyunsaturated fatty acids, γ-linolenic acid (GLA) and stearidonic acid (SDA), are required for the basal expression of innate immune effectors [12]. Here, we show that oleate is necessary for innate immune activation and resistance to bacterial infection in a manner distinct from the effects of GLA and SDA. Because oleate is among the most abundant fatty acids in cells, our data suggest an ancient link between cellular energy stores and immune activation.

RESULTS

An RNAi screen identifies a role for MUFAs in the activation of C. elegans innate immune effectors.

We previously conducted an RNAi screen of 1,420 intestinal genes for innate immune regulators in *C. elegans* [23]. We used an immunostimulatory small molecule called R24 (also called RPW-24) and a GFP-based transcriptional reporter, *irg-4::GFP,* which provides a convenient readout of innate immune activation [21, 23, 46-49]. The gene *irg-4* (F08G5.6) is transcriptionally upregulated during infection with multiple pathogens and contains a CUB-like domain, which is present in many of the secreted immune effectors in *C. elegans* [7, 21, 43]. *irg-4* is required for normal resistance to

bacterial infection, but does not modulate the normal lifespan of *C. elegans* or affect susceptibility to other stressors [12, 21, 43]. *irg-4* is also strongly upregulated by R24, a xenobiotic that protects nematodes from bacterial infection by boosting innate immune responses [21, 23, 46, 49]. Because of its potent immunostimulatory properties, R24 is a useful tool for dissecting the metabolic requirements of immune activation without altering the bacterial diet of *C. elegans* [21, 23, 46-49]. The RNAi screen identified 29 gene inactivations that are required for the R24-mediated induction of the innate immune reporter *irg-4::GFP* [23]. Interestingly, two of the genes identified in this screen are the stearoyl-coenzyme A (CoA) desaturases *fat-6* and *fat-7*, which function redundantly to synthesize oleate from stearic acid (Fig. 2.1A) [33]. RNAi-mediated knockdown of *fat-6* completely abrogated the induction of *irg-4::GFP* by R24 (Fig. 2.1B) while knockdown of *fat-7* partially suppressed its upregulation (Fig. 2.2A).

To validate the results of the RNAi studies in the *irg-4::GFP* transcriptional reporter, we used qRT-PCR to examine the transcriptional regulation of the *irg-4* gene in wild-type and in *fat-6(tm331);fat-7(wa36)* double mutant animals, which are deficient in oleate production (Fig. 2.1C) [33, 36]. The R24-mediated induction of *irg-4* was reduced in *fat-6(tm331);fat-7(wa36)* animals compared to wild-type animals. In addition, the induction of two other immune effectors, *irg-5*(F35E12.5) and *irg-6*(C32H11.1), was also attenuated in the *fat-6(tm331);fat-7(wa36)* double mutant (Fig. 2.1C). Like *irg-4*, *irg-5* and *irg-6* are strongly induced during infection with the bacterial pathogen *P. aeruginosa* and by the immunostimulatory xenobiotic R24 [21, 23, 46, 47]. In addition, knockdown of *irg-5* and *irg-6* makes *C. elegans* more susceptible to infection by *P. aeruginosa* [21]. The defect in immune activation by *fat-6(RNAi)* was also visualized

using the *irg-5::GFP* transcriptional reporter (Fig. 2.1D). Thus, stearoyl-CoA desaturases are required for the induction of at least three key immune effectors in *C. elegans*.

We performed fatty acid supplementation experiments to determine if the effect of the stearoyl-CoA desaturases on immune activation depends specifically on the production of the MUFA oleate. Interestingly, supplementation of exogenous oleate rescued, in a dose-dependent manner, the R24-mediated immune activation defect of the *irg-4::GFP* reporter strain in *fat-6(RNAi)* animals (Fig. 2.1B). Oleate is also required for the upregulation of *irg-5::GFP* by R24, as supplementation of this MUFA rescued the induction defect conferred by knockdown of *fat-6* (Fig. 2.1D).

Consistent with a key role for MUFAs in immune activation, knockdown of the elongase *elo-2*, which catalyzes the conversion of palmitic acid to stearic acid, the step immediately upstream of oleate synthesis, also suppressed the activation of *irg-4::GFP* by R24 (Fig. 2.1E). Importantly, oleate supplementation also fully complemented the immune activation defect of *elo-2(RNAi)* animals (Fig. 2.1E). These data demonstrate that lack of oleate, and not an accumulation of upstream stearic acid, is responsible for deficits in immune effector induction. In addition, knockdown of *fat-5*, the palmitoyl-CoA desaturase, which also preferentially acts on palmitic acid, but converts it to a different MUFA, palmitoleic acid (PLA), had no effect on the induction of *irg-4::GFP* (Fig. 2.1E).

Our RNAi screen also identified the mediator subunit *mdt-15* among the 29 gene inactivations that are required for the R24-mediated induction of the innate immune reporter *irg-4::GFP* [46]. We subsequently showed that *mdt-15* is required for the induction of innate immune effectors and for defense against the bacterial pathogen

Pseudomonas aeruginosa [46]. In addition to its role as an immune regulator, MDT-15 controls the transcription of a suite of fatty acid biosynthesis enzymes [50-52]. Interestingly, oleate supplementation did not rescue the induction of *irg-4::GFP* in *mdt-15(tm2182)* loss-of-function animals, indicating that *mdt-15* controls multiple steps in the activation of innate immune effectors (Fig. 2.2B).

Polyunsaturated fatty acids (PUFAs) are not required for immune effector induction by the immunostimulatory xenobiotic R24.

Monounsaturated fatty acids are converted to polyunsaturated fatty acids (PUFAs) by desaturases that initially use oleate as a substrate [34]. To determine if a PUFA is required for immune effector induction by the immunostimulatory xenobiotic R24, we used both genetic and fatty acid complementation experiments. We examined the induction of *irg-4::GFP* in animals deficient in the desaturase *fat-2*, which catalyzes the first step in PUFA synthesis (the conversion of oleate to linoleic acid), and also *fat-1(RNAi)* and *fat-3(RNAi)*, the enzymes that act downstream of *fat-2* in the synthesis of PUFAs (Fig. 2.1A) [34, 35]. Knockdown of *fat-1*, *fat-2,* or *fat-3* had no effect on the induction of *irg-4::GFP* by R24 (Fig. 2.3A). We confirmed this RNAi experiment using the *fat-2(wa17)* and the *fat-3(wa22)* loss-of-function mutants (Figs. 2.3B and 2.3C). Notably, the R24-mediated induction of the immune effectors *irg-4, irg-5,* and *irg-6* in the *fat-2(wa17)* and the *fat-3(wa22)* mutants were not significantly lower than in wild-type animals (Figs. 2.3B and 2.3C).

Supplementation of individual fatty acids to *fat-6(RNAi)* animals confirmed these genetic observations. Unlike oleate supplementation, addition of the 16 carbon MUFA

palmitoleic acid (PLA), which is synthesized by the desaturase *fat-5* (Fig. 2.1A), did not complement the *irg-4::GFP* induction defect in *fat-6(RNAi)* animals (Fig. 2.3D). In addition, supplementation of the PUFA linoleic acid (LA), which is synthesized by *fat-2* using oleate as a substrate (Fig. 2.1A), also failed to fully complement the *irg-4::GFP* induction defect of *fat-6(RNAi)* animals (Fig. 2.3D). Together, these data show that the fatty acid oleate, and not another MUFA or PUFA, is required for the induction of the innate immune effector genes by an immunostimulatory small molecule.

Stearoyl-CoA desaturase activity is required for immune effector induction.

To determine if stearoyl-CoA desaturase activity has a broad effect on the induction of innate immune effectors, we profiled the transcription of 118 immune and stress response genes in wild-type, *fat-6(RNAi)* and *fat-3(RNAi)* animals, each exposed to the solvent control (DMSO) or R24 (Fig. 2.4A). Of the 40 genes that were induced at least 4-fold by R24, the upregulation of 16 genes was significantly attenuated in *fat-6(RNAi)* animals (Figs. 2.4A and 2.4B, Table 2.1). As we observed in our studies of *irg-4, irg-5,* and *irg-6* in the *fat-3(wa22)* mutant (Fig. 2.3C), the induction of these 16 *fat-6*-dependent genes was not affected by knockdown of *fat-3* (Figs. 2.4A and 2.4B). For this transcription profiling experiment, we chose to use *fat-6(RNAi)* to examine the effects of oleate depletion on immune activation. Others have also used single knockdown of either *fat-6* or *fat-7* to recapitulate the phenotypes observed in the *fat-6(tm331);fat-7(wa36)* double mutant [31, 53]. Of note, the R24-mediated upregulation of *irg-4*, *irg-5,* and *irg-6* was not attenuated in the *fat-6(tm331)* or *fat-7(wa36)* single mutants (Fig. 2.2A and 2.2B), but the induction of these immune effectors was suppressed in *fat-6(RNAi)*

animals (Fig. 2.4B), as in the *fat-6(tm331);fat-7(wa36)* double mutants (Fig. 2.1C). We also confirmed by gas chromatography-mass spectrometry (GC-MS) that knockdown of *fat-6* significantly decreases the pool of oleate and causes accumulation of the upstream fatty acid stearate (Fig. 2.2C).

Interestingly, each of the 16 *fat-6*-dependent, *fat-3*-independent genes encode putative immune effectors that are induced during infection with at least one bacterial pathogen, a group that includes the innate immune effectors *irg-4, irg-5,* and *irg-6* (Fig. 2.4B). Twenty-four genes, however, were induced by R24 in a manner independent of *fat-6* (Table 2.1). Thus, *fat-6* modulates the transcription of a specific subset of genes, including a group of innate immune effectors. Moreover, the observation that the induction of these 16 genes was not controlled by *fat-3* further supports the specificity of *fat-6* in the regulation of innate immune responses.

Oleate is required for host resistance to *P. aeruginosa* infection.

Of the 16 genes whose R24-mediated induction was dependent on *fat-6*, ten are putative immune effectors that are also induced during infection with *P. aeruginosa*, including three known modulators of the host susceptibility to pseudomonal infection, *irg-4*, *irg-5*, and *irg-6* [12, 21, 43]. To determine if oleate is important for host defense in *C. elegans*, we performed pathogenesis assays with *P. aeruginosa*. The *fat-6(tm331);fat-7(wa36)* double mutant was more susceptible to infection by *P. aeruginosa* than wild-type animals, consistent with a prior report [12] (Figs. 2.7A and Table 2.2A). Importantly, *fat-6(tm331);fat-7(wa36)* animals have a similar lifespan as wild-type animals when grown under standard laboratory conditions [54]. These data suggest that

the hypersusceptibility to pathogen-mediated killing in the *fat-6(tm331);fat-7(wa36)* double mutant is not secondary to pleiotropic effects of these mutations on worm fitness. Supplementation of oleate to the *fat-6(tm331);fat-7(wa36)* animals fully complemented the enhanced susceptibility of this mutant to pathogen infection (Figs. 2.7A and Table 2.2A). Of note, *fat-6(tm331)* and *fat-7(wa36)* single mutant worms are not more susceptible to pathogen-mediated killing than wild-type animals, as noted previously [12] (Fig. 2.6 and Table 2.2B). Consistent with the key role of *fat-6* and *fat-7* in the regulation of innate immune responses, the fold induction of the innate immune effectors *irg-4, irg-5, irg-6, irg-1,* and *irg-2* during pseudomonal infection was significantly attenuated in the *fat-6(tm331);fat-7(wa36)* double mutant compared to wild-type (Fig. 2.7B).

Nandakumar et al. previously defined a role for two PUFAs, GLA and SDA, in the basal regulation of innate immune effectors and pathogen resistance in *C. elegans* [12]. We considered whether the effect of oleate on the activation of immune responses could occur through its metabolism to GLA and SDA; however, several lines of evidence show that this is not the case. The pathogen susceptibility and immune effector transcription profile of *fat-2(wa17)* mutants demonstrate that the effect of oleate on innate immune activation is not dependent on the production of PUFAs. The desaturase *fat-2* acts immediately downstream of oleate production to catalyze the first step in PUFA biosynthesis (Fig. 2.1A). *fat-2(wa17)* mutant animals are not more susceptible to *P. aeruginosa* infection than wild-type animals (Fig. 2.7C and Table 2.2A). In addition, the induction of the immune effectors *irg-4, irg-5, irg-6, irg-1,* and *irg-2* during pseudomonal infection was not compromised in *fat-2(wa17)* mutants compared to wild-

type (Fig. 2.7D), unlike what we observed for the *fat-6(tm331);fat-7(wa36)* double mutant (Fig. 2.7B). We also examined the desaturase *fat-3*, which acts downstream of *fat-2* in the synthesis of PUFAs, including GLA and SDA (Fig. 2.1A). Nandakumar et al. previously showed that *fat-3* is required for resistance to *P. aeruginosa* via the fatty acids GLA and SDA [12]. We found that exogenous oleate did not rescue the enhanced susceptibility of the *fat-3(wa22)* mutant to pseudomonal infection (Fig. 2.8 and Table 2.2D). Thus, *fat-6* and *fat-7* affect pathogen susceptibility specifically through the production of oleate, in a manner that is independent of PUFA synthesis via the enzymes *fat-2* or *fat-3*.

Stearoyl-CoA desaturases are required for the induction of immune effectors, such as *irg-4*, *irg-5*, and *irg-6*, whose basal, or resting, expression is dependent on the p38 MAPK PMK-1 innate immune pathway and those, like *irg-1* and *irg-2*, whose transcription are regulated independent of this canonical immune pathway (Fig. 2.7B) [7, 21, 23, 55]. Interestingly, knockdown of *tir-1*, the Toll/IL-1 (TIR) domain protein that is an integral component the p38 MAPK PMK-1 signaling cassette [44, 56, 57], further enhanced the susceptibility of *fat-6(tm331);fat-7(wa36)* mutants to pseudomonal infection (Fig. 2.7E and Table 2.2A). Likewise, knockdown of the bZIP transcription factor *zip-2*, which controls the induction of *irg-1* and *irg-2* during *P. aeruginosa* infection [55], caused *fat-6(tm331);fat-7(wa36)* to be more susceptible to killing by *P. aeruginosa* (Fig. 2.7F and Table 2.2A). These data suggest that *fat-6* and *fat-7* are required for the proper expression of a broad group of innate immune effectors via a mechanism that operates in parallel to the p38 MAPK PMK-1 and ZIP-2 immune pathways.

Stearoyl-CoA desaturase activity is necessary for protection against diverse bacterial pathogens.

We performed GC-MS to determine if R24 treatment changes the abundance of cellular oleate. Interestingly, GC-MS revealed that the fraction of both oleate and linoleic acid relative to the total fatty acid pool significantly increased in R24-treated samples compared to controls (Fig. 2.9A). Together, these data show that treatment with the immunostimulatory xenobiotic R24 shifts the fatty acid pool towards more oleate.

Because oleate is required for the induction of innate immune effectors and is increased in the presence of R24, we asked if this MUFA is sufficient for innate immune activation in *C. elegans*. However, the addition of oleate to the standard bacterial food source for *C. elegans* (*E. coli* OP50) did not activate GFP expression in the *irg-4::GFP* or the *irg-5::GFP* transcriptional reporters (Figs. 2.9B and 2.9C). The presence of oleate in the media also did not further augment the induction of *irg-5::GFP* during *P. aeruginosa* infection (Fig. 2.9C). In addition, oleate treatment did not extend the lifespan of wild-type *C. elegans* during *P. aeruginosa* infection (Fig. 2.9D and Table 2.2C). Thus, oleate is necessary, but not sufficient, for immune activation and resistance to *P. aeruginosa* infection in *C. elegans*.

Interestingly, *fat-6(tm331);fat-7(wa36)* mutant animals were also hypersusceptible to infection with the gram-positive pathogen *Enterococcus faecalis* (Fig. 2.9E and Table 2.2C) and *Serratia marcescens* (Fig. 2.9F and Table 2.2C), which, like *P. aeruginosa*, is a gram-negative bacteria. Importantly, the enhanced susceptibility of the *fat-6(tm331);fat-7(wa36)* mutants to infection with *E. faecalis* and *S. marcescens*

was rescued by treatment with exogenous oleate (Figs. 2.9E and 2.9F). Thus, oleate is required for host resistance to diverse bacterial pathogens.

CONCLUSIONS

This study defines a role for the MUFA oleate in *C. elegans* innate immune activation. We show that animals deficient in oleate production were hypersusceptible to killing by the bacterial pathogens *P. aeruginosa*, *E. faecalis,* and *S. marcescens* in a manner dependent on oleate. Oleate is among the most abundant fatty acids in cells. Thus, these data may explain how a metazoan animal limits the induction of protective immune defenses to times when the host has accumulated sufficient energy reserves to survive challenge from bacterial pathogens.

Nandakumar et al. previously identified two fatty acids, GLA and SDA, which are synthesized by the enzyme *fat-3* and are required for the basal expression of immune effectors [12]. Our data indicate that oleate and these PUFAs affect immune effector expression and pathogen resistance by different mechanisms. *C. elegans* with a loss-of-function mutation in *fat-2*, the enzyme that catalyzes the first step in PUFA synthesis, induced innate immune effector genes normally and were not more susceptible to *P. aeruginosa* pathogenesis. It is also important to note that knockdown of *fat-3* did not affect the R24-mediated induction of 16 *fat-6*-dependent innate immune effectors. In addition, exogenous supplementation of PUFAs to *fat-6(RNAi)* animals did not restore immune effector expression, whereas the addition of oleate fully complemented the induction defect of these animals. Also of note, the effect of *fat-3(wa22)* on susceptibility to bacterial infection was independent of oleate.

Han et al. recently found that oleate is sufficient to extend the lifespan of nematodes that were grown under standard laboratory conditions [29]. Interestingly, we found that treatment with oleate is not sufficient to provide protection during bacterial infection, but is required for proper immune gene transcription. Specifically, oleate is important for the pathogen-mediated induction of immune effectors that are downstream of the p38 MAPK PMK-1 pathway and for genes that are regulated by the bZIP transcription factor ZIP-2, which functions independently of the canonical PMK-1 pathway to mediate an early transcriptional response to *P. aeruginosa* infection [55]. Consistent with these data, RNAi mediated knockdown of *tir-1,* a component of the p38 MAPK PMK-1 signaling cassette, as well as *zip-2,* enhanced the susceptibility of *fat-6(tm331);fat-7(wa36)* animals to *P. aeruginosa* infection. Thus, oleate has diverse, health-promoting effects on lifespan and pathogen resistance in *C. elegans*.

In plants, oleate is also required for the proper expression of immune defense genes and resistance to pathogen infection, suggesting that the role for oleate in immune activation may be strongly conserved [58, 59]. However, the mechanism by which oleate regulates immune defenses is not known in either *C. elegans* or plants. Our supplementation studies indicate that oleate treatment itself does not activate immune gene transcription. Thus, oleate is unlikely to be a signal of immune activation in *C. elegans*, but rather functions as a licensing factor for the elaboration of anti-pathogen responses. Disruption of oleate biosynthesis alters membrane fluidity, which has pleiotropic consequences on membrane-bound organelles, including activating stress pathways associated with endoplasmic reticulum dysfunction [31]. Indeed, alterations of membrane fluidity have been linked to activation of G protein-coupled

receptors [60, 61]. Thus, changing the oleate content in *C. elegans* may modulate the ability of the host to mount protective defense responses, either directly or by disrupting lipid-protein interactions that are essential for immune pathway activation. Our findings present a previously unappreciated link between a highly abundant fatty acid and immune activation, which may represent an ancient connection between body energy stores and susceptibility to bacterial infection.

FIGURES

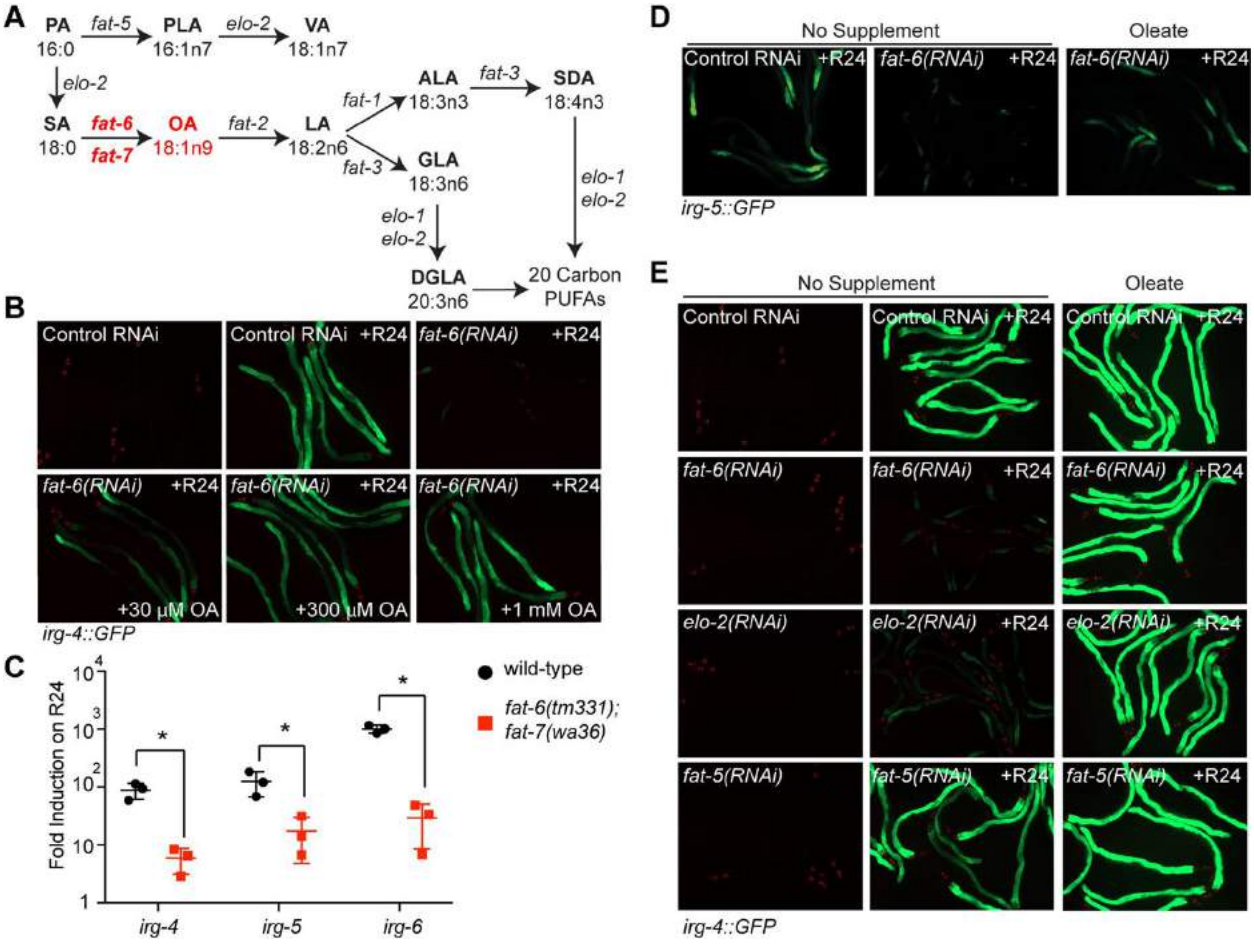

3. Figure 2.1: An RNAi screen identifies a role for MUFAs in the activation of *C. elegans* innate immune effectors.

A. A schematic of the long-chain fatty acid synthesis pathway in *C. elegans* adapted from [12, 27]. Fatty acid nomenclature: X:YnZ, X indicates the number of carbon atoms, Y denotes the number of double bonds, and Z designates the position of the terminal double bond relative to the methyl end of the molecule. Abbreviations: ALA, α-linoleic acid; DGLA, di-homo-γ-linoleic acid; GLA, γ-linoleic acid; LA, linoleic acid; OA, oleate; PA, palmitic acid; PLA, palmitoleic acid; SA, stearic acid; SDA, stearidonic acid; VA, vaccenic acid. **B.** The *C. elegans irg-4::GFP* immune reporter was exposed to control or *fat-6(RNAi)* bacteria seeded on plates containing control or the indicated levels of oleate. The animals were then transferred at the L4 stage to plates containing R24 for approximately 18 hours. Red pharyngeal expression is the *myo-2::mCherry* co-injection marker, which confirms the presence of the transgene. **C.** Expression of the immune effectors *irg-4, irg-5,* and *irg-6* were determined using qRT-PCR in wild-type or *fat-6(tm331);fat-7(wa36)* mutant animals exposed to R24 or solvent control (1% DMSO) for six hours. Data are the average of three independent replicates, each normalized to a control gene and presented as fold induction in R24-exposed vs. solvent control-exposed animals in the indicated genetic background. Error bars show standard deviation. Significance was determined by *t*-tests, * $p<0.05$. **D.** Animals containing the *irg-5::GFP* immune reporter were grown as described above and exposed to R24. All animals had a RoI phenotype, which confirms the presence of the transgene. **E.** *C. elegans* containing the *irg-4::GFP* immune reporter were fed RNAi bacteria targeting the indicated genes on plates containing control or oleate and exposed to R24, as described above.

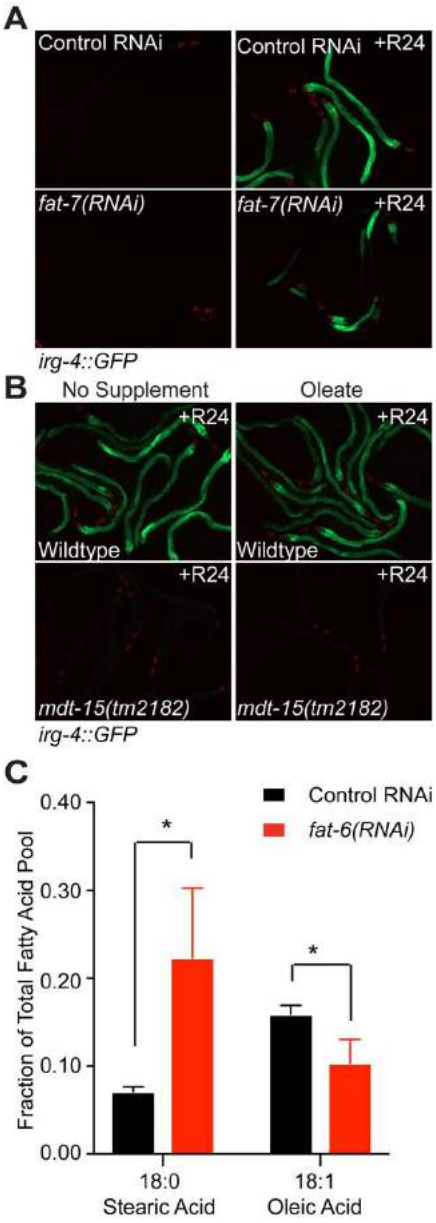

4. Figure 2.2: An RNAi screen identifies a role for MUFAs in the activation of *C. elegans* innate immune effectors.

A. *C. elegans* carrying the *irg-4::GFP* immune reporter grown on control or *fat-7(RNAi)* bacteria and exposed to R24 or solvent control at the L4 stage. **B.** Wild-type *C. elegans* or *mdt-15(tm2182)* loss-of-function *C. elegans* grown on control media or media supplemented with oleate and exposed to R24 at the L4 stage. **C.** GC-MS of L4-stage animals grown on control or *fat-6(RNAi)* exposed to solvent control for 24

hours. Data are the average of three independent replicates with error bars showing standard deviation. Statistical analyses performed using two-way ANOVA with Bonferroni correction. * $p<0.05$.

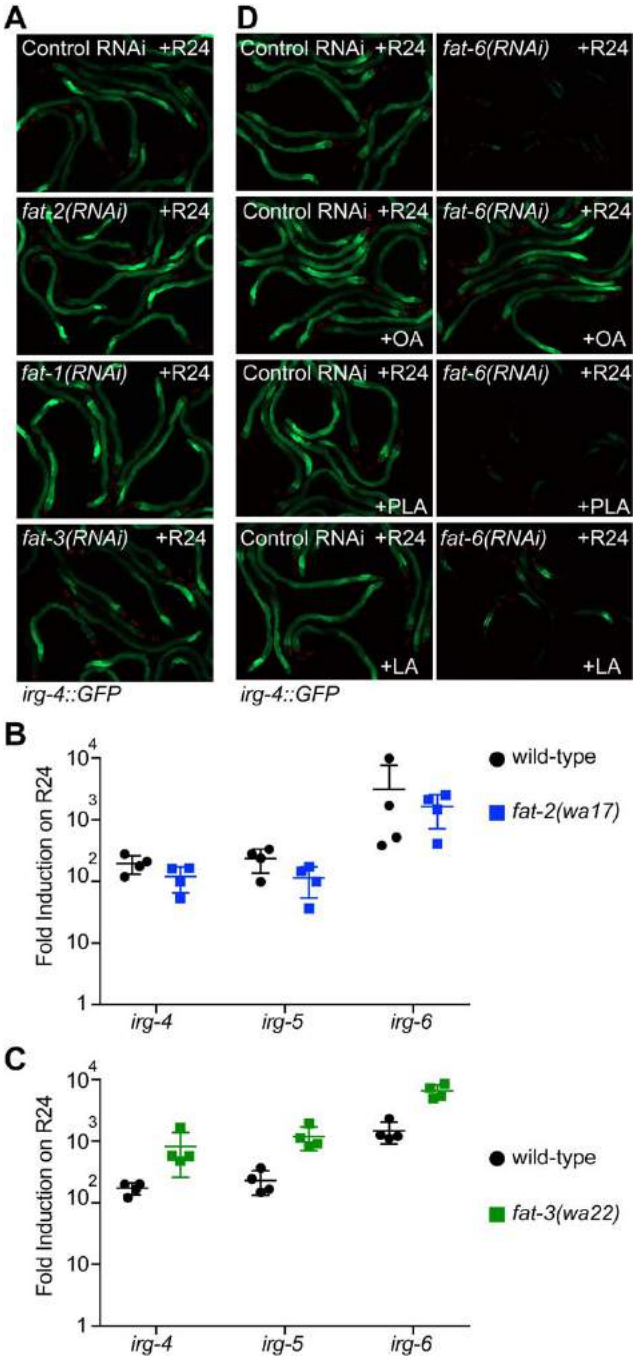

5. Figure 2.3: Polyunsaturated fatty acids are not required for immune induction by the immunostimulatory small molecule R24.

A. *C. elegans irg-4::GFP* immune reporter animals were fed the indicated RNAi bacteria and transferred at the L4 stage to plates containing R24 for approximately 18 hours. **B and C.** Expression of the immune effectors *irg-4, irg-5,* and *irg-6* were determined using qRT-PCR in wild-type, *fat-2(wa17),* and *fat-3(wa22)* mutant animals exposed to R24 or the solvent control (DMSO) for six hours. Data are the average of four independent replicates, each normalized to a control gene and presented as fold induction in R24-exposed vs. solvent control-exposed animals in the indicated genetic background. Error bars show standard deviation. Significance was determined by *t*-tests. There was no significant difference in the R24-mediated induction of the indicated gene in *fat-2(wa17)* animals or in *fat-3(wa22)* mutants for *irg-4*. In *fat-3(wa22)* animals, the induction of *irg-5* and *irg-6* by R24 was significantly higher than in wild-type ($p < 0.001$). **D.** *C. elegans irg-4::GFP* immune reporter animals were fed control or *fat-6(RNAi)* bacteria seeded on plates containing control or 500 μM of the indicated fatty acid. PLA is palmitoleic acid and LA is linoleic acid. The animals were then transferred at the L4 stage to plates containing R24 for approximately 18 hours. The presence of the transgene is confirmed by red pharyngeal expression of the *myo-2::mCherry* co-injection marker.

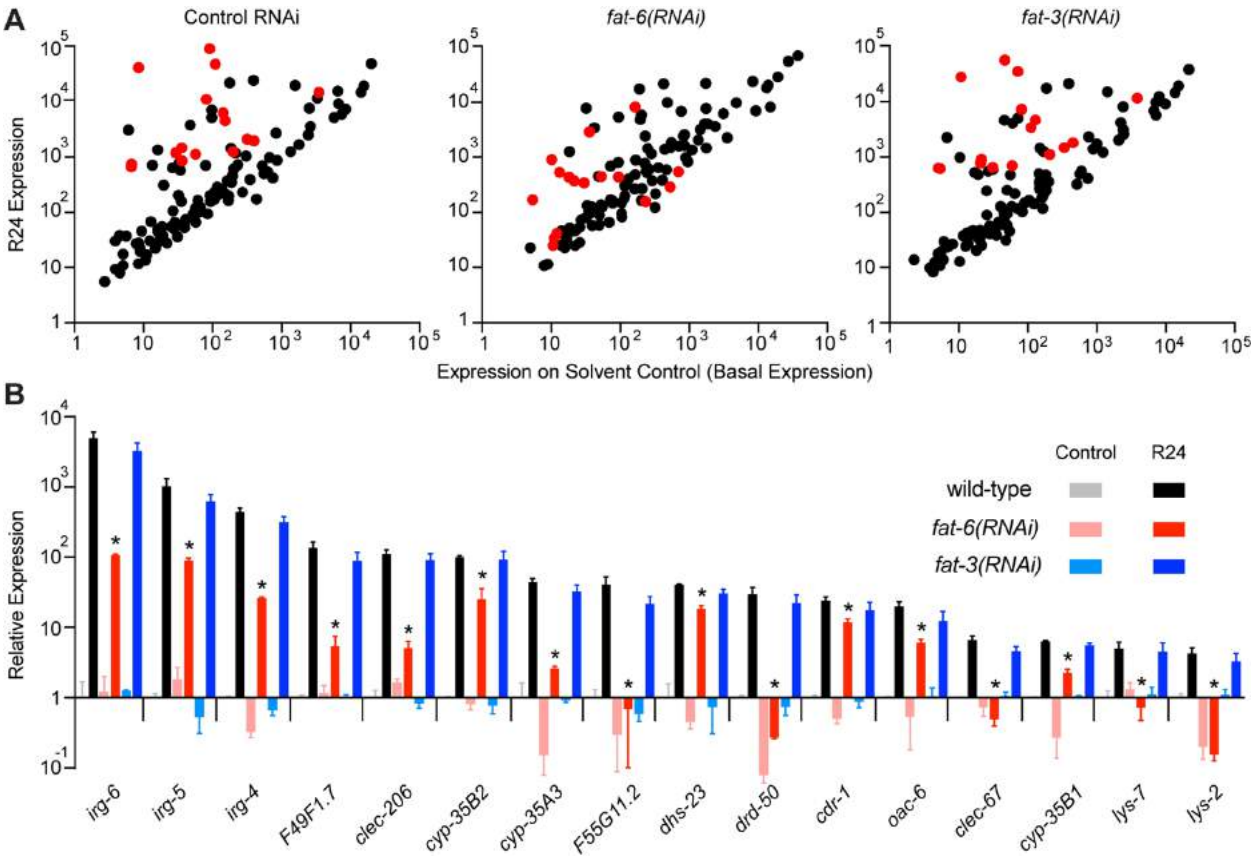

6. Figure 2.4: Stearoyl-CoA desaturase activity is required for the induction of an innate immune response in *C. elegans.*

A. Dot plots showing the NanoString nCounter gene expression analysis of 118 immune and stress response genes in *C. elegans* grown on the indicated RNAi bacteria and exposed to control or R24. Each dot represents one gene. Red dots highlight the 16 genes whose R24-mediated induction is significantly suppressed in *fat-6(RNAi)* animals. Data are the average of two independent replicates. **B.** The expression of the 16 *fat-6*-dependent genes in the indicated genotypes and conditions is shown relative to wild-type animals exposed to control. Significance was determined using *t*-tests, * $p<0.05$. Data are the average of two independent replicates, each normalized to three control genes and expressed relative to the baseline condition (wild-type animals exposed to control) for each gene. Error bars show standard deviation.

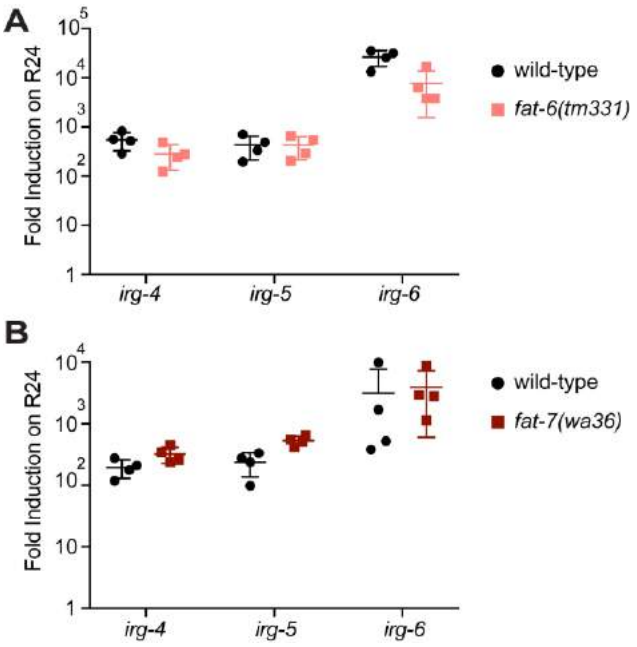

7. Figure 2.5. *C. elegans fat-6(tm331)* and *fat-7(wa36)* mutants do not affect the R24-mediated induction of innate immune effector genes.

qRT-PCR was used to assess the expression of the immune effector genes *irg-4, irg-5,* and *irg-6* in *fat-6(tm331)* **A.** and *fat-7(wa36)* **B.** animals exposed to the solvent control or R24 compared to wild-type. Data are the average of four independent replicates, each normalized to a control gene and presented as fold induction in R24-exposed vs. solvent control-exposed animals. Error bars show standard deviation.

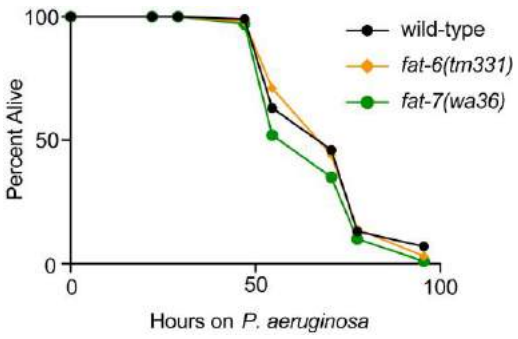

8. Figure 2.6: *C. elegans fat-6(tm331)* and *fat-7(wa36)* mutants are not more susceptible to killing by *P. aeruginosa* than wild-type animals.

A. *P. aeruginosa* pathogenesis assay of wild-type and the indicated mutant worms are presented. There is no significant difference between these conditions. Data are representative of two trials. Sample sizes, mean lifespan and p values for both trials are shown in Table 2.2B. Significance was determined using Kaplan-Meier survival curves and log-rank tests.

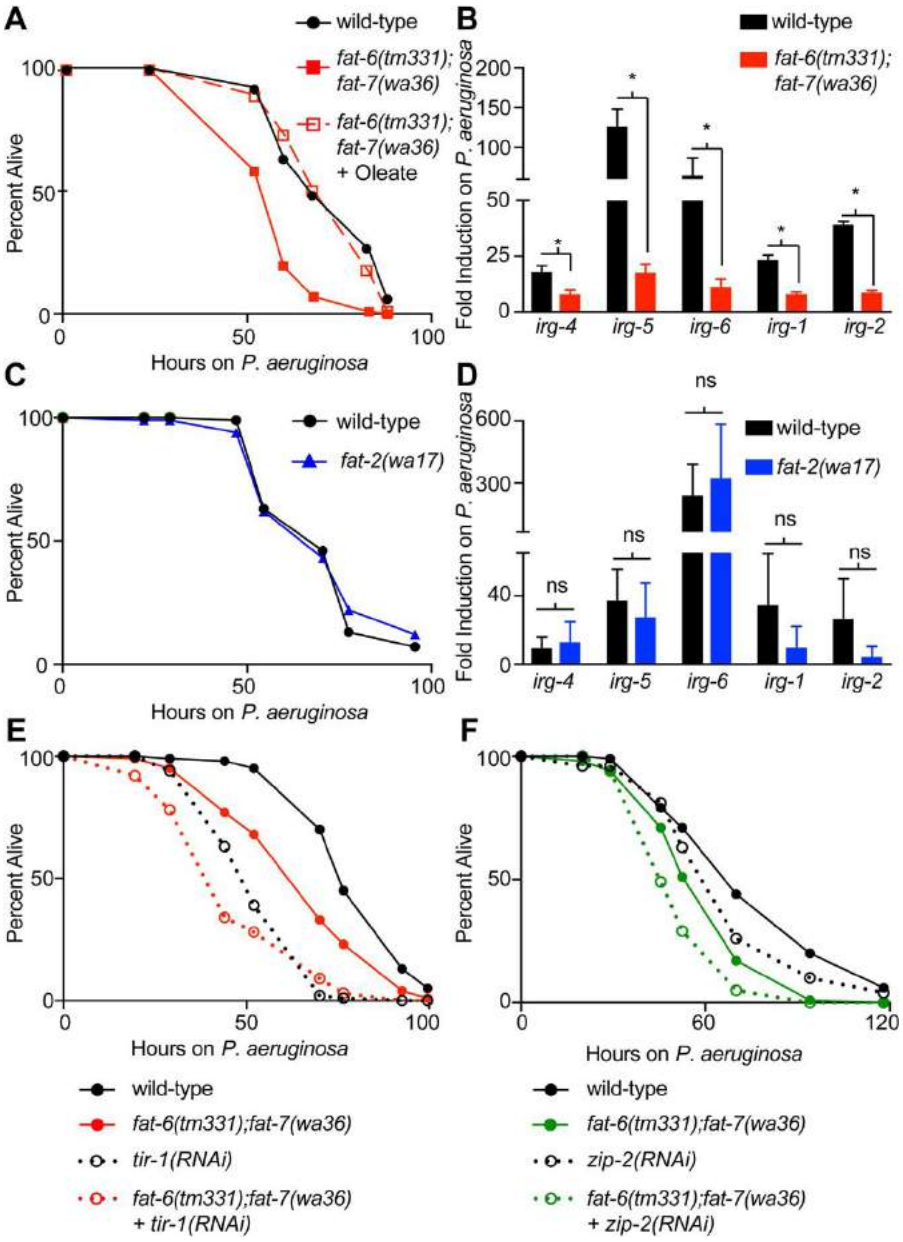

9. Figure 2.7: Oleate is required for host resistance to *P. aeruginosa* infection.

A and C. *P. aeruginosa* pathogenesis assays of wild-type and *fat-6(tm331);fat-7(wa36)* (A) or *fat-2(wa17)* (C) animals grown on control media or oleate-supplemented media, as indicated. Animals were transferred at the L4 stage to plates containing *P. aeruginosa*. Assay plates were not supplemented with oleate. Both *fat-6(tm331);fat-7(wa36)* and *fat-3(wa22)* are more susceptible to killing by *P. aeruginosa* ($p<0.01$). Oleate supplementation rescues the enhanced susceptibility to pathogens phenotype of the *fat-6(tm331);fat-7(wa36)* mutant ($p<0.01$). *fat-2(wa17)* animals are not hypersusceptible to killing (p=not significant). Data are representative of at least two trials. Sample sizes, mean lifespan, and p values for all trials are shown in Table 2.2A. Significance was determined using Kaplan-Meier survival curves and log-rank tests. **B and D.** Expression of the indicated genes measured by qRT-PCR in wild-type, *fat-6(tm331);fat-7(wa36), or fat-2(wa17)* double mutant animals exposed to *P. aeruginosa* at the L4 stage for 6 hours. Data are the average of three independent replicates, each normalized to a control gene and presented as fold induction in animals of the indicated genetic background infected with *P. aeruginosa* vs. animals fed the standard bacterial food source (*E. coli* OP50). Error bars show standard deviation. Statistical significance was determined using t-tests. * $p<0.05$. **E and F.** *P. aeruginosa* pathogenesis assays of wild-type and *fat-6(tm331);fat-7(wa36)* exposed to control RNAi bacteria, *tir-1(RNAi)* or *zip-2(RNAi)* bacteria, as indicated. *fat-6(tm331);fat-7(wa36)+ tir-1(RNAi)* animals are significantly more susceptible than *fat-6(tm331);fat-7(wa36)* mutants and *tir-1(RNAi)* animals ($p<0.05$). In addition, *fat-6(tm331);fat-7(wa36)+ zip-2(RNAi)* animals are significantly more susceptible than *fat-6(tm331);fat-7(wa36)* mutants and *zip-2(RNAi)* animals ($p<0.05$). Data are representative of at least two trials. Sample sizes, mean

lifespan, and p values for all trials are shown in Table 2.2A. Significance was determined using Kaplan-Meier survival curves and log-rank tests.

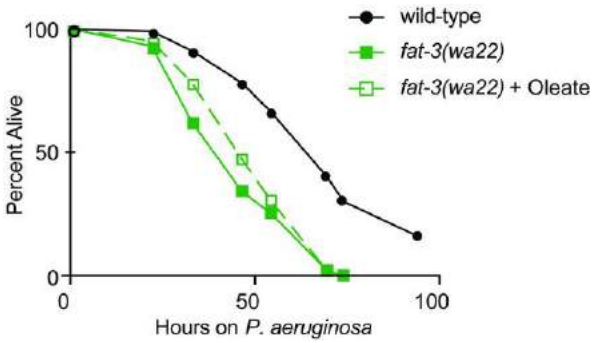

10. Figure 2.8: The effect of *fat-3(wa22)* on susceptibility to *P. aeruginosa* infection is independent of oleate.

P. aeruginosa pathogenesis assays of wild-type and *fat-3(wa22)* animals grown on control media or oleate-supplemented media, as indicated. Animals were transferred at the L4 stage to plates containing *P. aeruginosa*. Assay plates were not supplemented with oleate. The *fat-3(wa22)* mutant is more susceptible to killing by *P. aeruginosa* ($p<0.01$). Oleate supplementation did not rescue the enhanced susceptibility to pathogens phenotype of the *fat-3(wa22)* mutant (p is not significant). Data are representative of two trials. Sample sizes, mean lifespan, and p values for all trials are shown in Table 2.2D. Significance was determined using Kaplan-Meier survival curves and log-rank tests.

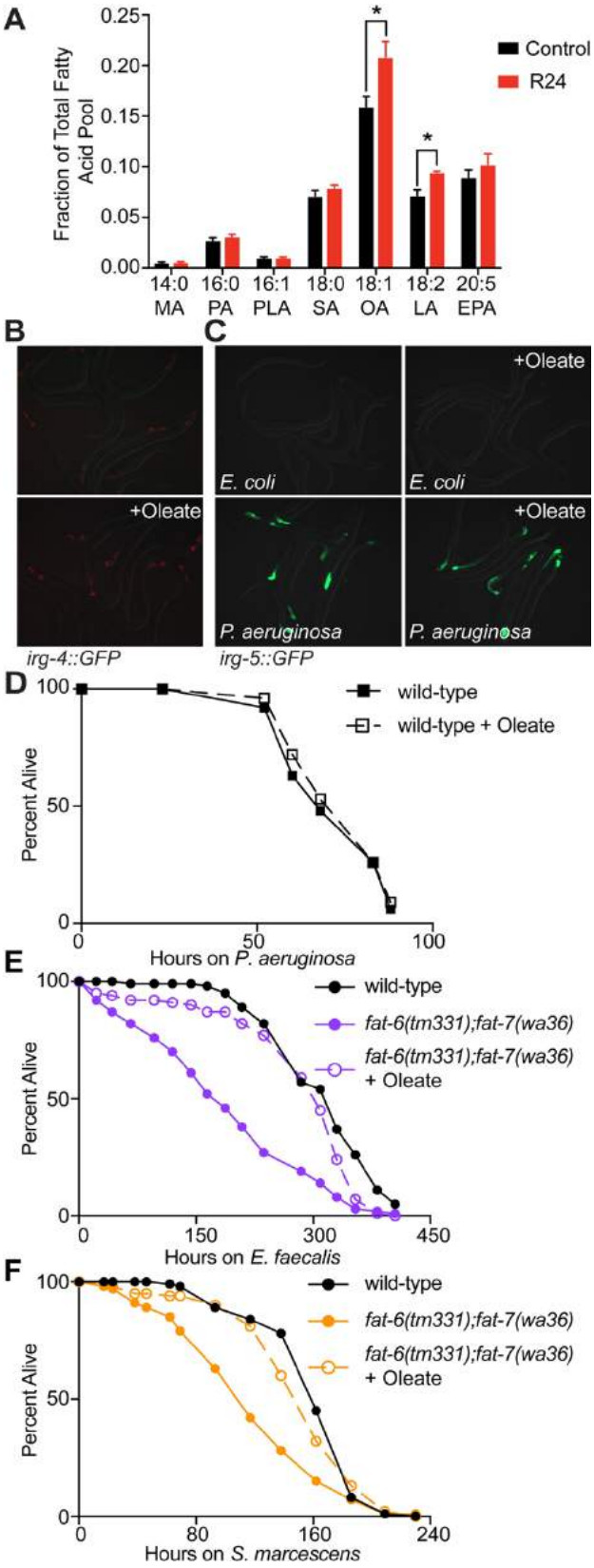
A
Fraction of Total Fatty Acid Pool
0.25
0.20
0.15
0.10
0.05
0.00
*
*
Control
R24
14:0 MA
16:0 PA
16:1 PLA
18:0 SA
18:1 OA
18:2 LA
20:5 EPA
B
C
+Oleate
E. coli
E. coli
+Oleate
+Oleate
P. aeruginosa
P. aeruginosa
irg-4::GFP
irg-5::GFP
D
Percent Alive
100
50
0
wild-type
wild-type + Oleate
0
50
100
Hours on P. aeruginosa
E
Percent Alive
100
50
0
wild-type
fat-6(tm331);fat-7(wa36)
fat-6(tm331);fat-7(wa36) + Oleate
0
150
300
450
Hours on E. faecalis
F
Percent Alive
100
50
0
wild-type
fat-6(tm331);fat-7(wa36)
fat-6(tm331);fat-7(wa36) + Oleate
0
80
160
240
Hours on S. marcescens

11. Figure 2.9: Oleate is necessary but not sufficient for pathogen resistance in *C. elegans.*

A. GC-MS of L4-stage animals exposed to R24 or solvent control for 24 hours. Data are the average of three independent replicates with error bars showing standard deviation. Statistical analyses performed using two-way ANOVA with Bonferroni correction. * $p<0.05$. Abbreviations: MA, myristic acid; PA, palmitic acid; PLA, palmitoleic acid; SA, stearic acid; OA, oleic acid; LA, linoleic acid; EPA, eicosapentaenoic acid. **B and C.** *C. elegans irg-4::GFP* (**B**) or *irg-5::GFP* (**C**) animals were grown on plates containing control or oleate, as indicated. The animals were then transferred at the L4 stage to plates containing *P. aeruginosa* or *E. coli* OP50, as indicated. **D, E, F.** *C. elegans* pathogenesis assays with *P. aeruginosa* (D), *E. faecalis* (E) and *S. marcescens* (F) in wild-type and *fat-6(tm331);fat-7(wa36)* animals grown on control media or oleate-supplemented media, as indicated. Animals were transferred at the L4 stage to plates containing the indicated pathogen. Assay plates were not supplemented with oleate. There is no significant difference between the conditions in D. In E and F, the *fat-6(tm331);fat-7(wa36)* mutants are more susceptible to killing by the indicated pathogen ($p<0.01$). Oleate supplementation rescues the enhanced susceptibility to pathogens phenotype of the *fat-6(tm331);fat-7(wa36)* mutant in both E and F ($p<0.01$). Data are representative of at least two trials. Sample sizes, mean lifespan, and p values for all trials are shown in Table 2.2C. Significance was determined using Kaplan-Meier survival curves and log-rank tests.

TABLES

See List of Online Files

MATERIALS AND METHODS

***C. elegans* and bacterial strains.** *C. elegans* strains were maintained on *E. coli* OP50 or HT115 bacteria on nematode growth media plates, as described [62]. The *C. elegans* strains used in this study were N2 Bristol [62], AU306 *agIs43* [*irg-4::GFP::unc-54-3'UTR; myo-2::mCherry*] [23], AY101 *acIs101* [p*DB09.1(irg-5::gfp)*; p*RF4(rol-6(su1006))*] [63], BX156 *fat-6(tm331);fat-7(wa36)* [37], BX106 *fat-6(tm331)* [33], BX153 *fat-7(wa36)* [33], BX30 *fat-3(wa22)* [34], and BX26 *fat-2(wa17)* [34]. *P. aeruginosa* strain PA14 [31], *E. faecalis* strain MMH594 [64] and *S. marcescens* strain Db11 [65] were used in this study.

Fatty Acid Supplementation. Fatty acids were obtained from Nu-Chek-Prep, Inc. and were prepared as previously described [66]. Assays were performed by growing synchronized L1 worms on the indicated fatty acid or control media containing tergitol (0.1%). Unless otherwise indicated, oleate was used at a concentration of 400 or 500 μM, except for Fig. 2.1E, which used 1 mM. Palmitoleic acid and linoleic acid were used at a concentration of 500 μM.

***C. elegans* Bacterial Infection and Other Assays.** "Slow killing" *P. aeruginosa* pathogenesis assays were performed as previously described [67]. The protocol for treatment of animals with 70 μM R24 has also been described [46]. The *E. faecalis* [64, 68] and *S. marcescens* [69] pathogenesis assays were performed as previously described. Fatty acid supplementation was performed as described above. For all

assays, L4 stage-matched animals raised from the L1 stage on media containing fatty acids or control were transferred to standard assay plates for the indicated experiment, which were not supplemented with fatty acids. Sample sizes, mean lifespan, and p values for all trials are shown in Table 2.2. The RNAi screen of 1,420 RNAi clones was previously described [23]. RNAi clones that were used in this study are from the Ahringer [70] or Vidal [71] libraries and were confirmed by sequencing.

NanoString nCounter Gene Expression Analyses and Quantitative RT-PCR (qRT-PCR). The codeset used for the NanoString nCounter Gene Expression Analysis was synthesized by NanoString and contained probes for 118 *C. elegans* genes, which has been described previously [23, 47]. Counts from each gene were normalized to three control genes: *snb-1*, *ama-1* and *act-1*. The qRT-PCR studies were performed as described previously [23, 46, 47], using previously published primer sequences [7, 23, 36, 46, 47]. All values were normalized against the control gene *snb-1*. Fold change was calculated using the Pfaffl method [72].

Gas Chromatography and Mass Spectrometry (GC-MS). Synchronized populations of approximately 6000 worms at the L4 stage were harvested 24 hours after exposure to 70 μM R24 or 1% DMSO control, washed with M9 buffer to remove excess bacteria, and frozen in ethanol on dry ice. Worm pellets were thawed, sonicated, and then dissolved in 1 mL of a 3:1 methanol: methylene chloride mixture with 50 μl of internal standard dissolved in hexane (17:0, Nu-Chek-Prep Inc.). While vortexing, 200 μl acetyl chloride was slowly added. Samples were subjected to methanolysis at 80°C for 1 hour.

After cooling to room temperature, the sample was neutralized with 4 mL of 7% K_2CO_3, and fatty acid methyl esters were extracted through the addition of 2 mL of hexane. Following hexane addition, samples were vortexed and then centrifuged at 2500 rpm for 10 minutes. The top hexane layer containing fatty acid methyl esters was transferred to a new borosilicate glass test tube and washed with 2 mL acetonitrile, vortexed and centrifuged at 2500 rpm for 5 min. The top hexane layer was transferred and dried under nitrogen. Fatty acid methyl esters were resuspended in 200 μl hexane, vortexed and transferred to Agilent vials with glass insert. Fatty acid methyl esters were analyzed by GC-MS using an Agilent 6890/5972 GC-MS system outfitted with a Supelcowax 10 column as previously described [73, 74]. The relative abundance of each fatty acid was determined by dividing each fatty acid by the total fatty acid pool.

Microscopy. Nematodes were paralyzed with 10 mM levamisole (Sigma), mounted on agar pads and photographed using a Zeiss AXIO Imager Z2 microscope with a Zeiss Axiocam 506mono camera and Zen 2.3 (Zeiss) software.

Statistical Analyses. *C. elegans* survival was assessed using the Kaplan-Meier method and differences were determined with the log-rank test using OASIS 2 [75]. Other statistical tests, which are indicated in the figure legends, were performed using Prism 7 (GraphPad Software).

Chapter III: Redirection of SKN-1 abates the negative metabolic outcomes of a perceived pathogen infection

PREFACE

This research chapter derives from a collaboration between several people and labs. Our work started as a collaboration with Cole Haynes and Nandhitha Uma Naresh where we generated data that ultimately became Figure 3.10E and F. Sean Curran and James Nhan are the original creators of this project that then contacted us to combine our work. We published this in PNAS with the title “Redirection of SKN-1 abates the negative metabolic outcomes of a perceived pathogen infection” in 2019. In this work, I am the third author, James Nhan is the first author, Christian Turner is the second author, Chia-An Yena, Hans Dalton, Dana Ruter, Nandhitha Uma Naresh, Cole Haynes, Alexander Soukas, and Read Pukkila-Worley are middle authors, and Sean Curran is the last author. James Nhan, Nandhitha Uma Naresh, Hilary Cheesman and I worked collaboratively to generate portions of Figures 3.10, 3.12, 3.13, and 3.14. These figures highlight my contributions to this work and are the key observations that relate to the role of oleate in the *C. elegans* innate immune response.

ABSTRACT

Early host responses toward pathogens are essential for defense against infection. In *Caenorhabditis elegans*, the transcription factor, SKN-1, regulates cellular defenses during xenobiotic intoxication and bacterial infection. However, constitutive activation of SKN-1 results in pleiotropic outcomes, including a redistribution of somatic lipids to the germline, which impairs health and shortens lifespan. Here, we show that

exposing *C. elegans* to *Pseudomonas aeruginosa* similarly drives the rapid depletion of somatic, but not germline, lipid stores. Modulating the epigenetic landscape refines SKN-1 activity away from innate immunity targets, which alleviates negative metabolic outcomes. Similarly, exposure to oxidative stress redirects SKN-1 activity away from pathogen response genes while restoring somatic lipid distribution. In addition, activating p38/MAPK signaling in the absence of pathogens, is sufficient to drive SKN-1–dependent loss of somatic fat. These data define a SKN-1– and p38-dependent axis for coordinating pathogen responses, lipid homeostasis, and survival and identify transcriptional redirection, rather than inactivation, as a mechanism for counteracting the pleiotropic consequences of aberrant transcriptional activity.

INTRODUCTION

The transcription factor SKN-1, the *Caenorhabditis elegans* ortholog of mammalian NRF2, mediates cytoprotective responses to diverse stresses to restore cellular homeostasis [76]. For example, SKN-1 induces the transcription of phase II detoxification genes during oxidative stress, promotes adaptation to proteotoxic and metabolic stress, and drives the induction of innate immune effector genes during pathogen exposure [77, 78].

Although SKN-1 activation in response to stress facilitates survival, when left unchecked, aberrant activation of SKN-1 and its mammalian ortholog NRF2 can have negative pathological outcomes in worms [79, 80] and humans [81, 82]. Specifically, constitutive activation of SKN-1 shortens lifespan [80, 83] and causes a reorganization of fat from the soma to the germline, termed age dependent somatic depletion of fat

(Asdf) [79]. Thus, although the activation of cytoprotective transcription factors is obligatory for maintaining homeostasis when organisms encounter stressful environments, the inability to turn off or control these transcriptional responses can be detrimental [80, 81, 83].

Here, we show that redirecting activated SKN-1 by modulating the epigenetic landscape abolishes negative metabolic outcomes associated with its aberrant activation, but at the cost of losing increased innate immune function. Specifically, abolishing H3K4me3 epigenetic marks directed SKN-1 activity away from innate immunity targets, thus, reestablishing pathogen sensitivity while also restoring health-promoting, age-dependent outcomes, including homeostatic distribution of lipids, restoration of stress resistance, and increased lifespan.

RESULTS

SKN-1 Activation Drives the Post Developmental Expression of Innate Immunity Pathway Genes

Our previous studies established that activation of SKN-1 results in the age-dependent loss of somatic lipids [79]. We demonstrated this finding by activating SKN-1 using environmental factors, loss of a negative regulator, or in a *skn1(lax188)* gain-of-function (gf) mutant (*skn-1gf*). To define the extent of transcriptional dysregulation in *skn-1gf* mutants at the time of somatic lipid depletion, we performed RNA sequencing (RNA-seq) on day 2 adult worms, when these animals begin to display the Asdf phenotype [79] (Fig. 3.1 A–C and Fig. 3.2). The *skn-1gf* mutants display dysregulation

of 1,986 genes (1,376 up-regulated and 610 down-regulated) as compared to wild type (WT) (Table 3.1).

Interestingly, genes induced in *skn-1gf* mutants were strongly enriched for immune and pathogen response by Gene Ontology (GO) analysis (Fig. 3.1 D and E and Table 3.1), in addition to oxidative stress response and xenobiotic detoxification (Fig. 3.1 D–F and Table 3.1). Of note, the major SKN-1 responsive genes were represented in this dataset [82-86] (Table 3.1). The transcription profile of day 2 adults was distinct from previous transcriptional analyses of *skn-1gf* mutants during development [83], which do not display GO-term enrichment for innate immunity and pathogen related genes (Fig. 3.1G and Table 3.1). This finding suggests that the age-related negative outcomes of *skn-1gf* mutants, like the loss of somatic fat at day 2 of adulthood, may stem from an increase in expression of innate immune response genes.

H3K4 Methylation by WDR-5 Is Required for SKN-1–Dependent Loss of Somatic Lipids

We performed chromatin immunoprecipitation (ChIP) followed by qPCR of SKN-1 and SKN-1gf protein at day 2 of adulthood and observed enrichment of SKN-1gf relative to wild-type SKN-1 at the promoters of several genes, which we identified by RNA-seq (Fig. 3.1 and Table 3.1), selecting representative genes from the innate immunity, oxidative stress, and metabolism GO classes, including: *endu-2, dod-24*, W06H8.2, *clec-66*, F17A4.9, and *acs-14* (Fig. 3.3A and Table 3.1). We hypothesized that manipulating epigenetic modifications to restrict the transcriptional activity of the *skn-1gf* mutants could mitigate the pleiotropic effects of SKN-1 constitutive activation.

Methylation of Histone H3 at lysine 4 (H3K4me) is an established effector of transcriptional activity and several conserved protein complexes regulate H3K4 di- and trimethylation states [87]. With this in mind, we screened a panel of epigenetic chromatin modifiers by RNA interference (RNAi). We found that reducing the expression of *wdr-5* or *rbbp-5*—2 SET1/MLL-like proteins that influence the H3K4me3 state—restored somatic fat in *skn-1gf* mutant animals (Fig. 3.4). This finding suggests that H3K4me3 mediates physiological outcomes in the *skn-1gf* mutant.

We confirmed this genetic relationship in *wdr-5lf(ok1417);skn1gf* double mutants at day 2 of adulthood, noting that the *wdr-5lf* mutant had wild-type lipid distribution between the soma and germline and that *skn-1gf* does not impact H3K4me3 levels in the *wdr-5lf* background (Fig. 3.3 B–D and Fig. 3.5 A and B). In support of the molecular connection between SKN-1gf activity and H3K4me3 epigenetic marks, the loss of *wdr-5* attenuated the shortened lifespan [83] phenotype of *skn-1gf* mutants (Fig. 3.5C). As previously documented, the *skn-1gf(lax188)* allele enhances resistance to hydrogen peroxide exposure when reproduction begins (Fig. 3.5D), but this resistance is lost when reproduction ceases, as somatic lipids are depleted (Fig. 3.5E) [79]. Loss of *wdr-5* restored resistance to acute oxidative stress in the *skn-1gf* mutant background at this later stage of life. Recent studies have linked oxidative stress [88] and lipid mobilization [89] to cold stress tolerance. Similar to the oxidative stress responses, *skn-1gf* mutant animals at day 2 of adulthood were more sensitive to exposure at 2°C than wild-type animals and this sensitivity was suppressed in the absence of *wdr-5* (Fig. 3.5 F and G); thus, cold stress resistance is associated with the abundance of somatic lipids. It should be noted that both *wdr-5lf* and *wdr-5lf;skn-1gf* worms develop at a slightly slower rate as

compared to wild-type and *skn-1gf* animals (Fig. 3.5H). However, even if examined 24 h later, at day 3 of adulthood, *wdr-5lf;skn-1gf* worms continue to display a suppression of Asdf (Fig. 3.5I). Taken together, these data reveal the importance of H3K4me3 marks for SKN-1–dependent metabolic and stress responses.

Loss of H3K4 Trimethylation Impacts SKN-1 Activation of Innate Immunity Genes

Next, we performed RNA-seq analysis on *wdr5lf;skn-1gf* double mutants to measure the impact of loss of H3K4me3 on SKN-1 transcriptional activity (Fig. 3.3E and Table 3.2). The genes with the most significant reduction in expression, when compared to *skn-1gf* mutants, were the pathogen resistance GO-term class of genes (Fig. 3.3F, Fig. 3.6A, and Table 3.2). Surprisingly, the expression of oxidative and redox homeostasis genes remained largely unchanged (Fig. 3.3G, Fig. 3.6B, and Table 3.2). These data revealed that H3K4me3 can influence the transcriptional focus of constitutively activated SKN-1 between classes of target genes and that redirecting the transcriptional focus away from pathogen response genes, but not oxidative stress genes, can alleviate the negative metabolic outcomes of deregulated SKN-1 transcriptional activity (Fig. 3.6C).

Redirection of Activated SKN-1 from Innate Immunity Genes Abates Metabolic Dysfunction

Our finding that oxidative stress gene targets were generally unaltered in the *wdr-5lf;skn-1gf* double mutants was unexpected, given the established role of H3K4me3

as a transcriptionally activating epigenetic mark and the impact its loss has on *skn-1gf* stress responses. Our previous study has shown that acute exposure to hydrogen peroxide can induce a loss of fat phenotype in wild-type animals [79]. We therefore examined how continuous expression of oxidative stress response genes would affect fat levels in an age-dependent manner. We used a subliminal amount of the superoxide-generating oxidant paraquat (PQ) (75 μM), in order to chronically induce an oxidative stress response, and found no apparent change in somatic or germline lipid pools in wild-type animals (Fig. 3.7A). Unexpectedly, this treatment suppressed the Asdf phenotype of *skn-1gf* animals, restoring their somatic lipid stores (Fig. 3.8 A–C and Fig. 3.7B). We next compared the transcriptional profiles of *skn-1gf* mutant animals treated with paraquat to vehicle treatment (Fig. 3.8D and Table 3.3). Exposure to paraquat maintained, and for some genes enhanced, the expression of SKN-1–dependent antioxidant pathway genes (Fig. 3.8E, Fig. 3.9A, and Table 3.3) but, remarkably, paraquat treatment reduced the expression of pathogen response genes that are activated in *skn-1gf* (Fig. 3.8E, Fig. 3.9B, and Table 3.3). Consistent with this finding, chromatin immunoprecipitation revealed that the association of SKN-1gf with the promoter regions of innate immunity genes was markedly reduced (Fig. 3.8G), utilizing *dod-24* and *endu-2* as representative reporters of innate immunity and SKN-1 responsive genes (Fig. 3.1E) [83, 85, 90, 91]. Importantly, association of SKN-1gf with the promoter of the oxidative stress genes *gst-4* and W06H8.2, previously identified as SKN-1 responsive to oxidative stress [92], was enhanced with PQ treatment (Fig. 3.8G). SKN-1 regulates transcriptional targets that perform highly diverse functions [83, 85, 93-96], but these data reveal that even when activated, the protective responses regulated

by SKN-1 can be refined to suit the current need to restore homeostatic balance (Fig. 3.9C). Moreover, our discovery reveals the important finding that the focus of activated transcription factors, as probed using SKN-1gf mutants, can be interrupted and redirected to improve health.

Pathogen Exposure Drives the Rapid Loss of Somatic Lipids

Because *C. elegans* feed on bacteria, they represent an established model to study host–microbe interactions [41]. Although live bacteria are routinely used as a food source, *C. elegans* can be maintained on dead bacteria and the loss of colonization and proliferation of bacterial cells in the intestine can increase lifespan [97], supporting the notion that, compared to other microbial diets, the standard OP50 *Escherichia coli* diet is modestly pathogenic [97, 98]. With this in mind, we examined lipid distribution in *skn-1gf* animals raised on dead bacteria and observed suppression of Asdf (Fig. 3.10A). We also examined animals moved to plates with 5-fluoro-2′-deoxyuridine (FUdR)-treated bacteria, which inhibits bacterial proliferation, and observed a similar suppression of Asdf (Fig. 3.10A). Taken together, these data suggest that the mobilization of lipids from the soma to the germline at the end of reproduction in our *skn-1gf* animals requires an interaction with live and proliferating bacteria.

Based on this finding, we explored whether immune activation itself was sufficient to drive lipid redistribution. In *C. elegans*, the p38 MAPK PMK-1 pathway is a canonical regulator of innate immune defenses [42, 99, 100]. Following pathogen exposure, NSY-1/ MAPKKK (the *C. elegans* ASK1 homolog) phosphorylates a p38 MAPK cascade with one of the final targets being SKN-1 [77, 78, 101]. We first

examined the lipid distribution of animals harboring a *nsy-1gf* allele, which drives constitutive immune activation [47]. Interestingly, *nsy-1gf* animals mobilize lipids from the soma to the germline in an age-dependent manner, just like the Asdf phenotype observed in *skn-1gf* mutants (Fig. 3.10B and C and Fig. 3.11A). Importantly, this loss of fat phenotype requires SKN-1 activity as both *skn-1(zu135)* loss-of-function (lf) allele and *skn-1* RNAi suppressed lipid redistribution in the *nsy-1gf* mutant background, thus confirming the placement of SKN-1 downstream of NSY-1/MAPKKK signaling for changes in metabolic homeostasis (Fig. 3.10D and Fig. 3.11B). Taken together with the transcriptome profiling data of the skn-1gf mutants, these data indicate that activation of SKN-1 by the NSY-1/PMK-1 pathways and the subsequent transcription of innate immunity target genes, drives the loss of somatic lipids.

To determine whether physiological activation of innate immune defenses in the context of pathogen infection is sufficient to drive changes in metabolic homeostasis, we exposed wild-type and *skn-1gf* mutant animals to the opportunistic human pathogen *Pseudomonas aeruginosa*, which also infects and kills nematodes [41, 67, 102, 103]. Post-developmental exposure to *P. aeruginosa* resulted in the rapid depletion of somatic lipids (Fig. 3.10E and F and Fig. 3.12A). Importantly, exposure to the virulence attenuated pseudomonal mutant gacA or rhlR [55, 67, 104], which do not robustly activate *C. elegans* immune defenses [7], did not cause loss of somatic fat (Fig. 3.10F and Fig. 3.12B and C). We previously demonstrated that the loss of somatic lipids in *skn-1gf* mutants was mediated by lipid transport from the soma to the germline by vitellogenins [79]. Similarly, *vit-5* RNAi-treated animals displayed reduced somatic fat loss when exposed to *P. aeruginosa*, indicating a shared mechanism of lipid loss

between *skn-1gf* mutants and pathogen exposure (Fig. 3.12D). In addition, loss of somatic lipids during infection with *P. aeruginosa* was accelerated in *skn-1gf* mutants (Fig. 3.10E) and delayed in *skn-1* RNAi-treated animals (Fig. 3.12F and G). It is noteworthy that the genes with the largest changes in expression in wild-type animals exposed to pathogens are also activated in *skn-1gf* mutant animals on nonpathogenic bacteria (e.g., *fmo-2, clec-71, cpt-4, sodh-1, clec-60, cyp-34A4*, F53A9.8, C34C6.7, T07G12.5, M60.2, *ugt-18*, and Y65B4BR0.4; for full list see Table 3.1) [91, 99, 105]. Taken together, these findings demonstrate that the immune response to pathogenic bacteria involves SKN-1–dependent redistribution of somatic lipids and provides evidence of a sophisticated relationship between these previously unconnected essential aspects of organismal homeostasis.

Somatic Lipid Abundance Is Associated with Pathogen Sensitivity

Our data suggest that *skn-1gf* animals would potentially display enhanced resistance to pathogen exposure. The effects of pathogens on host physiology are a result of the presence of the microbe itself and the toxins it secretes [106]. Exposure of wild-type animals to *P. aeruginosa* can result in “slow-killing” of *C. elegans*, which reflects the colonization of *C. elegans* intestine and subsequent lethal infection. Altering the media on which the *P. aeruginosa* are grown prior to *C. elegans* exposure results in hyperproduction of phenazine toxins, which causes rapid intoxication of nematodes, an assay which is also called “fast-killing” [102, 103]. Although each of the modes of killing have been well studied, several aspects of pathogenesis remain unanswered, but it is clear that it is multifactorial. We challenged wild-type and *skn-1gf* animals to the fast-kill

and slow-kill models of pathogen-induced death. Interestingly, *skn-1gf* mutants were resistant to *P. aeruginosa* fast killing, in a manner dependent on the production of phenazine toxins (Fig. 3.13A and Fig. 3.14A), but surprisingly the effect in the slow-killing scenario was unremarkable (Fig. 3.13B).

The pathogen resistance phenotype of *skn-1gf* animals was suppressed in the absence of *wdr-5*, which is consistent with our findings that loss of H3K4me3 epigenetic marks on chromatin diminishes the transcriptional output of SKN-1–associated pathogen defense genes. Collectively, these findings support a biological framework for host–pathogen responses where the presence of a pathogen drives SKN-1 activation of pathogen defense genes (Fig. 3.13C). This program enables resistance to pathogen-derived toxins, but occurs at the expense of organismal lipid homeostasis, which impairs organismal health later in life. Importantly, this program is malleable and the loss of lifelong health can be restored, albeit at the cost of changes in pathogen susceptibility, by dampening SKN-1 activity at these specific gene targets.

Activated SKN-1 Drives Preferential Utilization of Diet-Derived and Short Unsaturated Lipids

Several events that immediately precede somatic lipid depletion in animals with SKN-1 activation have been described [79]; however, a full account of the metabolic state once somatic lipids have been depleted is lacking. We applied a tandem transcriptomic and lipidomic assessment of animals at the peak of somatic lipid depletion (day 2 of adulthood). We examined our RNA-seq data (Table 3.1-3.4) for changes in the expression of lipid metabolism genes in animals with activated SKN-1

that was dampened in the absence of H3K4me3 or when SKN-1 was redirected by PQ treatment. Several metabolism genes fit these criteria (Fig. 3.15 and Fig. 3.16), including mitochondrial and peroxisomal B-oxidation genes *acox-1.3, acs-7*, and *acs-14* (Fig. 3.15A); lipolysis genes *lipl-1* and *lipl-3* (Fig. 3.15B); and lipid binding genes like *lbp-7* (Fig. 3.15C). We also measured a reduction in several lipid biosynthesis genes, including *cpt-6* and *fat-5*, whose expression is restored when SKN-1 is redirected (Fig. 3.16A and B). These data reveal that SKN-1 activation induces a metabolic state where lipid utilization pathways are activated while de novo biosynthesis is suppressed, both of which could contribute to the observed depletion of somatic lipids. Our previous studies of L4-stage *skn-1gf* mutant animals identified the differential abundance of multiple lipid species as compared to age-matched wild-type animals before Asdf occurs [79]. To connect the transcriptomic analysis with the lipid signature of animals with a depletion of somatic lipids, we used quantitative Nile Red staining of lipids [107] and gas chromatography coupled to mass spectrometry (GCMS) [108]. At day 2 of adulthood, *skn-1gf* animals have 60% less total fat compared to wild-type animals (Fig. 3.15D and Fig. 3.16C) and we identified several classes of lipids with differential abundance in *skn-1gf* mutants as compared to wild-type animals (Fig. 3.15E–H). Specifically, bacterial diet-derived cyclopropane fatty acids (Fig. 3.15E) and synthesized 16:1 and 18:2 species (Fig. 3.15F) were all reduced. There was also a modest increase in monomethyl branched-chain fatty acids (Fig. 3.15G) and a more significant increase in synthesized mono- and polyunsaturated fat species of longer lengths, including eicosatetraenoic acid 20:4(n-3) lipid species (Fig. 3.15F and H). The relative abundance of these lipids in *skn-1gf* mutants is an important biomarker as it defines the lipid

species that are a hallmark of Asdf and also which lipid species are lost in response to SKN-1 activation.

Taken together, our data identify redirection of an activated cytoprotective transcription factor, like SKN-1, as a powerful mechanism to abate pleiotropic consequences of unchecked transcriptional activity, including age-dependent loss of lipid homeostasis that normally accompanies pathogen infection and chemosensitivity, respectively (Fig. 3.17).

CONCLUSIONS

We report a mechanism by which the pleiotropic outcomes stemming from the activation of SKN-1 can be ameliorated by redirecting transcriptional activity. Modulation of transcriptional outputs, rather than inactivation of the transcription factor, provides a model for the treatment of pathologies stemming from transcriptional dysregulation.

Importantly, we report the rapid loss of somatic lipid stores as one of the earliest documented pathological symptoms of pathogen exposure, which is dependent on SKN-1 activity. Although early responses to pathogens are essential for optimal health, the long-term effects of these responses are uncharacterized. Our data reveal that SKN-1 activation depletes somatic lipids while providing pathogen resistance. However, aberrant SKN-1 activation ultimately impedes oxidative stress resistance and shortens lifespan. Dampening the innate immunity axis of SKN-1 activation increases lifespan, restores oxidative stress resistance, and reestablishes the healthy distribution of lipids, but compromises the ability to survive pathogen challenge.

We previously found that depletion of the monounsaturated fatty acid oleate drives the redistribution of somatic lipids in *skn-1* gain-of-function mutants, or Asdf phenotype [79]. Of note, oleate is also necessary for the pathogen-mediated induction of host defense genes and resistance to diverse bacterial pathogens [109]. Taken together with data from this study that immune activation during pathogen infection drives the Asdf phenotype, these studies emphasize that oleate sufficiency is a key marker of health, depletion of which triggers protective reallocation of somatic fat and suppression of immune defenses, thereby allowing energy reserves to be devoted to the preservation of evolutionary fitness. Oleate is also required for proper immune defenses in plants [58, 59, 110], which suggests that cytoprotective redistribution of host lipids and energy stores is evolutionarily ancient.

Our previous work showed that diet can influence loss of somatic lipids in the context of our *skn-1gf* worms, as the bacteria *E. coli* OP50/B leads to fat loss but not *E. coli* HT115/K-12 [79]. This was not the case for exposure to *P. aeruginosa*, as virulence attenuated strains of the pathogen did not lead to depletion of somatic lipids. Thus, some aspect associated with *P. aeruginosa* virulence drives somatic lipid depletion, which is partially dependent on SKN-1, as RNAi against *skn-1* attenuates the lipid depletion. Our observation that animals with reduced SKN-1 activity eventually lose somatic fat following exposure to *P. aeruginosa* indicates the presence of additional factors that mediate pathogen-dependent fat loss. Additionally, we observed that wild-type animals exposed to *P. aeruginosa* displayed a rapid loss of somatic lipids—about 4 to 6 h for fat loss to occur. The speed of this response is intriguing as the “slow-killing” model requires bacteria to colonize the intestine and during the first 24 h of exposure

there are neither disease symptoms nor appreciable mortality. Moreover, SKN-1gf mutant animals, which are already primed for an innate immune response, deplete somatic lipids even more rapidly than wild-type animals and loss of SKN-1 attenuates the somatic lipid depletion in animals with constitutive activation of p38 signaling. As these host–pathogen interactions are mediated, at least in part, by intestinal epithelial cells [42, 47, 91, 111], the loss of lipids in this tissue is one of the first detectable physiological responses to pathogen exposure.

H3K4 methylation marks are epigenetic signatures of active gene expression, but they are not essential for all transcriptional activity [112] and their deposition at loci after transcription to maintain an active transcriptional state has been documented [113]. Our transcriptomic analysis revealed that loss of H3K4me3 resulted in reduced expression of certain genes but not others. For instance, in the *skn-1gf* animals, the loss of H3K4me3 marks suppressed the expression of innate immune targets, but not oxidative stress response genes. The observation that loss of H3K4me3 marks has differential effects on the expression of specific stress response genes could indicate a role for these marks for the recruitment of additional transcriptional regulators beyond SKN-1. Additionally, H3K4me3 can also facilitate transcriptional reinitiation, which can impact total transcriptional output of specific loci [114]. It should be of note that our RNAseq was performed on whole worms, which precludes tissue specific resolution of H3K4me3-sensitive targets. Nevertheless, our study identifies that the maintenance of H3K4me3 epigenetic marks is critical for the regulation of lipid homeostasis and pathogen resistance. Our previous study indicates a relationship between the Asdf phenotype and a reallocation of lipids to the germline to increase reproductive output.

Loss of WDR-5 activity can impact reproduction, but the loss of *wdr-5* exerts effects on progeny output at temperatures higher than those used in this study [115].

In contrast to acute hydrogen peroxide exposure, chronic exposure to a low dose of paraquat (a superoxide-producing agent) suppressed Asdf. Our discovery that paraquat exposure refines the transcriptional focus of activated SKN-1 suggests that transcriptional redirection is a powerful approach to curb the negative pleiotropies of unregulated transcriptional activity. It remains possible that low-dose exposure to paraquat reduces the pathogenicity of the OP50 *E. coli* diet. Exposure to much higher concentrations of paraquat can result in reduced *E. coli* B strain growth; however, treatment with 75 μM only slightly impaired OP50 viability (Fig. 3.7 C and D). Intriguingly, *E. coli* K-12 strains that do not induce Asdf [79] are resistant to the effects of paraquat [116], which supports further examination of dietary effects on SKN-1–dependent pathogen responses. Nevertheless, our results reveal that the induced expression of oxidative stress response genes does not drive the metabolic pleiotropies observed in *skn-1gf* animals. The shared suppression of pathogen response genes suggests the activation of immune responses drives the Asdf phenotype in *skn-1gf* mutants (Table 3.4). Moreover, the similarities in phenotypes between wild-type worms exposed to pathogens and our *skn-1gf* worms support our transcriptional data that it is the expression of innate immunity genes in our mutant worms that is driving its associated pleiotropies. Importantly, our data also reveal that once activated, SKN-1 remains responsive and can be redirected away from pathogen response genes to alleviate negative health outcomes. Determining whether the ability to redirect other

transcription factors, like NRF2, is a generalizable approach to treat diseases with aberrant transcription is an exciting avenue for future investigation.

FIGURES

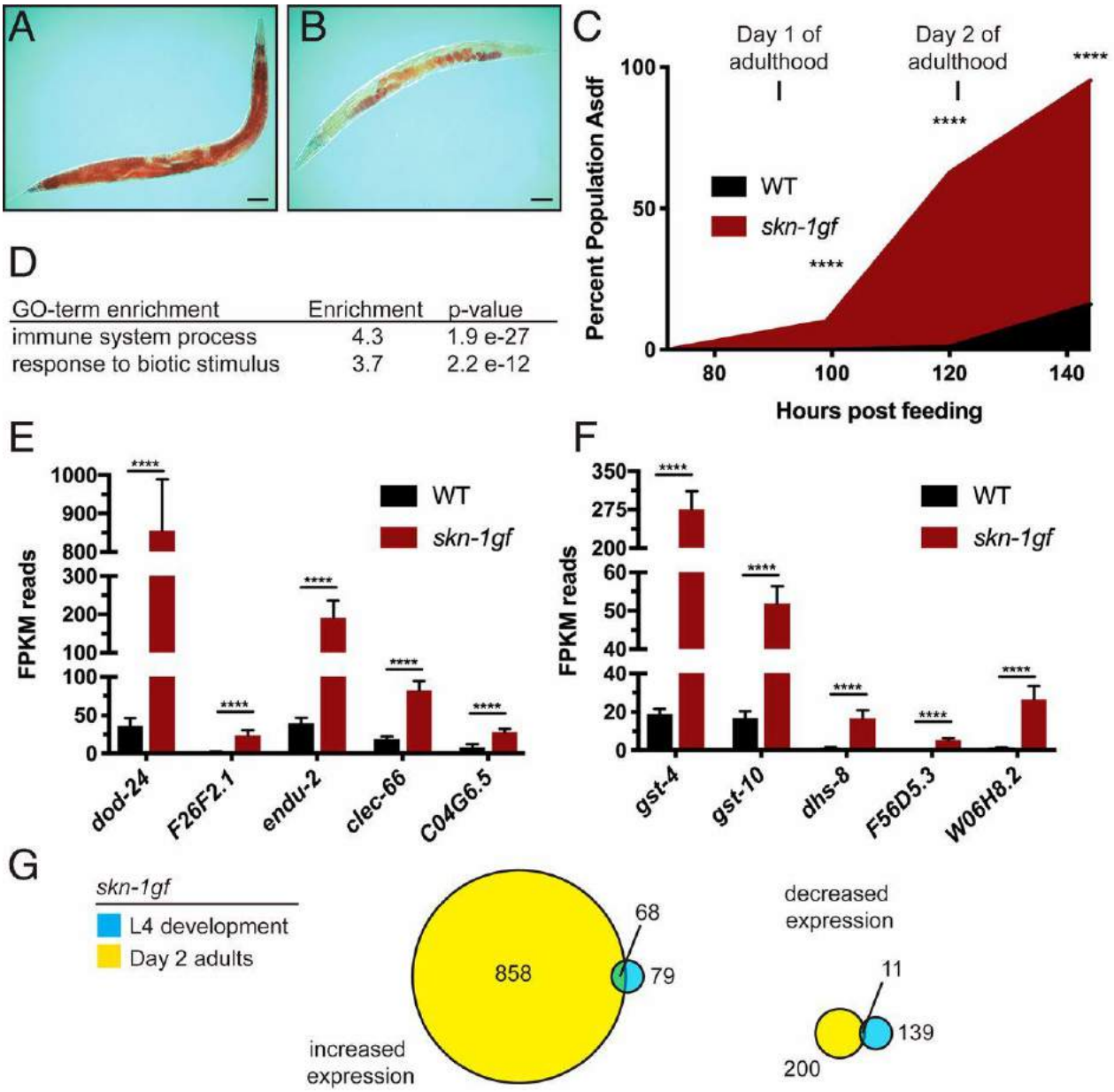

12. Figure 3.1: SKN-1 activation causes redistribution of somatic lipids and activation of immune defense genes.

(A) Normal lipid distribution in wild-type animals (representative image from n = 873) as compared to (B) somatic depletion of fat (Asdf) in animals with activated SKN-1 (representative image from n = 759) that occurs with age (C). (D) GO-term enrichment analysis of differentially expressed genes from RNA-seq of day 2 adult skn-1gf mutant animals as compared to age-matched WT controls. Analysis of the mRNA reads of the indicated genes related to (E) innate immunity and pathogen resistance and (F) oxidative stress and xenobiotic responses; see Table 3.1 for all RNA-seq measurements. (G) Venn diagram of gene expression changes with at least 2-fold change in *skn-1gf(lax188)* mutants during development (L4 stage) and day 2 of adulthood. See also Table 3.11 and 3.44 for all RNA-seq measurements. (Scale bar, 50 μm.) ****P < 0.0001. FPKM, fragments per kilobase of transcript per million mapped reads.

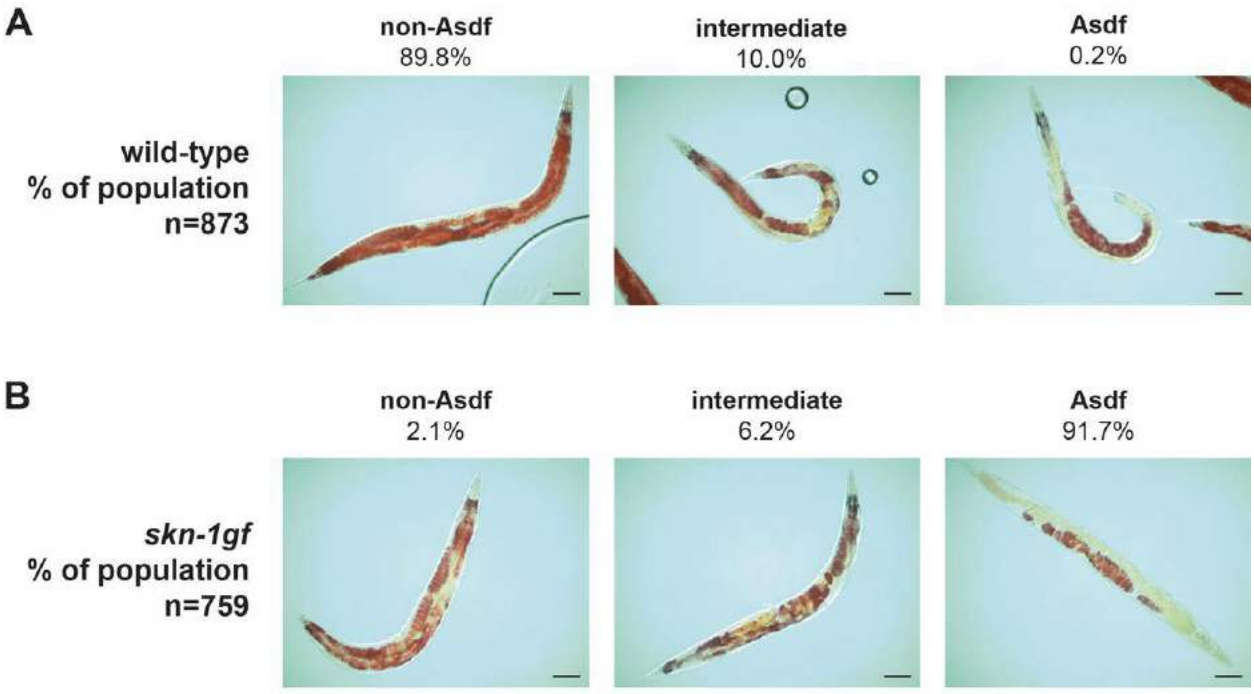

13. Figure 3.2. Categorization of fat levels for wild-type and *skn-1gf* worms.

Representative images of lipid level distribution for ORO stained wild-type (A) and *skn-1gf* (B) worms, along with population of worms scored and proportion of population displaying each phenotype at 120 hours post feeding. At this time point, *skn-1gf* worms display a strong loss of somatic fat phenotype, while a majority of wild-type worms retain fat throughout their body. The criteria for lipid level categorization is described in the methods. All experiments were performed in a minimum of three biological replicates and lipid distribution was assessed in at least 300 animals. Scale bar = 50μm.

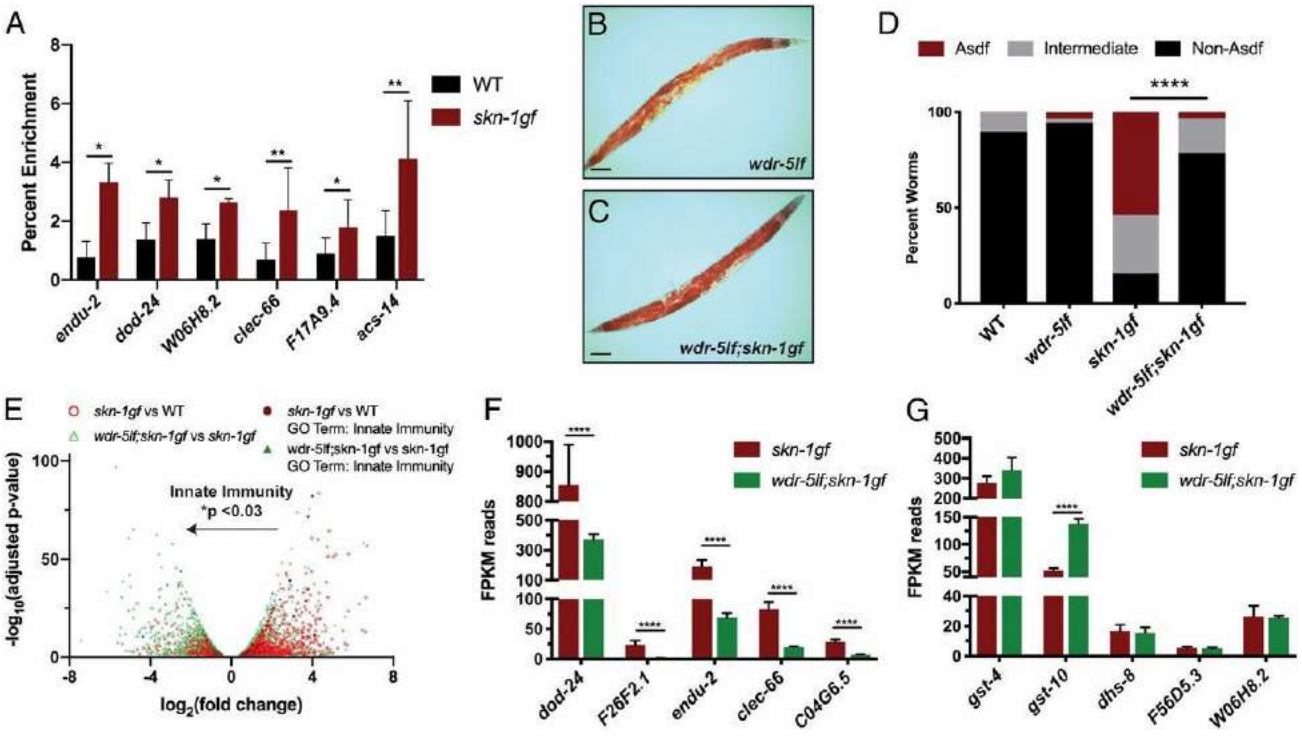

14. Figure 3.3. Loss of Histone H3 trimethylation restricts SKN-1gf transcriptional activity and suppresses the loss of somatic lipids.

(A) ChIP-qPCR reveals SKN-1gf enrichment at the promoter of target genes relative to wild-type SKN-1. (B and C) ORO staining of lipid stores in C. elegans. (B) *wdr-5lf(ok1417)* mutants display normal distribution of lipids across tissues (representative

image from n = 415). (C) The loss of somatic lipid stores observed in SKN-1gf mutant animals is restored in *wdr-5lf(ok1417);skn-1gf(lax188)* double mutants (representative image from n = 892). (D) Quantification of lipid distribution across tissues. All experiments were performed in a minimum of 3 biological replicates and lipid distribution was assessed in at least 300 animals. (See also Fig. 3.5 for all measurements.) (E) Volcano plot of differentially expressed genes in *skn-1gf* compared to WT (red), genes altered by loss of *wdr-5lf* (green), and innate immunity genes (black); changes in immune genes analyzed by unpaired, nonparametric, t test (Mann–Whitney). (F and G) Analysis of the mRNA reads of the indicated genes related to (F) innate immunity and pathogen resistance and (G) oxidative stress and xenobiotic responses. See Table 3.2 and 3.4 for RNA-seq measurements. (Scale bar, 50 μm.) *P < 0.05; **P < 0.01; ****P < 0.0001. FPKM, fragments per kilobase of transcript per million mapped reads.

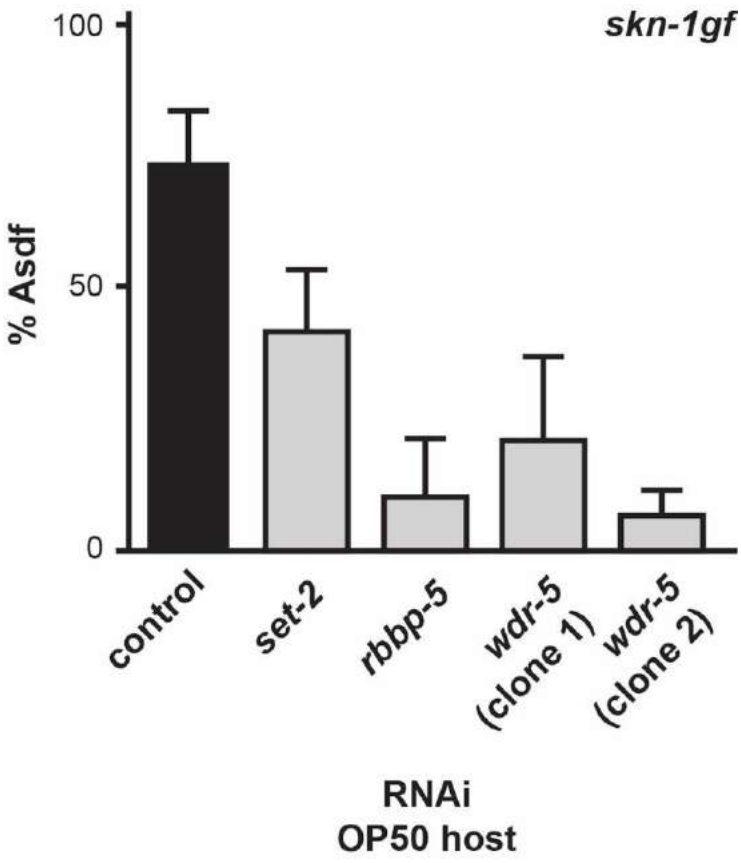

15. Figure 3.4. RNAi screen of chromatin modifiers effect on Asdf levels in *skn-1gf*. RNAi screen of *skn-1gf* worms done using OP50 RNAi clones. Chromatin modifiers associated with H3K4me3 complex, *wdr-5* and *rbbp-5*, suppressed the Asdf phenotype in *skn-1gf* worms. The RNAi screen was performed in biological triplicate and 50 worms were scored for each experiment. Two independent *wdr-5* RNAi clones tested positive. *set-2* RNAi animals were developmentally delayed and asynchronous at time of scoring.

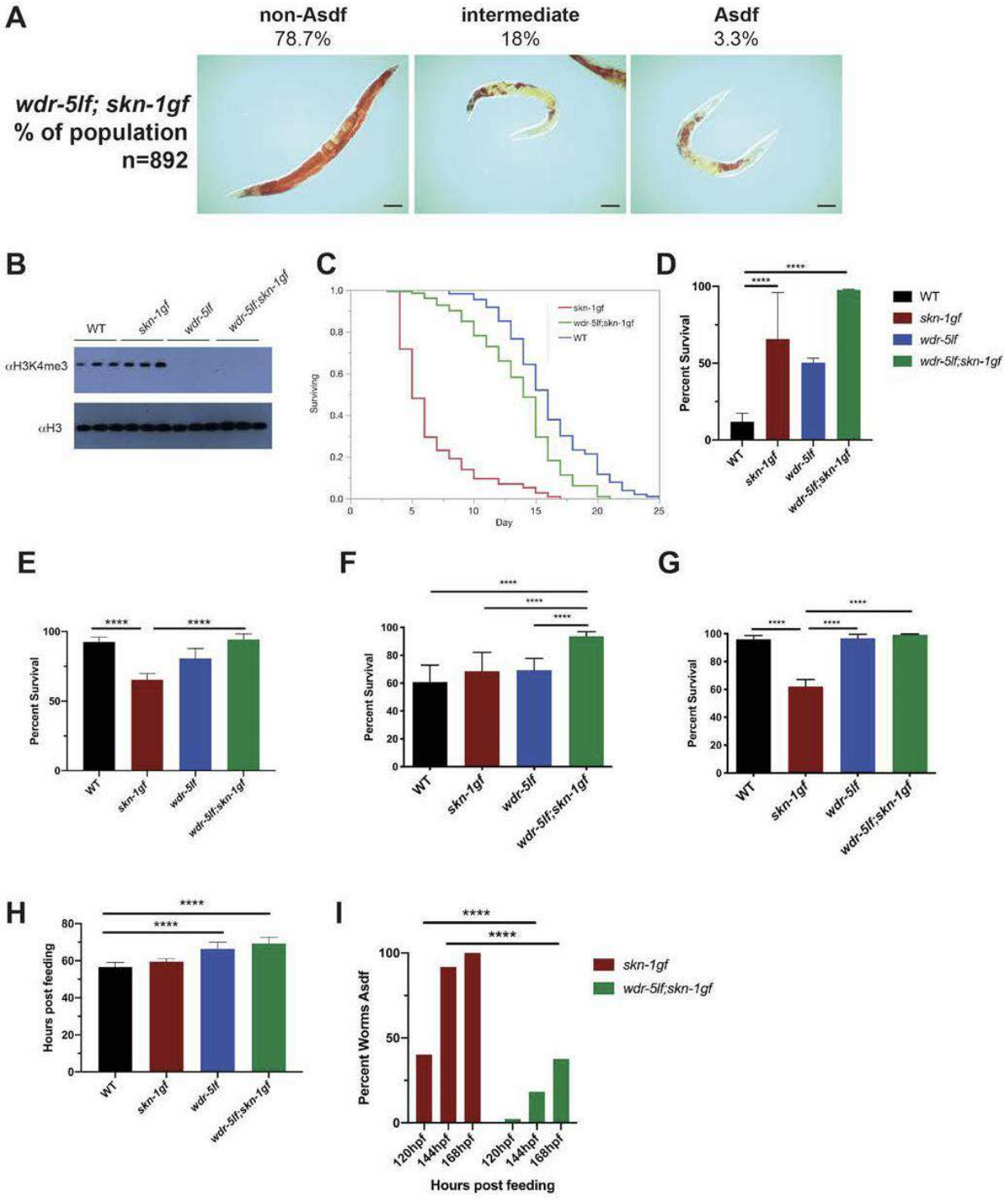

16. Figure 3.5 Loss of *wdr-5* suppresses pleiotropic phenotypes of *skn-1gf* animals

(A) Representative images of lipid level distribution for ORO stained *wdr-5lf;skn-1gf* worms, along with population of worms scored and proportion of population displaying

each phenotype at 120 hours post feeding. Loss of *wdr-5* suppresses fat loss in *skn-1gf* worms. (B) *wdr-5lf* abolishes H3K4me3 chromatin marks. (C) *skn-1gf* worms have a shortened lifespan, which is partially rescued by loss of *wdr-5*. Graph shows the combination of three biological replicates of the lifespan assay with >50 worms in each replicate (after censoring – WT n=127; *skn-1gf* n=241; *wdr-5lf; skn-1gf* n=304). (D-E) *skn-1gf* mutants are resistant to oxidative stress early in adulthood (80hpf) (D) that is lost later in life (120hpf) (E). This increased sensitivity is abolished in the absence of WDR-5. (F-G) Worms at 48 hours post feeding display similar survival levels following cold stress assay except for *wdr-5lf;skn-1gf*, which has an increased survival percentage, possibly due to the slower growth rate of the double mutant and reflecting the younger developmental stage of the animal at the time of the assay (F). (G) At 144 hours post feeding, *skn-1gf* worms display a decreased survival to cold stress, which may be due to the loss of fat phenotype seen during this age. This decreased survival is suppressed by the *wdr-5lf(ok1417)* mutation. (H) *wdr-5lf(ok1417)* animals reach egg laying adulthood at a slower rate (less than 24 hours) than wild type animals. (I) *wdr-5lf;skn-1gf* display suppressed levels of Asdf. ****P<0.0001 Fisher's exact two-tailed test used to compare stress survival percentage and log-rank test for lifespan analysis. All experiments were performed in a minimum of three biological replicates and lipid distribution was assessed in at least 300 animals. Scale bar = 50μm.

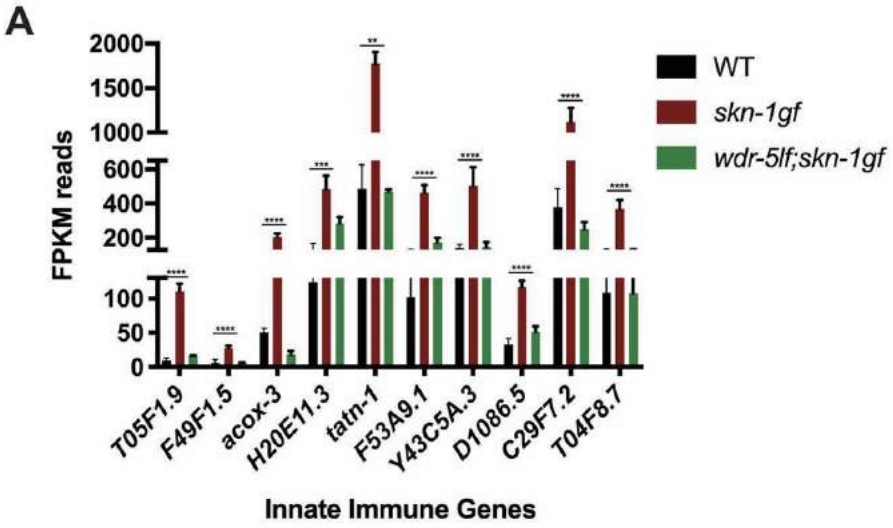
A
FPKM reads
2000
1500
1000
600
400
200
100
50
0
WT
skn-1gf
wdr-5lf;skn-1gf
T05F1.9
F49F1.5
acox-3
H20E11.3
tatn-1
F53A9.1
Y43C5A.3
D1086.5
C29F7.2
T04F8.7
Innate Immune Genes

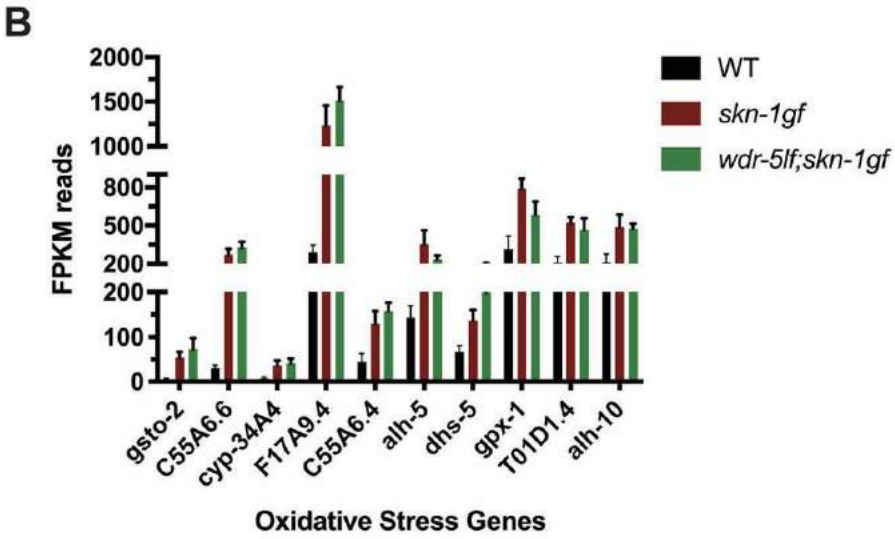
B
FPKM reads
2000
1500
1000
800
500
200
200
100
0
WT
skn-1gf
wdr-5lf;skn-1gf
gsto-2
C55A6.6
cyp-34A4
F17A9.4
C55A6.4
alh-5
dhs-5
gpx-1
T01D1.4
alh-10
Oxidative Stress Genes

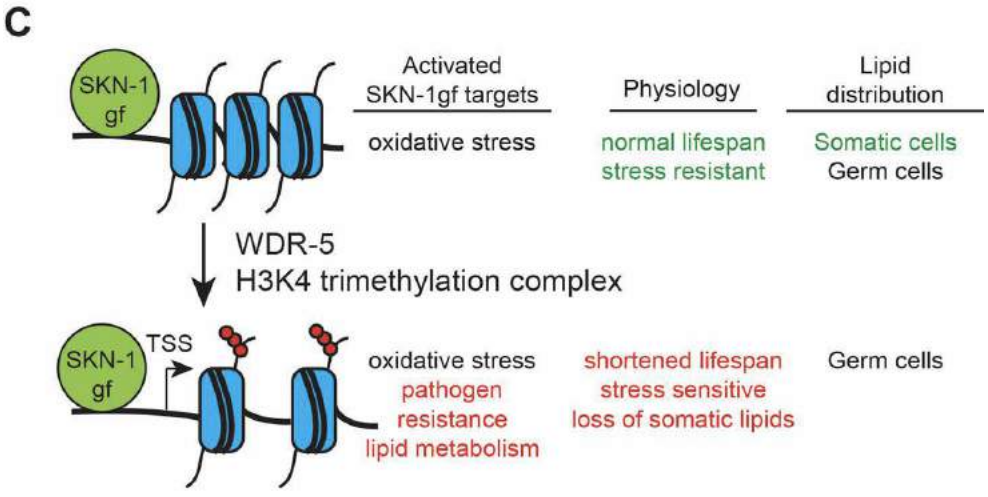
C
SKN-1
gf
Activated
SKN-1gf targets
oxidative stress
Physiology
normal lifespan
stress resistant
Lipid
distribution
Somatic cells
Germ cells
WDR-5
H3K4 trimethylation complex
SKN-1
gf
TSS
oxidative stress
pathogen
resistance
lipid metabolism
shortened lifespan
stress sensitive
loss of somatic lipids
Germ cells

17. Figure 3.6. Comparison of transcript levels in *wdr-5lf;skn-1gf* relative to *skn-1gf* animals at 120 hours post feeding using RNA-seq

(A-B) RNA-seq analysis of *wdr-5lf;skn-1gf* worms reveals genes associated with innate immune responses (A) are downregulated in *wdr-5lf;skn-1gf* worms when compared to *skn-1gf* worms, but oxidative stress genes (B) remain at the same. This suggests that the pleiotropic consequences suppressed in the *wdr-5lf;skn-1gf* double mutant may be due to the suppression of innate immune response genes. (C) Model of the impact of loss of Histone H3 trimethylation evokes on the transcriptional activity of SKN-1 and physiological responses. **P<0.01, ***P<0.001. ****P<0.0001

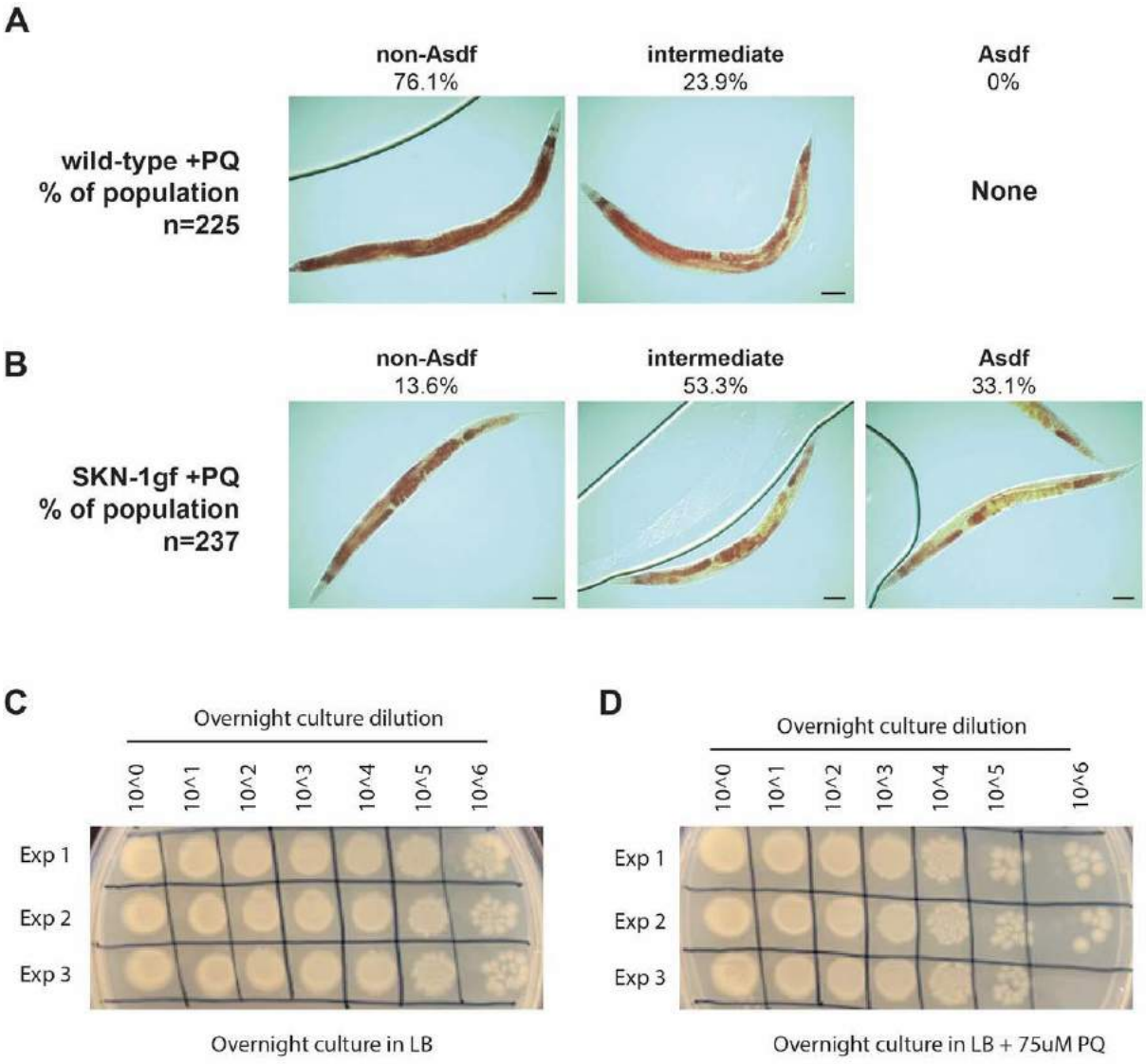

18. Figure 3.7. Representative images of fat level categorization 134 for WT and *skn-1gf* worms treated with paraquat

Representative images of lipid level distribution for ORO stained (A) wild-type and (B) *skn-1gf* worms treated with 75 µM paraquat (PQ), along with the population of worms scored and proportion of population displaying each phenotype at 120 hours post feeding. Exposure to 75 µM of PQ results in a relatively unchanged lipid level distribution in wild-type worms, while *skn-1gf* worms show a suppression of the Asdf

phenotype and an overall increase in lipid levels compared to untreated *skn-1gf* worms. (C-D) PQ treatment does not abolish OP50 bacteria growth. OP50 was inoculated in either LB (C) or LB + 75uM PQ (D) and grown overnight with shaking. Cultures were then diluted and 5µl plated on LB and allowed to grow to assess culture viability by colony count. All experiments were performed in a minimum of three biological replicates and lipid distribution was assessed in at least 200 animals. Scale bar = 50µm.

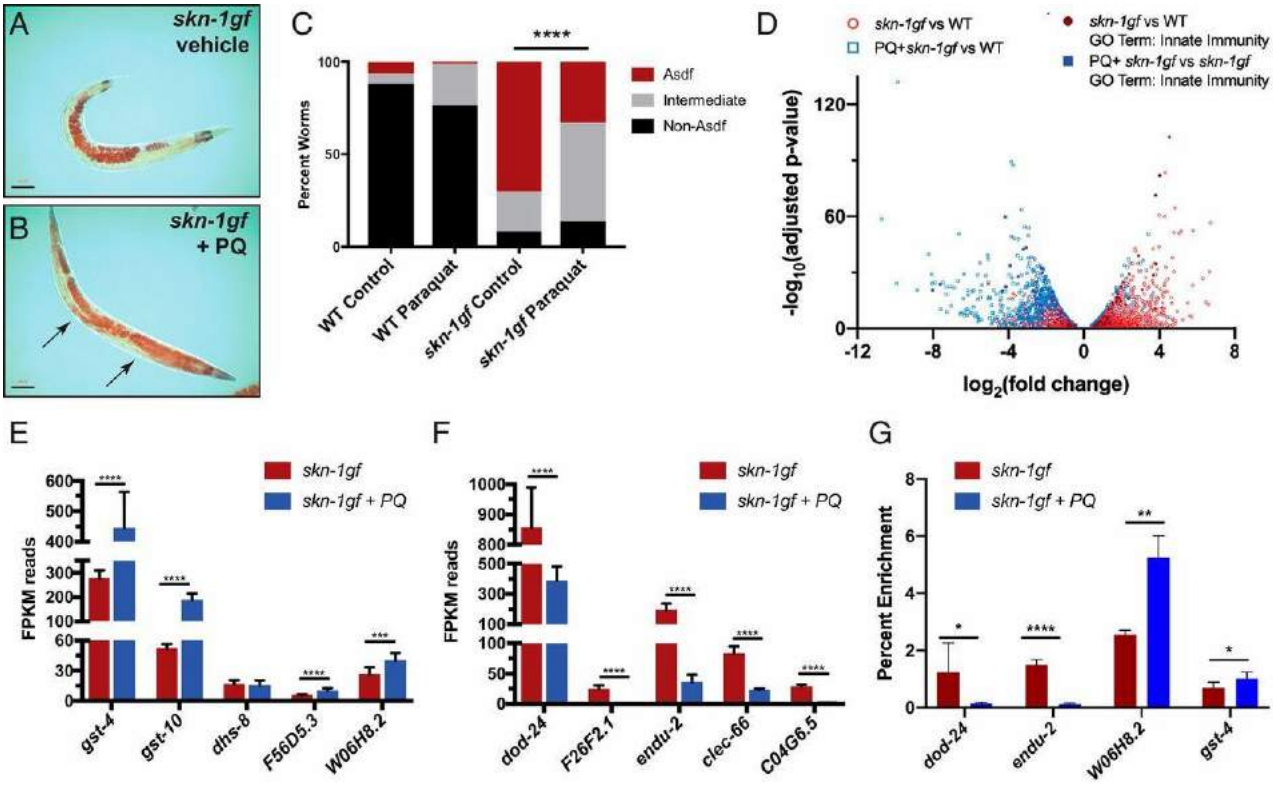

19. Figure 3.8 Oxidative stress redirects SKN-1gf transcriptional activity while restoring somatic lipid distribution.

(A–C) The absence of somatic lipids in SKN-1gf mutants treated with vehicle (control) (A) is restored in animals exposed to 75 µM PQ (B) (representative image from n = 237); arrows indicate somatic lipids. (C) Quantification of lipid distribution across tissues. All experiments were performed in a minimum of biological triplicates and lipid

distribution was assessed in at least 300 animals. (See also Fig. 3.7 and Table 3.3 for all measurements.) (D) Volcano plot of differentially expressed genes in *skn-1gf* compared to WT (red), genes altered by PQ exposure (blue), and innate immunity genes (black); changes in immune genes analyzed by unpaired, nonparametric, t test (Mann– Whitney). (E and F) Analysis of the mRNA reads of the indicated genes related to (E) oxidative stress and xenobiotic responses and (F) innate immunity and pathogen resistance. See also Tables 3.3 and 3.4 for RNA-seq measurements. (G) ChIP-qPCR reveals PQ treatment redirection of SKN-1gf activity is associated with a loss of recruitment at innate immunity gene promoters. (Scale bar, 50 μm.) *P < 0.05; **P < 0.01; ***P < 0.001; ****P < 0.0001. FPKM, fragments per kilobase of transcript per million mapped reads.

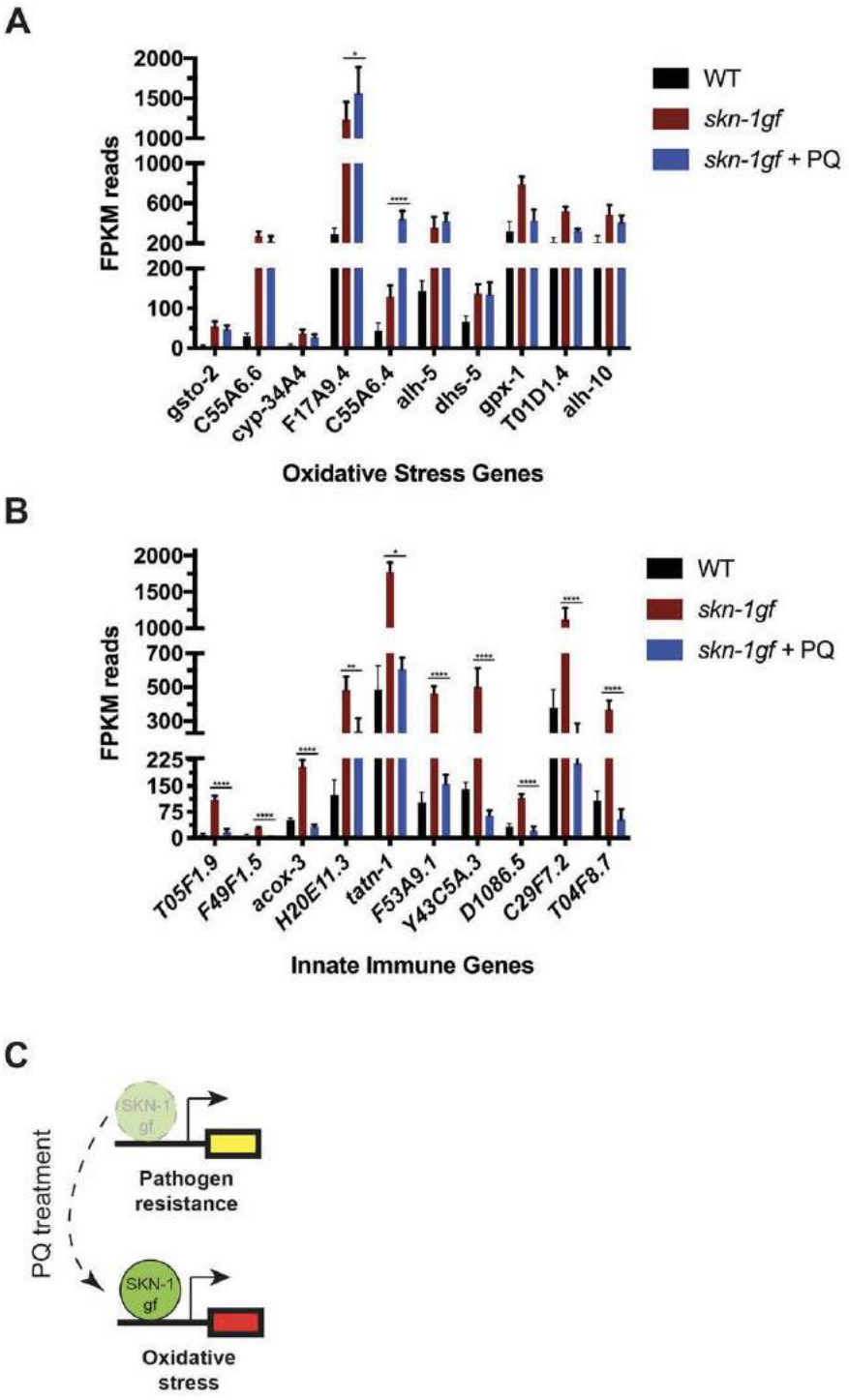

20. Figure 3.9. Comparison of transcript levels in *skn-1gf* worms that were untreated or treated with paraquat at 120 hours post feeding.

RNA-seq analysis of *skn-1gf* worms treated with paraquat (PQ) reveals that oxidative stress genes (A) remain unchanged or increased when compared to untreated *skn-1gf*

worms. Read counts for genes associated with the innate immune response (B) are significantly lower in PQ treated skn-1gf worms compared to untreated *skn-1gf* worms. This trend in gene expression remains consistent with *wdr-5lf;skn-1gf*, another suppressor of the Asdf phenotype in *skn-1gf* worms. (C) Depiction of overall change in transcriptional focus of SKN-1gf activity in response to oxidative stress. *P<0.05, **P<0.01, ****P<0.0001.

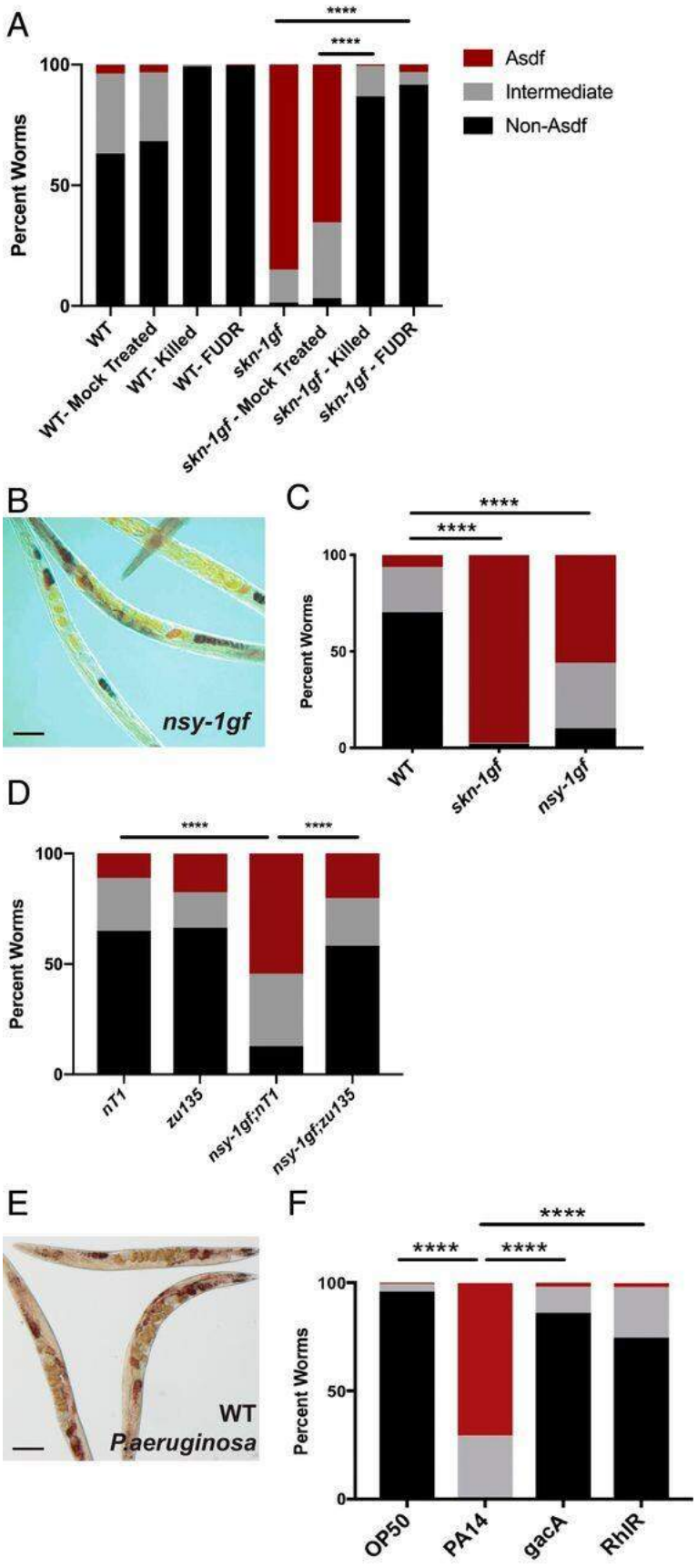
A
****
****
Asdf
Intermediate
Non-Asdf
Percent Worms
100
50
0
WT
WT- Mock Treated
WT- Killed
WT- FUDR
skn-1gf
skn-1gf - Mock Treated
skn-1gf - Killed
skn-1gf - FUDR
B
nsy-1gf
C
****
****
Percent Worms
100
50
0
WT
skn-1gf
nsy-1gf
D
****
****
Percent Worms
100
50
0
nT1
zu135
nsy-1gf;nT1
nsy-1gf;zu135
E
WT
P.aeruginosa
F
****
****
****
Percent Worms
100
50
0
OP50
PA14
gacA
RhlR

21. Figure 3.10. Exposure to pathogens drives a rapid and SKN-1–dependent loss of somatic lipids.

(A) Somatic lipid depletion requires live bacteria. (A) Bactericidal treatment of OP50 bacteria with UV+antibiotics (“killed”) or FUdR reduces Asdf in *skn-1gf* animals relative to mock-treated bacteria. (B and C) Constitutive activation of the p38 MAPK pathway in *nsy-1gf(ums8)* mutant animals displays age-dependent somatic depletion of fat (Asdf) at 144 h postfeeding; representative image (B) and quantification of population (C). (D) Lipid reallocation in *nsy-1gf(ums8)* mutant animals requires *skn-1*. (E and F) Exposure of 72-h postfed animals to *P. aeruginosa* results in the rapid loss of somatic lipid stores; representative image (E) and quantification of population (F). All experiments were performed in a minimum of biological triplicate and lipid distribution was assessed in at least 200 animals. (Scale bar, 50 μm.) ****P < 0.0001.

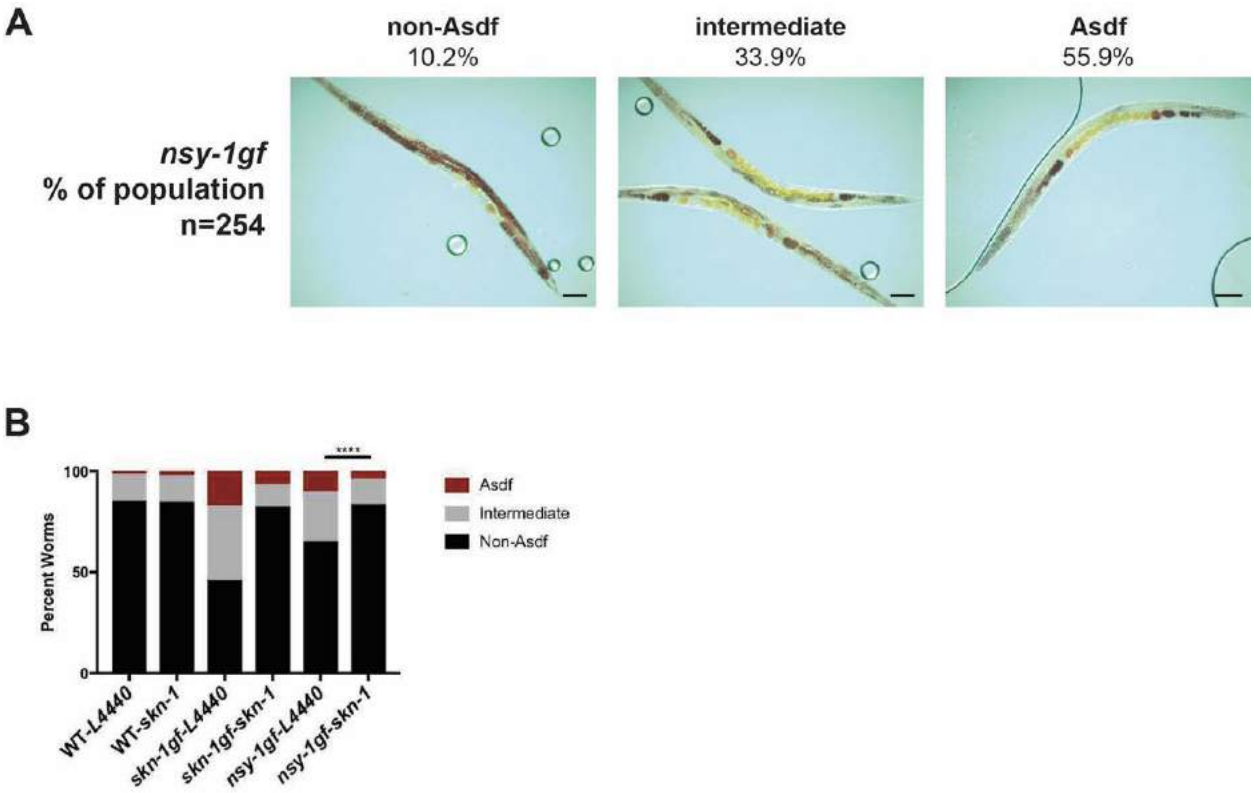

22. Figure 3.11. *nsy-1gf* worms display a similar age-dependent fat loss as *skn-1gf* worms

(A) Representative images of lipid level distribution for ORO stained *nsy-1gf* worms, along with the population of worms scored and the proportion of the population displaying each phenotype at 144 hours post feeding. Constitutive activation of *nsy-1*, a MAP3K involved in the innate immune pathway, causes worms to undergo a similar age-dependent depletion of lipids in somatic tissues at 144 hours post feeding. (B) This loss of fat at 144hpf is *skn-1* dependent as RNAi of *nsy-1gf* worms for *skn-1* seems to result in more non-Asdf worms when compared to L4440 RNAi. All experiments were performed in a minimum of three biological replicates and lipid distribution was assessed in at least 250 animals. ****P<0.0001 Fisher's exact two-tailed test used to compare survival percentage. Scale bar = 50μm.

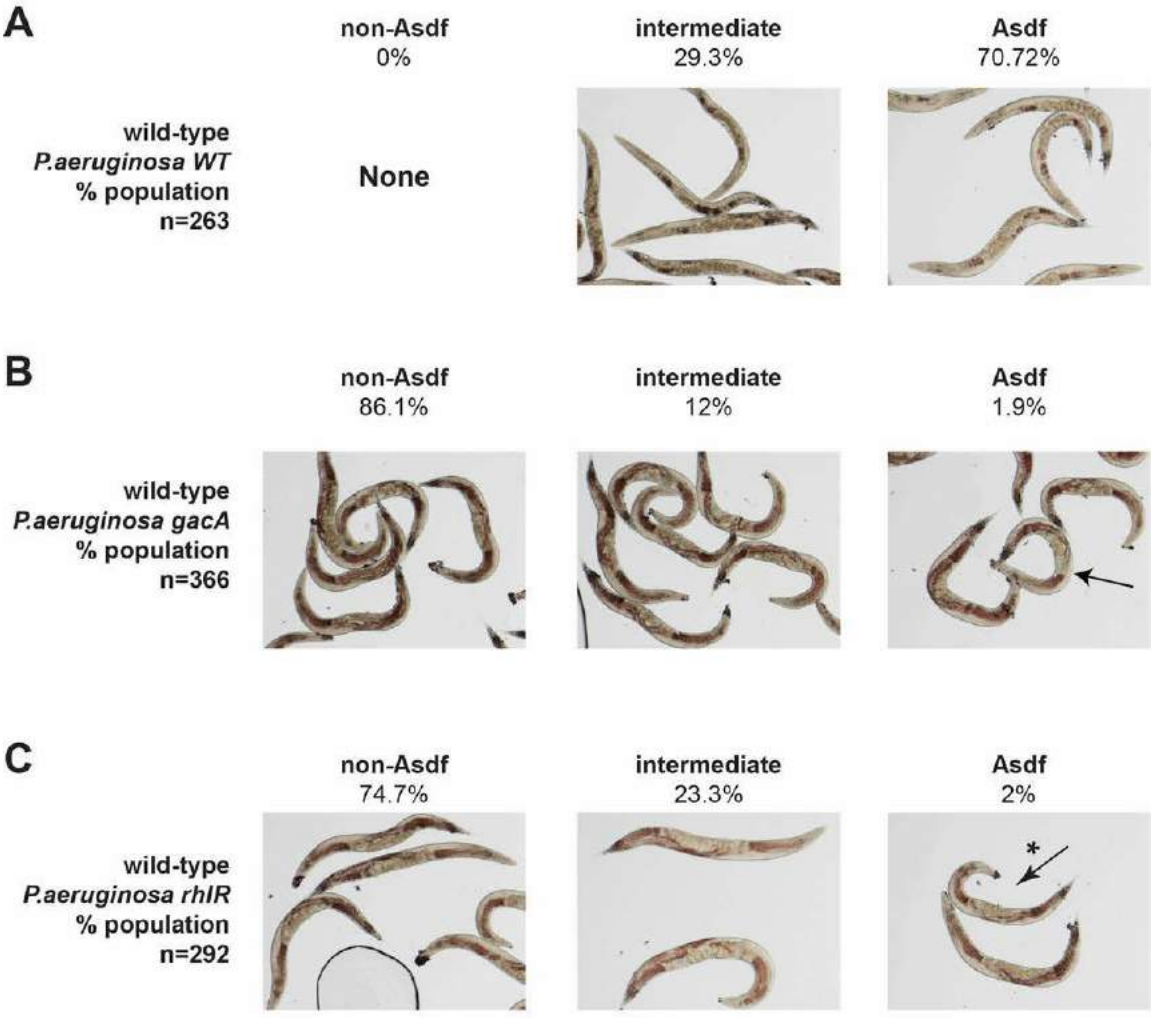
A
non-Asdf
0%
intermediate
29.3%
Asdf
70.72%
wild-type
P.aeruginosa WT
% population
n=263
None
B
non-Asdf
86.1%
intermediate
12%
Asdf
1.9%
wild-type
P.aeruginosa gacA
% population
n=366
C
non-Asdf
74.7%
intermediate
23.3%
Asdf
2%
wild-type
P.aeruginosa rhlR
% population
n=292
*

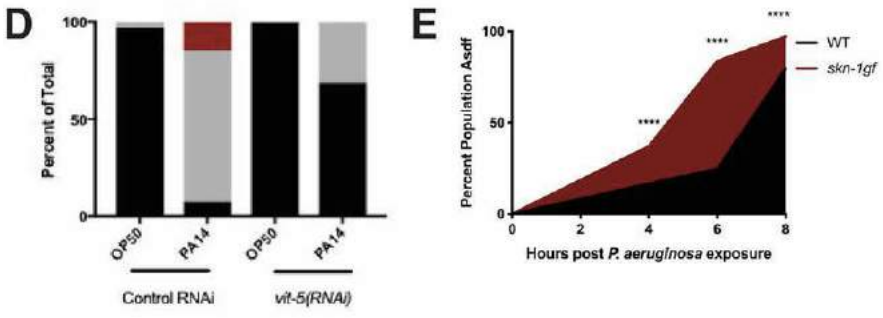
D
Percent of Total
100
50
0
OP50
PA14
OP50
PA14
Control RNAi
vit-5(RNAi)
E
Percent Population Asdf
100
50
0
0
2
4
6
8
Hours post P. aeruginosa exposure
****
****
****
WT
skn-1gf

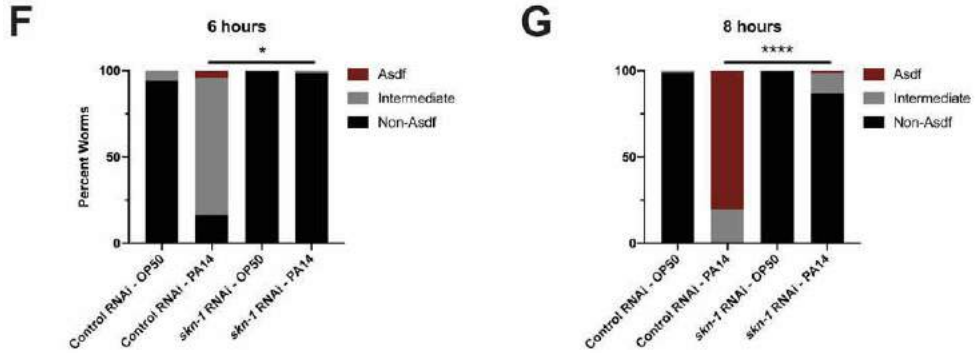
F
6 hours
*
Percent Worms
100
50
0
Asdf
Intermediate
Non-Asdf
Control RNAi - OP50
Control RNAi - PA14
skn-1 RNAi - OP50
skn-1 RNAi - PA14
G
8 hours
****
100
50
0
Asdf
Intermediate
Non-Asdf
Control RNAi - OP50
Control RNAi - PA14
skn-1 RNAi - OP50
skn-1 RNAi - PA14

23. Figure 3.12. Exposure to the pathogen *Pseudomonas aeruginosa* results in SKN-1 dependent fat loss and is attenuated by non-virulent strains.

Representative images of the lipid level distribution for wild-type worms exposed for 4 hours to *P. aeruginosa* (A) and 2 other non-virulent mutants *gacA* (B), or *rhlR* (C). Worms were stained with ORO 72 hours post feeding. The population of worms scored and the percentage displaying each phenotype are provided. Wild-type worms exposed to pathogens exhibited a similar fat loss phenotype to that seen in *skn-1gf* and *nsy-1gf* worms. This phenotype is not observed in wildtype worms exposed to non-virulent mutant pathogens. (D-E) The loss of somatic lipids in response to *P. aeruginosa* exposure is attenuated in *vit-5* RNAi treated animals (D) and enhanced in SKN-1gf mutants (E). (F-G) RNAi of *skn-1* delays somatic fat loss in response to pathogen. At least two biological replicates were performed and a minimum of 100 animals were analyzed in each replicate. *P<0.05, ****P<0.0001 Fisher's exact two-tailed test used to compare non-Asdf to Asdf worms

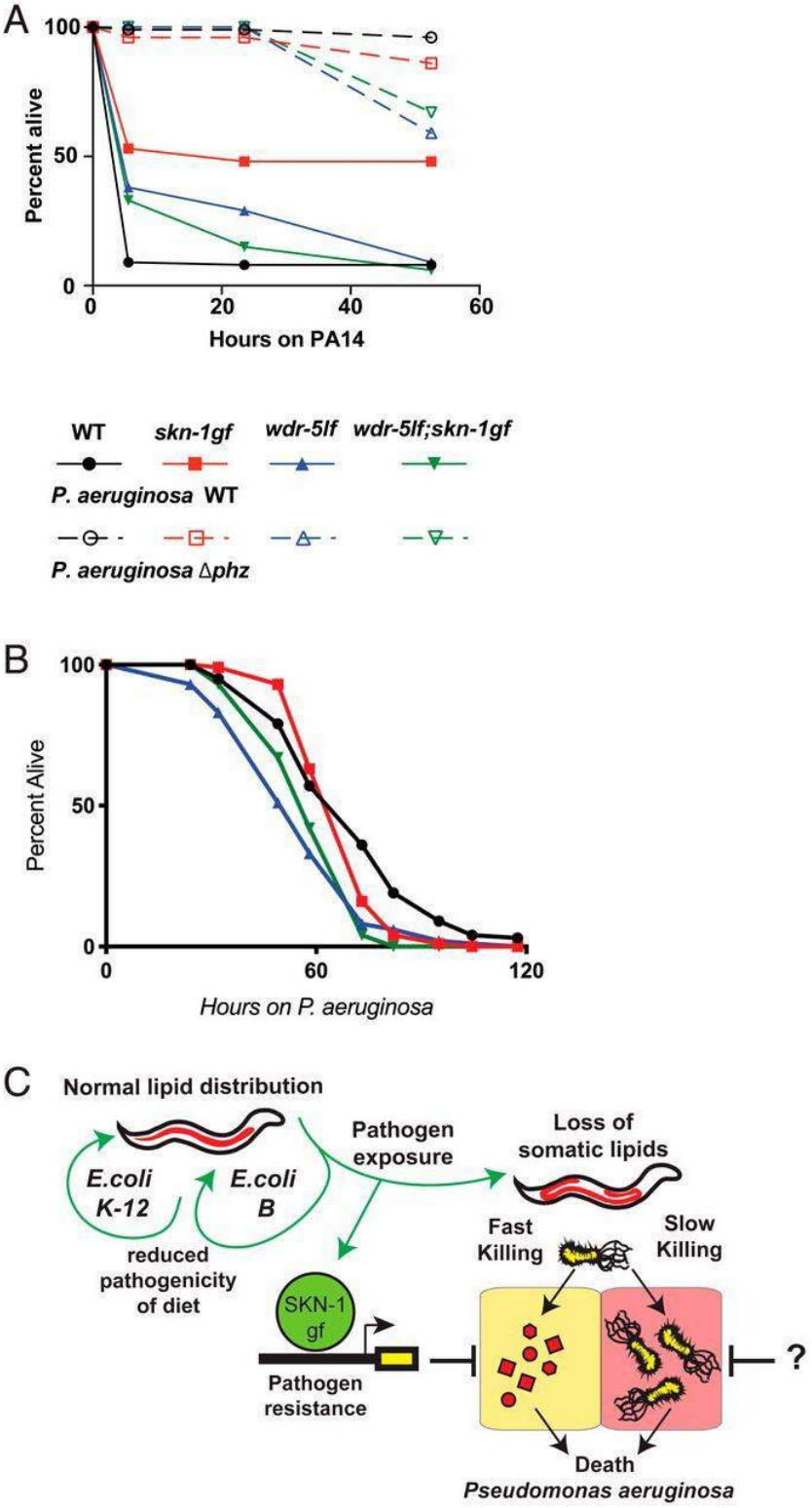

24. Figure 3.13. Redirection of SKN-1gf negates pathogen resistance.

(A–B) Pathogen sensitivity assays. Wild-type (black), *skn-1gf(lax188)* mutants (red), *wdr5lf(ok1417)* mutants (blue), or *wdr-5lf(ok1417);skn-1gf(lax188)* double mutants (green) were exposed to *P. aeruginosa* (A) “fast-kill” or (B) “slow kill” pathogen stress plates. Activated SKN-1 supports resistance to pathogenic *P. aeruginosa* specifically on fast-kill plates, which is abolished in the absence of H3K4me3. (C) Model for the impact of SKN-1gf on physiological responses to *P. aeruginosa* secreted factors “fast killing.” “?”, the role of SKN-1gf on colonization “slow killing” is unclear and requires further study. All experiments were performed in a minimum of biological triplicate.

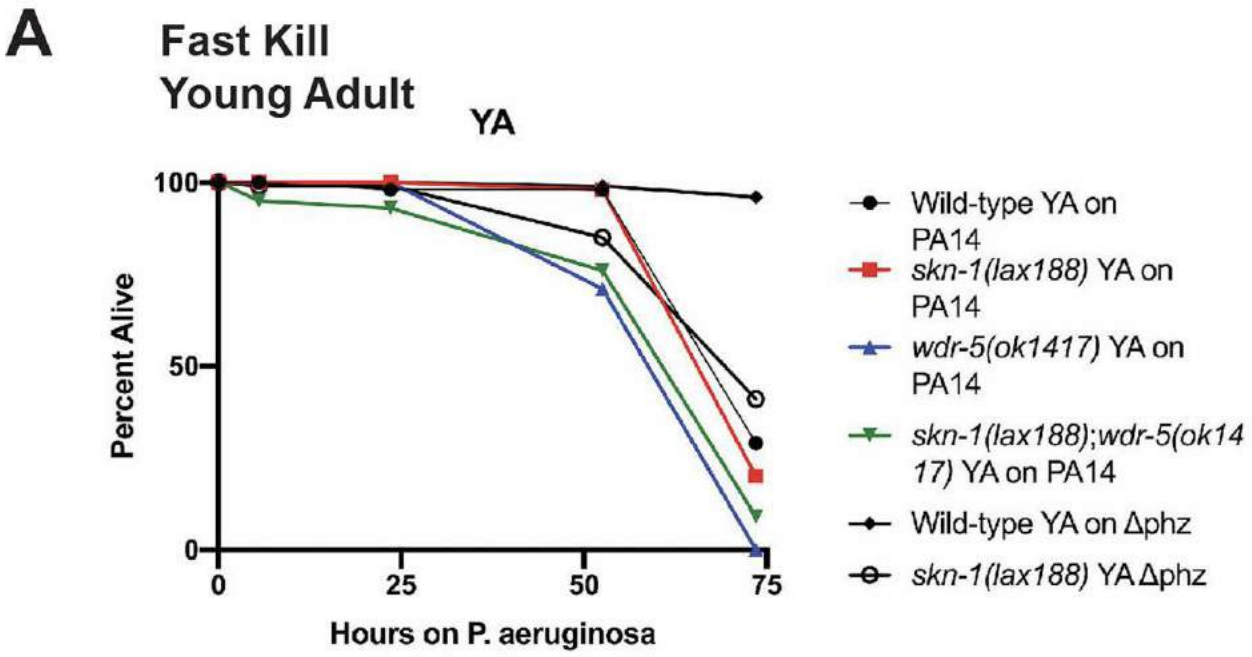

25. Figure 3.14. Adult animals are resistant to *P. aeruginosa* fast-killing.

Wild 182 type (black), *skn-1gf(lax188)* mutants (red), *wdr-5lf(ok1417)* mutants (blue), or *wdr-5lf(ok1417);skn-1gf(lax188)* double mutants (green) were exposed to *Pseudomonas aeruginosa* “fast-kill” as young adults (YA). As previously described, post-developmental animals are less sensitive to *P. aeruginosa* fast-kill exposure as compared to larval stage 4 (L4) animals.

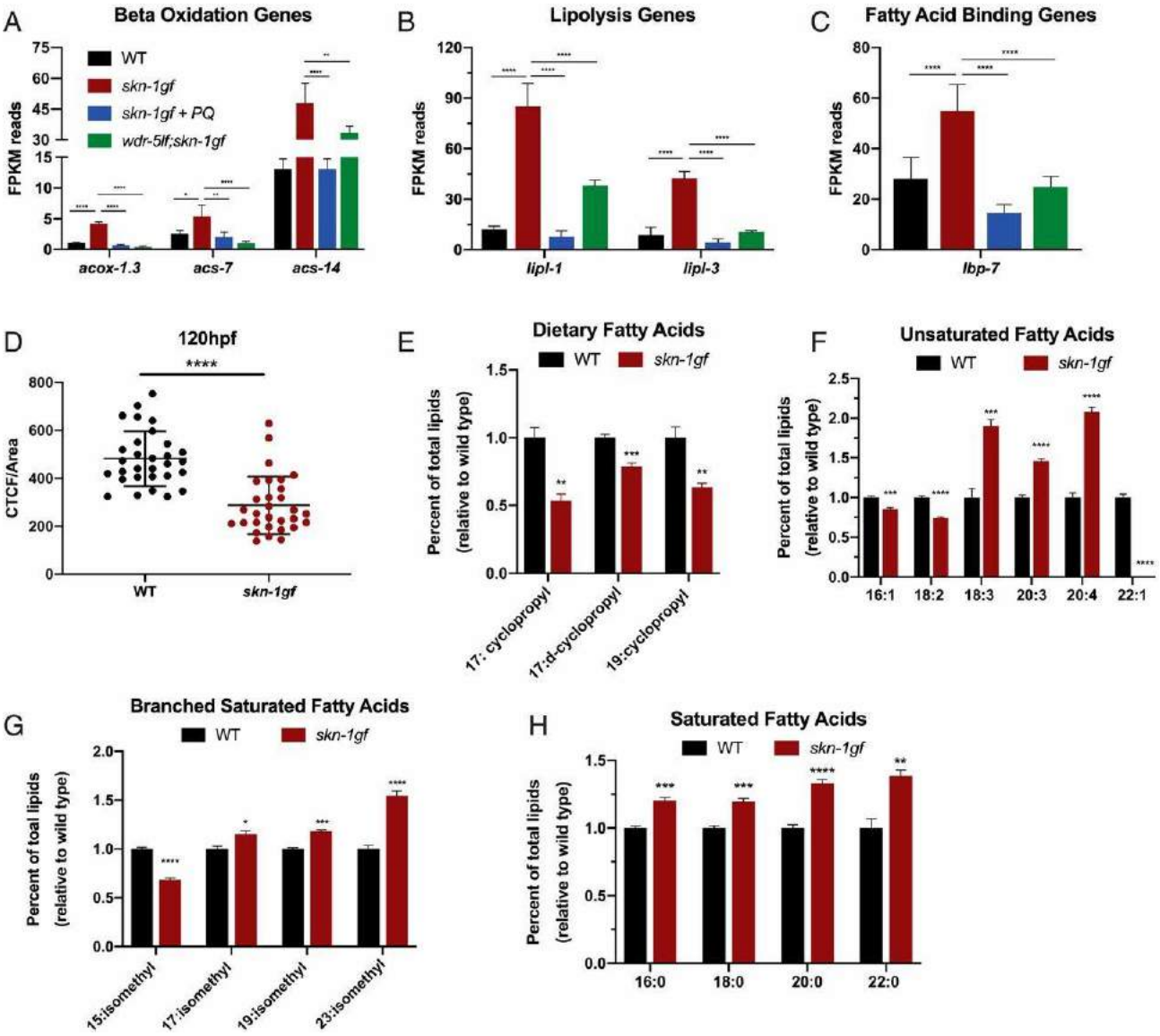

26. Figure 3.15. SKN-1 activation drives lipid utilization during Asdf.

(A–C) Analysis of the mRNA reads of the indicated genes related to lipid utilization: (A) lipid beta-oxidation and (B) lipolysis; and (C) lipid binding, which collectively reveal a scenario where activated SKN-1 drives lipid utilization while suppressing de novo synthesis (see also Fig. 3.16). (D) Fixed Nile Red staining reveals *skn-1gf(lax188)* mutants have a ~60% reduction in total fat (n = 30). (E–H) GCMS analysis of total fatty acids in the triglyceride fraction of wild-type (black) and *skn-1gf(lax188)* mutant (red)

animals fed an OP50 diet at day 2 of adulthood when Asdf is most prominent, 2-tailed t test. See also Tables 3.1–3.4 for all RNA-seq measurements. *P < 0.05; **P < 0.01; ***P < 0.001; ****P < 0.0001. FPKM, fragments per kilobase of transcript per million mapped reads.

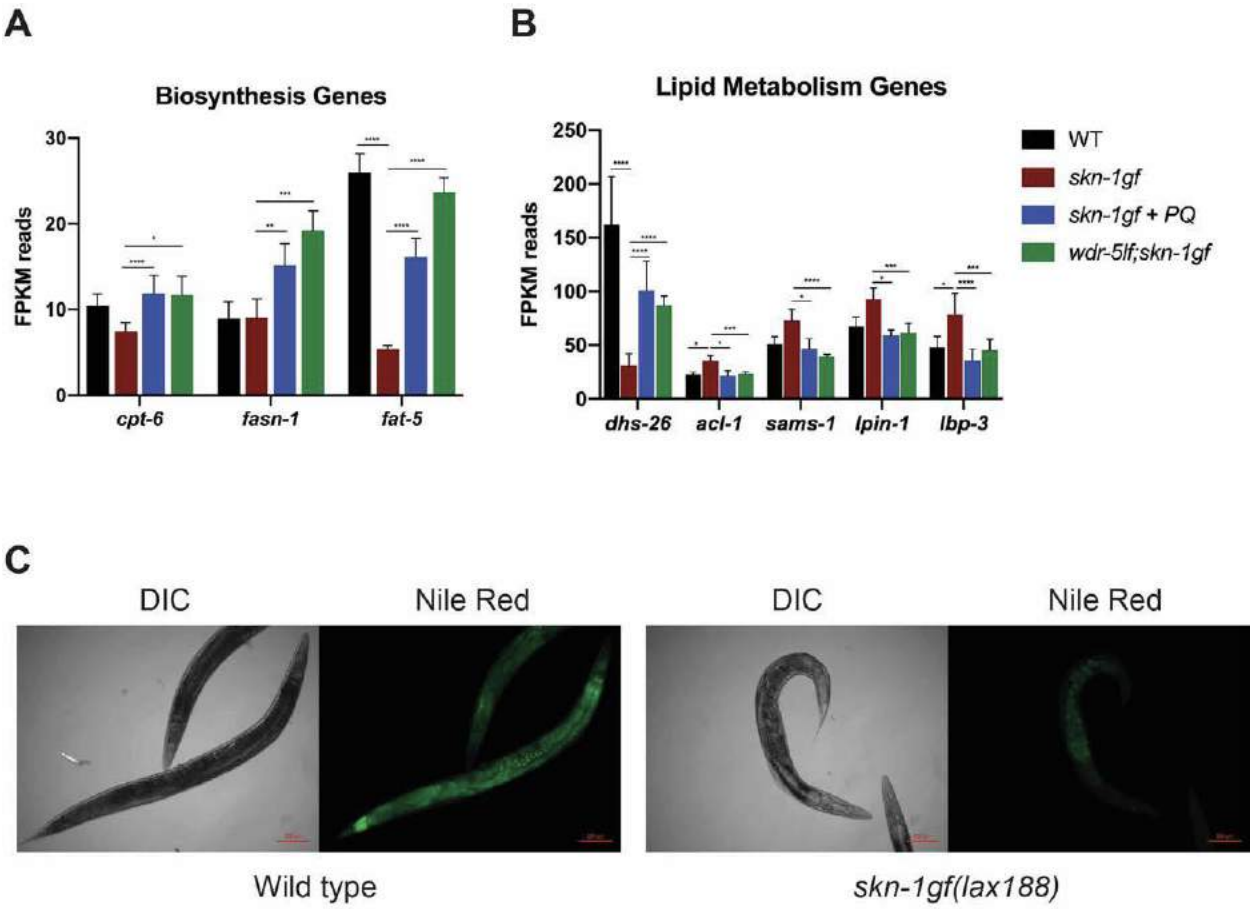

27. Figure 3.16 Metabolic phenotypes of SKN-1gf activity and subsequent redirection.

(A-B) Analysis of the mRNA reads of the indicated genes related to metabolism. (C) Representative images of Nile Red (NR) stained wildtype and *skn-1gf(lax188)* mutants reveals a 60% reduction in total lipids at day 2 of adulthood. See also Tables 3.1 thru 3.4 for all RNA-seq measurements. *P < 0.05; ***P < 0.001; ****P < 0.0001 by two-tailed t-test. Scale bar = 50μm.

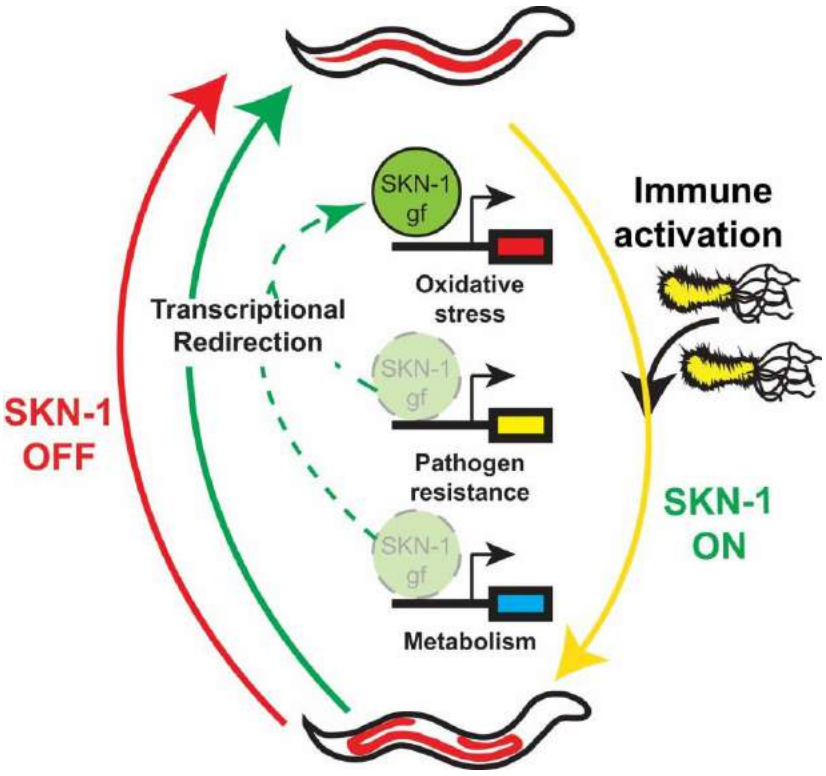

28. Figure 3.17. Transcriptional redirection of SKN-1 activity mitigates pleiotropic outcomes.

In the presence of pathogens, SKN-1 is activated (yellow arrow) and induces the expression of several classes of target genes (e.g., oxidative stress and pathogen resistance). The induction of pathogen resistance genes drives the depletion of somatic lipids with age that leads to poor health outcomes. Transcriptional redirection (green arrows) does not completely turn off all SKN-1 activity (red arrow), but rather focuses the gene targets that are activated. Redirection of activated SKN-1 away from pathogen resistance genes and toward oxidative stress genes abates the loss of metabolic homeostasis.

TABLES

See List of Online Files

MATERIALS AND METHODS

***C. elegans* and Bacterial Strains Used and Culturing Methods.** Worms were grown following standard culture protocols at 20 °C, unless otherwise noted. The following strains were used: WT, N2 Bristol strain; SPC227*, skn-1(lax188);* RB1304, *wdr-5lf(ok1417);* SPC415, *wdr-5lf(ok1417);skn-1gf(lax188);* RPW43, *nsy-1(ums8);* LG340, *skn-1(zu135);* and SPC425, *nsy-1gf(ums8);skn-1(zu135)*.

Oil Red O Staining. Oil Red O (ORO) staining of lipids was performed as previously described [79, 107, 117, 118]. In brief, synchronized worms were collected using 1 mL of 1× PBS + 0.01% Triton X-100 (PBST) into a microcentrifuge tube and allowed to gravity settle. Supernatant was aspirated and washed 3 additional times with 1 mL PBST. After the final wash, supernatant was removed until 100 µL was left and then 600 µL of 60% isopropanol was added, and samples were rocked for 3 min at room temperature. Samples were spun down at 25 × g and supernatant was removed until 100 µL was left. Worms were then stained for 2 h with 600 µL of ORO working solution (0.5 g of ORO in 100 mL of 100% isopropanol) while rotating at room temperature and destained in 600 µL of PBST for 30 min. All staining was done on synchronous populations of day 2 adult animals (120 h postfeeding starting from a synchronous L1 population), unless otherwise stated.

Asdf Quantification. ORO-stained worms were placed on glass slides and a coverslip was placed over the sample. Worms were scored, and images were taken using a Zeiss

microscope at 10× magnification. Fat levels of worms were placed into 3 categories: non-Asdf, intermediate, and Asdf. Non-Asdf worms display no loss of fat and are stained a dark red throughout most of the body (somatic and germ cells). Intermediate worms display significant fat loss from the somatic tissues, with portions of the intestine being clear, but ORO-stained fat deposits are still visible (somatic < germ cells). Asdf worms have had most, if not all, observable somatic fat deposits depleted (germ cells only).

Hydrogen Peroxide Stress Survival Assay. Acute exposure to H2O2 was performed as previously described [79, 119]. In brief, age-synchronized worms were exposed to 10 mM H2O2 in M9T at room temperature while rotating for 20 min. Samples were washed in 1 mL of M9T 3 times and then dropped directly on the OP50 bacterial lawn on a nematode growth media (NGM) plate. Scoring of dead or alive worms was done 24 h post H2O2 exposure. Worms were considered dead either when they were unresponsive to gentle prodding from a platinum-tipped wire or when they showed signs of internal larval hatching.

Pathogen Exposure Experiment. An overnight culture of *P. aeruginosa* strain PA14 (WT), PA14ΔgacA, or PA14ΔrhlR mutant was seeded on 6 cm “slow-killing” media plates, prepared as previously described [67]. Synchronized L1 stage *C. elegans* of the indicated genotypes were grown to day 0 adult stage then transferred to seeded plates and incubated at 20 °C for indicated time points. Plates were incubated at 20 °C to slow the kinetics of the *P. aeruginosa*-induced Asdf phenotype. Worms were then collected

and stained for fat and scored for fat levels as previously described [67, 120]. *P. aeruginosa* “fast kill” pathogenesis assays were conducted as previously described [102, 103]. Late L4 animals obtained from timed egg lays were used.

Additional *C. elegans* and bacterial strains used and culturing methods.

For experiments involving reproductive adults, progeny worms were separated from parents by washing adult worms daily onto new plates using M9 + 0.01% Triton X-100. For staging synchronous animals, hours post feeding (hpf) designates the time lapsed after starvation mediated synchronized L1 larvae were placed onto food and allowed to grow. *E. coli* strain OP50 was used for all experiments unless otherwise stated. OP50 bacteria was cultured overnight at 10 37°C in LB + streptomycin and 250 µL of the culture was seeded on NGM plates the following day. Plates were allowed to dry, and bacteria allowed to grow on NGM plates for at least 2 days before use. For experiments using FUdR, 10 µL at a concentration of 100 mg/mL of the drug was dropped on regular NGM plates. Killed OP50 was attained by growing the bacteria in normal culture conditions for 12 hours and subsequently adding both kanamycin and ampicillin to the culture at 1:25 concentration and incubating while shaking for an additional 12 hours. The treated OP50 was then spun down and resuspended to 5X concentration with M9 and was exposed to 12500 µJ of UV and subsequently seeded on NGM plates and allowed to dry overnight.

Lifespan Experiment

Synchronized L1-stage larval worms were dropped directly onto OP50 bacterial lawn and allowed to grow. Once worms reach adulthood, around 72 hours post feeding, they were transferred daily to a fresh plate using a platinum wire to separate parental worms from progeny. Transferring was done until no more progeny were observed on the plate. Scoring for dead worms was done by gentle prodding with a platinum wire, and worms were considered dead either when they were unresponsive to touch or internal progeny hatching occurred. Each genotype was assayed in biological triplicate using >50 animals in each independent lifespan experiment. Animals that crawled off the plate were censored.

Cold stress assay

Age-synchronized worms, either at 48 or 144 hours post feeding, were placed at 2°C for 48 hours. Following cold exposure, worms were removed from 2°C and allowed to recover at room temperature for 1 hour. Worms were then scored for survival and were considered dead if they were unresponsive to a gentle prodding from a platinum tip wire.

Paraquat Exposure Experiment

Paraquat (PQ) exposure was done by supplementing NGM plates with 75 µM paraquat. A 10 mM paraquat stock solution was made by dissolving paraquat (methyl viologen dichloride hydrate; Sigma Aldrich) in ddH2O, which can then be stored for several months at 4°C. 7.5 mL of 10 mM paraquat solution was added to 1 L of liquid NGM media at 55°C, and then plates were poured and seeded as normal with OP50.

Synchronized L1 larval worms were dropped on to 75 µM paraquat treatment plates. Worms are washed daily to new treatment plates to separate parents from progeny, until the stated age. At that time point, they were collected and stained with ORO and scored for fat distribution.

Chromatin immunoprecipitation (ChIP)

Synchronous populations of ~700,000 animals in triplicate were grown to day 2 of adulthood (120 hpf) on NGM plates or PQ treatment plates and treated with 1.1% formaldehyde to crosslink SKN 1 or SKN-1gf protein to chromatin. Worms were pelleted and flash frozen in FA Buffer (WormBook). Samples were thawed and chromatin isolated by sonication in a Diagenode Bioruptor as previously described [76]. SKN-1 or SKN-1gf bound to chromatin was immunoprecipitated and the associated DNA released by heating to 65°C overnight. Enrichment was assessed by qPCR of the promoter region of each gene in the ChIP DNA relative to the total starting material. All comparisons of enrichment at the promoter region were normalized to a qPCR of the 3'UTR region of the same gene.

RNA interference (RNAi) Experiment

OP50 RNAi strains were used for RNAi experiments [77]. OP50 RNAi was grown overnight in LB + ampicillin and seeded the following day on NGM plates with IPTG and allowed to express dsRNA overnight. Synchronized L1 worms were dropped onto plates containing appropriate OP50 RNAi and cultured until stated age. Animals were then collected and used for experiments.

Nile Red Staining and Quantification

A working Nile Red solution was made by diluting 6 µL of stock solution (0.5 mg/mL) in 1 mL 40% isopropanol and adding 10 µL of DAPI per samples being stained. Synchronized worms at the stated age were collected using 1 mL of 1X PBS + 0.01% Triton X-100 (PBST) into a microcentrifuge tube and allowed to gravity settle. Supernatant was aspirated and washed three additional times with 1 mL PBST. After the final wash, supernatant was removed until 100 µL was left and then 600 µL of 60% isopropanol was added, and samples were rocked for 3 minutes at room temperature. Samples were spun down at 25xg and supernatant was removed until 100 µL was left. Worms were then stained with 600 µL of Nile Red working solution and left in the dark for 2 hours. Following staining, 600 µL of the supernatant was removed, and the samples were de-stained with 600 µL of PBST for 30 minutes in the dark. Samples were placed on glass slides and images were taken using the green fluorescence channel of a Zeiss Axiocam MRm. The intensity of lipid droplets was quantified using ImageJ.

RNA sequencing

At least 1000 age synchronized day 2 adult worms were washed off plates in triplicate with 1.5 mL of M9 buffer + 0.01% Triton X-100 (M9T) into a microcentrifuge tube and spun down at 1000xg. The supernatant was removed, and the pellet was washed and spun down twice more to remove any residual bacteria from the sample. After the last wash, the supernatant was aspirated and 500 µL of TRI reagent was added. The sample was then frozen at -80°C overnight. Subsequently, the sample was thawed and

lysed using a syringe and needle. RNA extraction was then performed following Zymo Direct-zol RNA isolation kit protocol. RNA samples were sequenced and analyzed by Novogene.

Chapter IV: Redistribution of the monounsaturated fatty acid oleate promotes resistance to pathogen infection

PREFACE

This research chapter derives from work that begun after the publication of the role of oleate in immune activation and pathogen defense (Chapter II). It is combined with work performed by Nicholas Peterson and is intended as a preliminary manuscript with the potential title of “Systemic adaptation to pathogen infection by the monounsaturated fatty acid oleate.” The authors who currently have contributed to this work are Nicholas Peterson, me, Hilary Cheesman, and Read Pukkila-Worley. Nicholas Peterson performed all the experiments in Figure 4.1 and Table 4.1, including experimental preparation and RNA sequencing analysis. Nick Peterson and Hilary Cheesman are responsible for Figure 4.2. and Table 4.2. I performed the tissue specific cloning and Hilary Cheesman performed the microinjections to generate the strains made in this work. I performed the experiments that make up the remainder of the Figures and Tables. However, this project and data chapter would never have come together without the ideas from Nicholas Peterson and Read Pukkila-Worley.

ABSTRACT

Evolution of nematodes has been driven by the fact that their source of nutrients is also a source of disease. This has shaped an evolutionarily conserved balance between metabolism and immunity. Indeed, intestinal epithelial cells are both a factory and warehouse for macromolecules, such as lipids, and anti-microbial peptides. Therefore, the coordination of maintaining both metabolic and immune function in

intestinal epithelial cells is critical for survival. We previously showed a requirement for the monounsaturated fatty acid (MUFA) oleate in immune activation and pathogen defense. Here, we show that transcriptional suppression of MUFA synthesis occurs during pathogen infection, in a virulent dependent manner. Additionally, genetic rescue of oleate synthesis in distal tissues restores intestinal immune responses. This suggests a novel virulence induced metabolic change that is compensated by systemic redistribution of MUFAs for survival.

INTRODUCTION

Pseudomonas aeruginosa is a gram negative opportunistic human pathogen that can cause life-threating infections in patients with burns, cystic fibrosis, or immunosuppression. *P. aeruginosa* is well characterized, with many known virulence factors, including the master virulence regulator gene *gacA* [120]. Using the nematode *C. elegans,* a well-established model for the study of *P. aeruginosa*, we can further elucidate how these virulence factors affect the conserved host responses that exist during infection with this pathogen [67].

Previously, we showed a requirement for the monounsaturated fatty acid (MUFA) oleate in the pathogen-mediated induction of innate immune genes. Animals that lack the stearoyl-CoA desaturases *fat-6* and *fat-7,* which are required to synthesis oleate, are hypersusceptible to infection with diverse pathogens, including *P. aeruginosa*. Oleate supplementation was able to restore immune phenotypes but was insufficient to activate immune responses alone in wild-type animals [109]. This suggests oleate acts

as a licensing factor for the activation of anti-pathogen responses. Stearyl-CoA desaturases are also critical for proper lipid storage [121].

In a related study, we found that infection with *P. aeruginosa* causes a rapid somatic depletion of fat. Reduction of lipid stores occurs within eight hours of infection in a virulence dependent manner. During *P. aeruginosa* infection the conserved p38 MAPK PMK-1 pathway is activated, triggering the induction of many innate immune response genes. A gain of function within this pathway, in the MAPKKK NSY-1, constitutively activates immune responses independent of diet [47]. We found that activation of this pathway also causes somatic depletion of fat [122]. This demonstrates a systemic change in the metabolism of *C. elegans* during infection, potentially as a consequence of immune activation. These data suggest that metabolism is intricately involved in the host response against *P. aeruginosa,* but it is unclear how these observations may be related.

To better understand these processes and define novel virulence mechanisms of *P. aeruginosa* we hoped to further understand the systemic host metabolic changes that occur during infection. We identified a virulence dependent and diet independent suppression of MUFA synthesis, but not PUFA synthesis. Specifically, *fat-7* expression was suppressed during infection with virulent strains of *P. aeruginosa* but was restored during infection with non-pathogenic strains. Lastly, we found rescue of oleate synthesis in a single tissue distal from the intestine was able to restore survival during pathogen infection in a *fat-6(tm331);fat-7(wa36)* mutant. This suggests that *C. elegans* overcomes suppression of MUFA synthesis during infection by redistributing oleate from distal tissues for pathogen defense.

RESULTS

Pseudomonas aeruginosa infection suppresses MUFA synthesis genes in a virulence dependent manner

We hypothesized that metabolic adaptions that occur during infection can be captured transcriptionally. Therefore, we preformed RNA sequencing and plotted the expression of genes when animals are infected with pathogenic *P. aeruginosa* compared to animals exposed to the normal *E. coli* OP50 diet against expression of genes when infected with a virulence attenuated *gacA* mutant compared to a wild-type strain of *P. aeruginosa.* This allowed us to identify genes that are specifically virulence repressed and virulence induced in a manner unrelated to diet. We found that all genes ($r = -0.403$) and differentially expressed genes were significantly correlated ($r = -0.582$). Surprisingly, fatty acid synthesis genes, defined by DAVID Gene Ontology, were also significantly correlated ($r = -0.786$) (Fig. 4.1A). To understand this further we performed a gene set enrichment analysis. We identified a significant enrichment for fatty acid synthesis genes among genes that are suppressed by *P. aeruginosa* virulence ($q<0.01$) (Fig. 4.1B). Interestingly, individual gene expression analysis identified a specific suppression of MUFA synthesis genes, whereas PUFA synthesis genes were unchanged (Fig. 4.1C). Together, this data indicates that *P. aeruginosa* virulence suppresses MUFA synthesis in a diet independent manner.

Due to the critical role of oleate during infection, we looked directly at stearoyl-CoA desaturase activity by utilizing a transgenic worm that expresses green fluorescent protein (GFP) under a *fat-7* promoter. We confirmed our RNA-seq results, that infection

with wild-type *P. aeruginosa,* but not a virulence attenuated *P. aeruginosa gacA* mutant strain*,* decreased *fat-7* expression (Fig. 4.2A). We tested additional *P. aeruginosa* strains that have varying levels of virulence, based on the previously published median lifespan of animals infected with each bacterial strain [123]. Interestingly, we can see as *fat-7* expression increased there was also an increase in lifespan, supporting a virulence dependent suppression of stearoyl-CoA desaturase activity (Fig. 4.2B).

To take an unbiased approach and identify bacterial factors required for *fat-7* suppression, we performed a screen using our *fat-7p::GFP* reporter strain. We infected animals with a *P. aeruginosa* transposon mutant library and scored for animals that had restored *fat-7* expression compared to wild-type *P. aeruginosa.* We identified 28 *P. aeruginosa* genes that were required to suppress *fat-7* out of 5,590 mutations (Fig. 4.2C). Previous work utilized the same *P. aeruginosa* transposon mutant library to identify genes required for pathogen virulence [104]. Interestingly, we observed a significant overlap (hypergeometric p value 1.65e−15) between the two screens, further supporting that suppression of stearoyl-CoA expression occurs in a virulence dependent manner (Fig. 4.2C). These data show that genes required to synthesis oleate are suppressed, independent of dietary changes, during infection with virulent *P. aeruginosa*.

Genetic rescue of oleate synthesis genes restores innate immune activation through a cell non-autonomous mechanism

To further understand the role of oleate we sought to determine the tissue in which oleate was sufficient to restore innate immune responses. The expression of *fat-6*

and *fat-7* have been previously characterized in the intestine and *fat-6* has been shown to be expressed in the hypodermis [36, 61]. However, these conclusions are based on GFP expression, and we cannot exclude undetectable expression in distal tissues.

The *fat-6(tm331);fat-7(wa36)* mutant animals in our *irg-4$_p$::GFP* reporter background lack the ability to induce *irg-4* on our immunostimulatory molecule R24, as is observed with *fat-6(RNAi)* (Fig. 4.3A). By expressing *fat-6* and *fat-7* under their native promoters we can genetically restore oleate synthesis. We hypothesized that this would allow us to drive *irg-4$_p$::GFP* induction on R24 in a manner that resembled rescue by supplementation with exogenous oleate [109]. Indeed, stearoyl-CoA desaturase activity under their own promoters was sufficient to induce *irg-4* to wild-type levels (Fig. 4.3B).

Next, we tested if *fat-6* and *fat-7* expression in a single tissue would be sufficient to restore immune gene induction. Expression of *fat-6* and *fat-7* under the intestinal specific promoter *ges-1* was able to restore *irg-4$_p$::GFP* induction on R24 (Fig. 4.3C). As *fat-6* is expressed in the hypodermis, we drove *fat-6* and *fat-7* expression in the hypodermis under the *vha-7* promoter. Interestingly, we were able to restore *irg-4$_p$::GFP* expression in the intestine by driving expression of stearoyl-CoA desaturases only in the hypodermis (Fig 4.3D). Lastly, we made transgenic animals that expressed *fat-6* and *fat-7* under the *unc-119* promoter to drive transcription exclusively in the neurons. Surprisingly, we also observed *irg-4$_p$::GFP* expression in the intestine of animals on R24 (Fig. 4.3E). This indicates that expression in tissues distal from the intestine, where *fat-6* and *fat-7* are either not expressed or very lowly expressed, oleate is able to induce innate immune effector induction.

Oleate production in tissues other than the site of infection can partially restore survival during infection on pathogen

As *fat-6* and *fat-7* expression in any of the tested tissues was able to induce *irg-4$_p$::GFP* expression, we sought to identify if this mechanism of oleate was sufficient to promote survival during pathogen infection. Expression of these stearoyl-CoA desaturases under their native promoters was sufficient to restore survival during infection as expected (Fig 4.4A and Table 4.3A). Under an intestinal specific promoter, expression of *fat-6* and *fat-7* were at least partially able to restore survival during infection (Fig 4.4B and Table 4.3B). Interestingly, hypodermal specific expression of *fat-6* and *fat-7* was also able to restore survival during infection (Fig 4.4C and Table 4.3C). Surprisingly, expression of *fat-6* and *fat-7* in only the neurons was able to fully restore survival during infection to that of wild-type levels (Fig 4.4D and Table 4.3D). This indicates that oleate synthesis in a single tissue can restore pathogen defense, even in tissues that are distal from the site of infection. This suggests that oleate utilizes a cell-nonautonomous mechanism to activate immune responses for defense against pathogen infection.

Developmental delay of stearoyl-CoA desaturase mutants is restored by rescue in a single tissue

In order to understand the cell non-autonomous mechanism of oleate we hypothesized that additional phenotypes, independent of innate immune responses, of the *fat-6(tm331);fat-7(wa36)* mutants would be restored if oleate was being redistributed among tissues. We measured the number of animals in wild-type, *fat-6(tm331);fat-*

7(wa36) mutants, and each transgenic rescue strain that were L4 or older after approximately 72 hours. Indeed, restoration of oleate synthesis in the intestine, hypodermis, or neurons alone was sufficient to restore the developmental delay that presents in the absence of oleate (Fig 4.5). This suggests that oleate is redistributed among tissues to restore this phenotype and overall health of animals. However, the mechanism of transport or redistribution remains unknown.

CONCLUSIONS

Here we show that MUFA synthesis, but not PUFA synthesis, is suppressed by infection with wild-type *P. aeruginosa* but not by a virulence attenuated *P. aeruginosa* mutant. Specifically, *fat-7* expression is negatively correlates with the virulence of *P. aeruginosa.* Furthermore, synthesis of the MUFA oleate in only the intestine, hypodermis, or neurons alone was able to restore *irg-4*$_p$*::GFP* induction on our small immunostimulatory molecule R24. Survival during infection with *P. aeruginosa* was also at least partially restored to wild-type levels when oleate synthesis occurred in any one of these tissues. Rescue of oleate synthesis in any individual tissue was also able to restore the developmental delay of *fat-6(tm331);fat-7(wa36)* mutants, suggesting a redistribution of this MUFA to restore non-immune phenotypes. We have uncovered a cell non-autonomous mechanism of host adaptation to pathogen infection by the MUFA oleate. Together this work supports the vital role of oleate during pathogen infection and defines a significant metabolic change that occurs during infection.

FIGURES AND TABLES

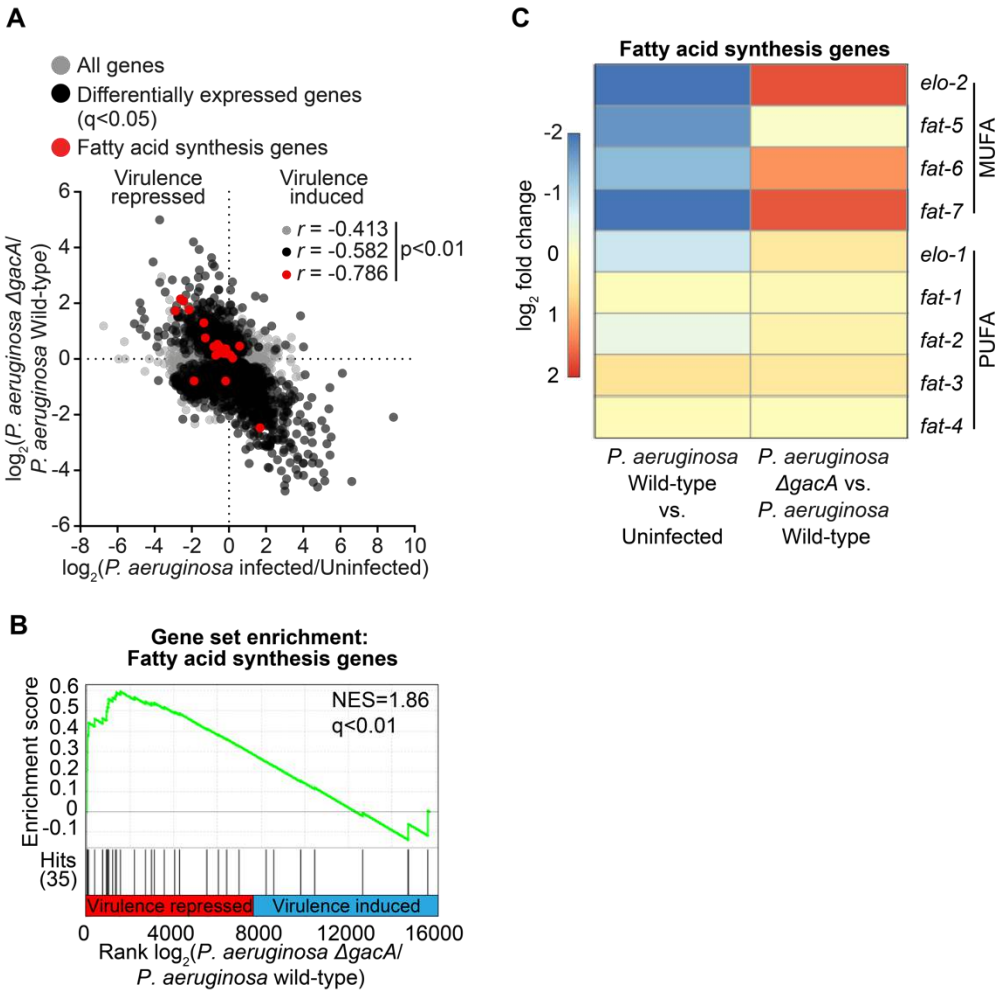

29. Figure 4.1. *Pseudomonas aeruginosa* virulence suppresses monounsaturated fatty acid synthesis genes.

A. Data from an mRNA-seq experiment of indicated conditions are represented in a scatter plot. All genes are shown in gray. Genes that were differentially expressed during infection with wild-type *P. aeruginosa* versus *E. coli* compared to a virulence attenuated *P. aeruginosa* strain versus wild-type *P. aeruginosa* are shown in black. Genes involved in fatty acid synthesis are highlighted in red. Pearson correlations for each gene set is indicated. **B.** Gene set enrichment analysis (GSEA) of differentially expressed genes in animals exposed to virulence attenuated *P. aeruginosa* strain versus wild-type *P. aeruginosa.* Results for DAVID GO fatty acid synthesis gene set are

shown. **C.** Heat map displaying fold change expression of MUFA and PUFA fatty acid synthesis genes under indicated conditions.

1. Table 4.1: RNA Sequencing Data

Table 4.1: RNA sequencing data

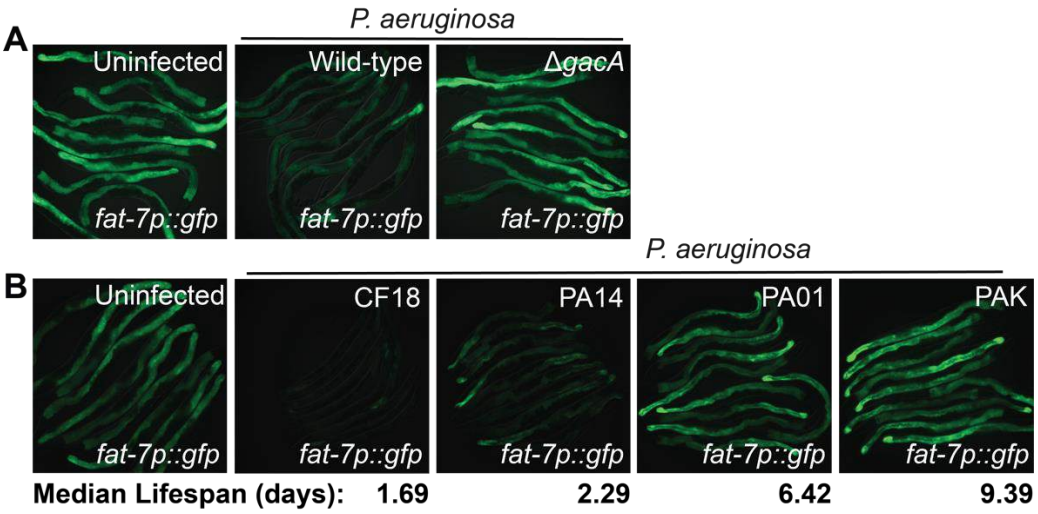

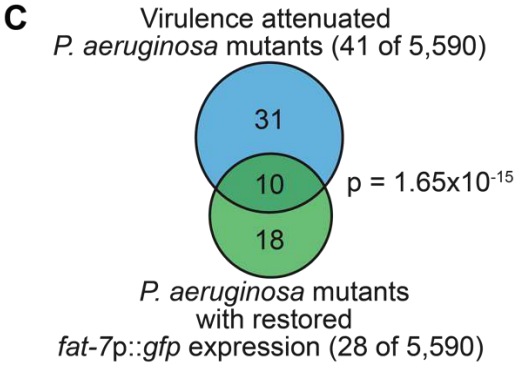

30. Figure 4.2: *Pseudomonas virulence* is required for *fat-7$_p$::GFP* suppression.

A. The *fat-7$_p$::GFP* reporter was transferred at L4 stage to plates seeded with indicated bacteria and imaged after 24 hours. **B.** Animals imaged as in A. The previously published median lifespan of *C. elegans* on each *P. aeruginosa* strain is indicated underneath each image [123]. **C.** A Venn diagram shows the overlap of *P. aeruginosa* strains identified to restore *fat-7$_p$::GFP* with those previously identified as virulence attenuated [104].

2. Table 4.2: Screen Data

"Active" Gene Locus	PA01	"Active" Gene Name	"Active" Gene Description	Score
PA14_53950	***PA0795***	***prpC***	***citrate synthase 2***	4
PA14_30650	***PA2586***	***gacA***	***response regulator GacA***	3.5
PA14_44440	PA1549	copA2	Cu2+ cation-transporting P-type ATPase	3
PA14_27700	***-***		***putative transcriptional regulator***	3
PA14_69810	***PA5288***	***glnK***	***Nitrogen regulatory protein PII***	3
PA14_04410	***PA0337***	***ptsP***	***phosphoenolpyruvate-protein phosphotransferase***	3
PA14_52260	***PA0928***	***gacS***	***sensor/response regulator hybrid***	3
PA14_42470	PA1706	pcrV	type III secretion protein PcrV	2.5
PA14_57690	PA4441		conserved hypothetical protein	2.5
PA14_72390	***PA5484***	***kinB***	***putative two-component sensor***	2.5
PA14_19120	***PA3477***	***rhlR***	***acylhomoserine lactone dependent transcriptional regulator***	2.5
PA14_59370	-		Hypothetical protein	2.5
PA14_62490	PA4723	dksA	suppressor protein DksA	2.5
PA14_27640	-		putative protein associated with synthesis and assembly of refractile incl	2
PA14_61840	PA4674	HigA	antitoxin protein	2
PA14_67210	-		conserved hypothetical protein	2
PA14_19630	PA3438	folE1	GTP cyclohydrolase I precursor	2
PA14_72450	PA5489	dsbA	thiol:disulfide interchange protein DsbA	2
PA14_07620	PA0584	cca	tRNA nucleotidyl transferase	2
PA14_07170	PA0551	epd	D-erythrose 4-phosphate dehydrogenase	1.5
PA14_52630	***PA0901***	***aruE***	***succinylglutamate desuccinylase***	1.5
PA14_12370	PA3978		hypothetical protein	1.5
PA14_63160	PA4777	pmrB	two-component sensor	1.5
PA14_07700	PA0590	apaH	bis(5'-nucleosyl)-tetraphosphatase	1.5
PA14_54640	***PA0745***	***dspI***	***probable enoyl-CoA hydratase/isomerase***	1.5
PA14_45940	***PA1432***	***lasI***	***autoinducer synthesis protein LasI***	1.5
PA14_62770	PA4745	nusA	N utilization substance protein A	1.5
PA14_48640	PA1211		conserved hypothetical protein	1.25

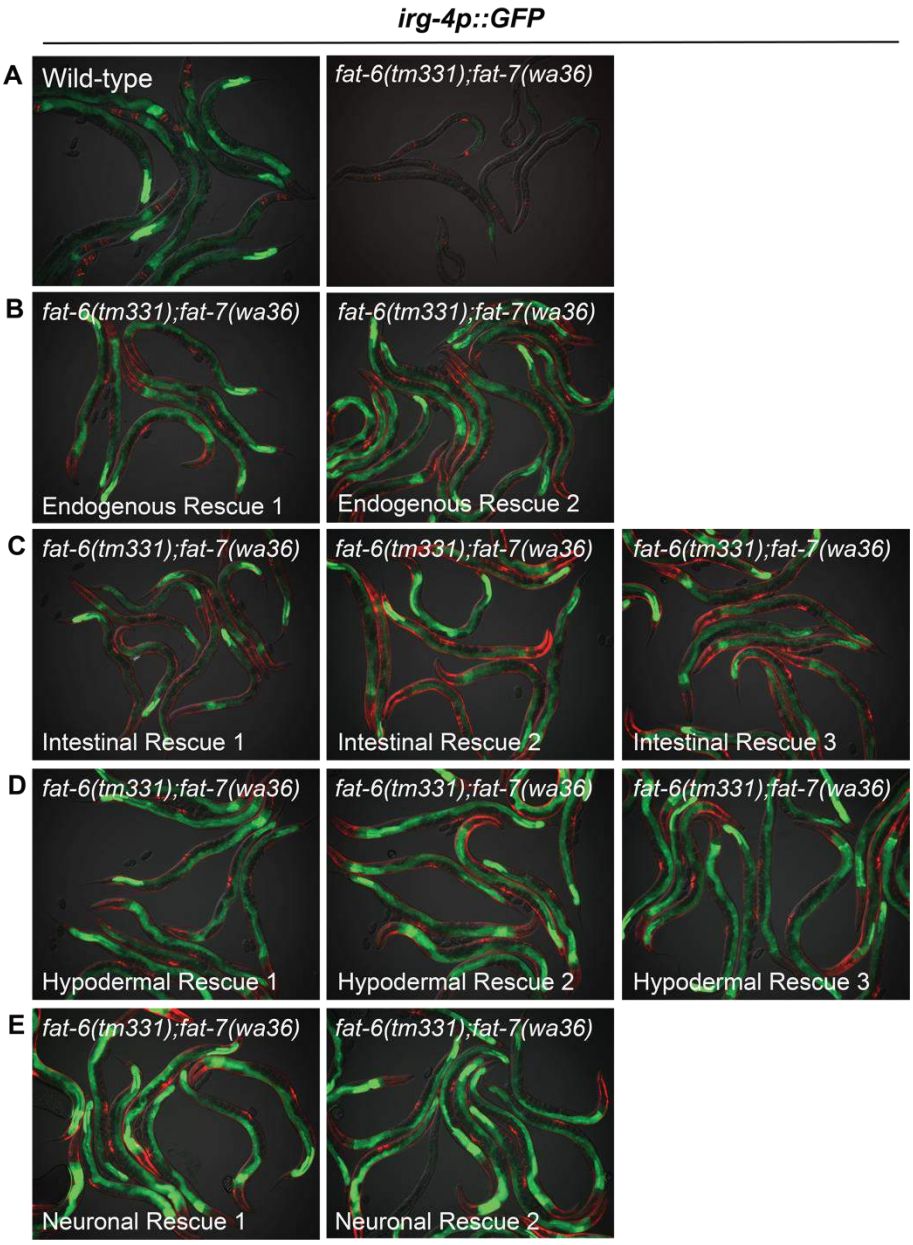

31. Figure 4.3. Tissue specific rescue of oleate synthesis restores *irg-4$_p$::GFP* induction on the small immunostimulatory molecule R24.

A-E. The *irg-4$_p$::GFP* immune reporter with the indicated genetic background were transferred at L4 stage to plates containing 70 uM R24 for approximately 18 hours. Red pharyngeal expression is the *myo-2$_p$::mCherry* co-injection marker, which confirms the presence of the *irg-4$_p$::GFP* transgene. The *myo-3$_p$::mCherry* co-injection marker indicates the presence of the extrachromosomal array that contains *fat-6$_p$::fat-6* + *fat-*

7$_p$::fat-7 (**B**), *ges-1$_p$::fat-6 + ges-1$_p$::fat-7* (**C**), *vha-7$_p$::fat-6 + vha-7$_p$::fat-7* (**D**), or *unc-119$_p$::fat-6 + unc-119$_p$::fat-7* (**E**).

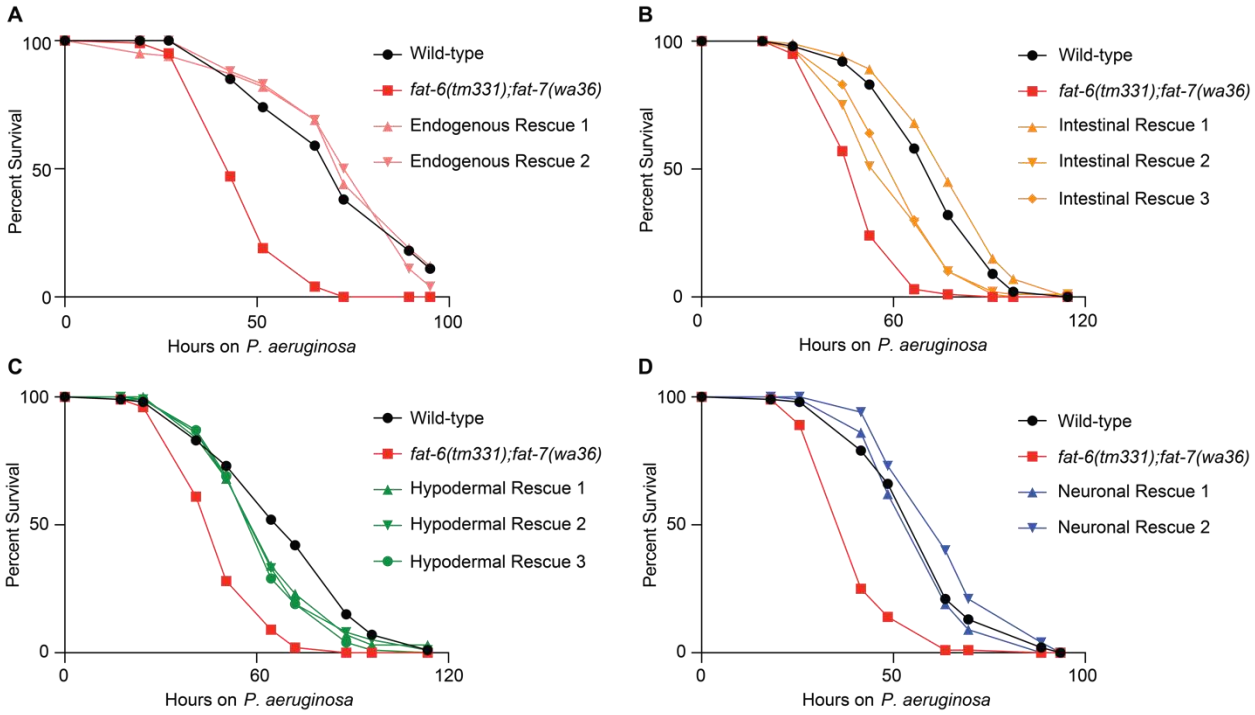

32. Figure 4.4. Survival during pathogen infection is at least partially restored by tissue specific rescue of oleate synthesis.

C. elegans pathogenesis assay conducted with the indicated genotypes. **A.** Endogenous (*fat-6$_p$::fat-6 + fat-7$_p$::fat-7)* **B.** Intestinal (*ges-1$_p$::fat-6 + ges-1$_p$::fat-7)* **C.** Hypodermal *(vha-7$_p$::fat-6 + vha-7$_p$::fat-7)* **D**. Neuronal (*unc-119$_p$::fat-6 + unc-119$_p$::fat-7)*. Sample sizes, mean lifespan, and p values for all trials are shown in Table 4.2. Significance was determined using Kaplan-Meier survival curves and log-rank tests.

3. Table 4.3: Killing Assay Statistics

Table 4.3 Killing Assay Statistics: All trials for the pathogenesis assays presented in Figure 4.4. **A.** Endogenous rescue trials. **B.** Intestinal rescue trials. **C.** Hypodermal rescue trials. **D.** Neuronal rescue trials.

Date	Genotype	n	Mean lifespan (hours)		
Table 4.3A: Endogenous					
12.9.19	*irg-4p::GFP*	111	58.84±1.54		
12.16.19	***irg-4p::GFP***	**164**	**72.09±1.44**		
7.20.20	*irg-4p::GFP*	178	73.72±1.56		
				P value vs. wild-type	
12.9.19	*irg-4p::GFP;fat-6(tm331);fat-7(wa36)*	112	52.32±1.21	0.001	
12.16.19	***irg-4p::GFP;fat-6(tm331);fat-7(wa36)***	**114**	**48.99±0.97**	**<0.0001**	
7.20.20	*irg-4p::GFP;fat-6(tm331);fat-7(wa36)*	154	45.58±1.05	<0.0001	
				P value vs. *fat-6(tm331);fat-7(wa36)*	P value vs. wild-type
12.9.19	*irg-4p::GFP;fat-6(tm331);fat-7(wa36) + Endogenous Rescue 1*	79	58.86±1.42	0.0009	0.9049
12.16.19	***irg-4p::GFP;fat-6(tm331);fat-7(wa36) + Endogenous Rescue 1***	**108**	**73.89±1.94**	**<0.0001**	**0.3611**
7.20.20	*irg-4p::GFP;fat-6(tm331);fat-7(wa36) + Endogenous Rescue 1*	162	64.34±1.43	<0.0001	0.000037
				P value vs. *fat-6(tm331);fat-7(wa36)*	P value vs. wild-type
12.9.19	*irg-4p::GFP;fat-6(tm331);fat-7(wa36) + Endogenous Rescue 2*	81	60.6±1.66	0.0001	0.801
12.16.19	***irg-4p::GFP;fat-6(tm331);fat-7(wa36) + Endogenous Rescue 2***	**94**	**75.98±1.75**	**<0.0001**	**0.7887**
7.20.20	*irg-4p::GFP;fat-6(tm331);fat-7(wa36) + Endogenous Rescue 2*	118	51.95±1.36	0.0015	<0.0001
Table 4.3B: Intestinal					
12.9.19	*irg-4p::GFP*	111	58.84±1.54		
12.16.19	*irg-4p::GFP*	164	72.09±1.44		
1.13.20	***irg-4p::GFP***	**122**	**74.73±1.55**		
				P value vs. wild-type	
12.9.19	*irg-4p::GFP;fat-6(tm331);fat-7(wa36)*	112	52.32±1.21	0.001	
12.16.19	*irg-4p::GFP;fat-6(tm331);fat-7(wa36)*	114	48.99±0.97	<0.0001	
1.13.20	***irg-4p::GFP;fat-6(tm331);fat-7(wa36)***	**103**	**51.96±1.09**	**<0.0001**	
				P value vs. *fat-6(tm331);fat-7(wa36)*	P value vs. wild-type
12.9.19	*irg-4p::GFP;fat-6(tm331);fat-7(wa36) + Intestinal Rescue 1*	69	79.1±1.68	<0.0001	<0.0001
12.16.19	*irg-4p::GFP;fat-6(tm331);fat-7(wa36) + Intestinal Rescue 1*	99	63.14±1.51	<0.0001	<0.0001
1.13.20	***irg-4p::GFP;fat-6(tm331);fat-7(wa36) + Intestinal Rescue 1***	**85**	**79.95±1.92**	**<0.0001**	**0.0295**
				P value vs. *fat-6(tm331);fat-7(wa36)*	P value vs. wild-type
12.9.19	*irg-4p::GFP;fat-6(tm331);fat-7(wa36) + Intestinal Rescue 2*	97	64.08±1.53	<0.0001	0.0733
12.16.19	*irg-4p::GFP;fat-6(tm331);fat-7(wa36) + Intestinal Rescue 2*	45	79.92±2.7	3.16.20	0.0413
1.13.20	***irg-4p::GFP;fat-6(tm331);fat-7(wa36) + Intestinal Rescue 2***	**141**	**61.52±1.38**	**<0.0001**	**<0.0001**
				P value vs. *fat-6(tm331);fat-7(wa36)*	P value vs. wild-type
12.9.19	*irg-4p::GFP;fat-6(tm331);fat-7(wa36) + Intestinal Rescue 3*	111	66.95±1.29	<0.0001	0.004
12.16.19	*irg-4p::GFP;fat-6(tm331);fat-7(wa36) + Intestinal Rescue 3*	115	61.26±1.55	<0.0001	<0.0001
1.13.20	***irg-4p::GFP;fat-6(tm331);fat-7(wa36) + Intestinal Rescue 3***	**123**	**64.11±1.37**	**<0.0001**	**<0.0001**
Table 4.3C: Hypodermal					
1.6.20	*irg-4p::GFP*	101	63.28±1.42		
1.20.20	***irg-4p::GFP***	**122**	**71.78±2.0**		
2.24.20	*irg-4p::GFP*	131	75.32±1.65		
6.8.20	*irg-4p::GFP*	141	62.23±1.52		
				P value vs. wild-type	
1.6.20	*irg-4p::GFP;fat-6(tm331);fat-7(wa36)*	77	52.29±1.55	0.0000015	
1.20.20	***irg-4p::GFP;fat-6(tm331);fat-7(wa36)***	**175**	**51.0±0.96**	<0.0001	
2.24.20	*irg-4p::GFP;fat-6(tm331);fat-7(wa36)*	105	51.33±1.19	<0.0001	
6.8.20	*irg-4p::GFP;fat-6(tm331);fat-7(wa36)*	109	50.76±1.16	<0.0001	
				P value vs. *fat-6(tm331);fat-7(wa36)*	P value vs. wild-type
1.6.20	*irg-4p::GFP;fat-6(tm331);fat-7(wa36) + Hypodermal Rescue 1*	87	60.24±1.7	0.0006	0.3141
1.20.20	***irg-4p::GFP;fat-6(tm331);fat-7(wa36) + Hypodermal Rescue 1***	**186**	**65.82±1.32**	**<0.0001**	**0.0099**
2.24.20	*irg-4p::GFP;fat-6(tm331);fat-7(wa36) + Hypodermal Rescue 1*	128	69.01±1.42	<0.0001	0.0006
6.8.20	*irg-4p::GFP;fat-6(tm331);fat-7(wa36) + Hypodermal Rescue 1*	95	65.81±1.54	<0.0001	1
				P value vs. *fat-6(tm331);fat-7(wa36)*	P value vs. wild-type
1.6.20	*irg-4p::GFP;fat-6(tm331);fat-7(wa36) + Hypodermal Rescue 2*	100	58.49±1.43	0.0061	0.0268
1.20.20	***irg-4p::GFP;fat-6(tm331);fat-7(wa36) + Hypodermal Rescue 2***	**136**	**65.49±1.6**	**<0.0001**	**0.0098**
6.8.20	*irg-4p::GFP;fat-6(tm331);fat-7(wa36) + Hypodermal Rescue 2*	124	81.18±1.51	<0.0001	<0.0001
				P value vs. *fat-6(tm331);fat-7(wa36)*	P value vs. wild-type
1.6.20	*irg-4p::GFP;fat-6(tm331);fat-7(wa36) + Hypodermal Rescue 3*	107	63.87±1.54	<0.0001	0.4232
1.20.20	***irg-4p::GFP;fat-6(tm331);fat-7(wa36) + Hypodermal Rescue 3***	**114**	**64.51±1.53**	**<0.0001**	**0.0005**
6.8.20	*irg-4p::GFP;fat-6(tm331);fat-7(wa36) + Hypodermal Rescue 3*	119	86.47±1.96	<0.0001	<0.0001
Table 4.3D: Neuronal					
1.6.20	*irg-4p::GFP*	101	63.28±1.42		
1.27.20	***irg-4p::GFP***	**130**	**72.89±1.82**		
3.16.20	*irg-4p::GFP*	131	60.32±1.34		
				P value vs. wild-type	
1.6.20	*irg-4p::GFP;fat-6(tm331);fat-7(wa36)*	77	52.29±1.55	0.0000015	
1.27.20	***irg-4p::GFP;fat-6(tm331);fat-7(wa36)***	**132**	**65.95±1.54**	**0.001**	
3.16.20	*irg-4p::GFP;fat-6(tm331);fat-7(wa36)*	145	43.81±0.89	<0.0001	
				P value vs. *fat-6(tm331);fat-7(wa36)*	P value vs. wild-type
1.6.20	*irg-4p::GFP;fat-6(tm331);fat-7(wa36) + Neuronal Rescue 1*	82	61.99±1.78	0.000046	0.9501
1.27.20	***irg-4p::GFP;fat-6(tm331);fat-7(wa36) + Neuronal Rescue 1***	**151**	**75.38±1.58**	**0.000044**	**0.5083**
3.16.20	*irg-4p::GFP;fat-6(tm331);fat-7(wa36) + Neuronal Rescue 1*	118	59.58±1.23	<0.0001	0.4446
				P value vs. *fat-6(tm331);fat-7(wa36)*	P value vs. wild-type
1.6.20	*irg-4p::GFP;fat-6(tm331);fat-7(wa36) + Neuronal Rescue 2*	79	66.02±1.52	<0.0001	0.2469
1.27.20	***irg-4p::GFP;fat-6(tm331);fat-7(wa36) + Neuronal Rescue 2***	**166**	**52.47±0.98**	**<0.0001**	**<0.0001**
3.16.20	*irg-4p::GFP;fat-6(tm331);fat-7(wa36) + Neuronal Rescue 2*	109	65.67±1.42	<0.0001	0.0082

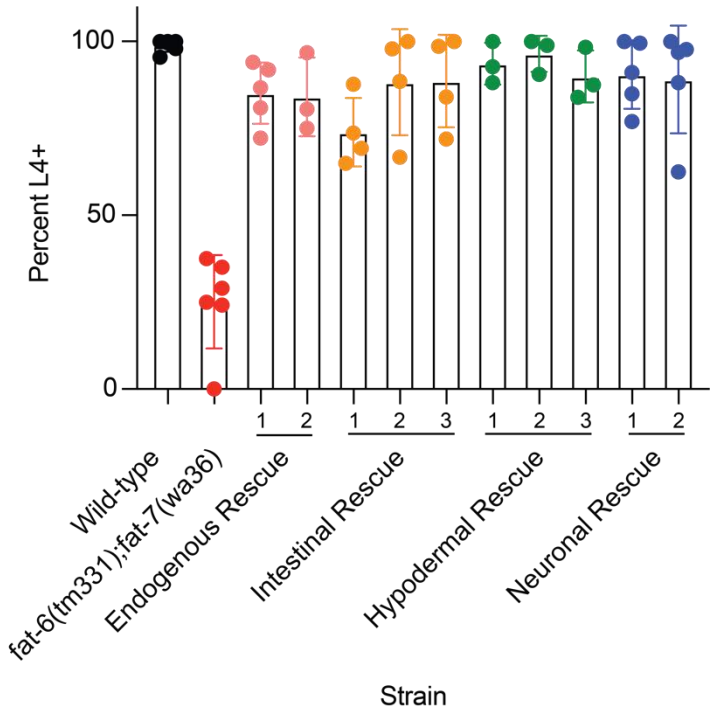

33. Figure 4.5. Developmental delay of *fat-6(tm331);fat-7(wa36)* animals is restored by tissue specific rescue of oleate synthesis.

Developmental assays were performed with the indicated genotypes. The stage of the animals was recorded at the same time point, approximately 72 hours after eggs were laid. Wild-type development was significantly different from *fat-6(tm331);fat-7(wa36)* ($p<0.0001$) and intestinal rescue line 1 ($p = 0.04$) but not significantly different from any other genotype by one-way ANOVA.

4. Table 4.4: Primers Used and Strains Generated

Table 4.4: Primers used for generation of transgenic *C. elegans* and strains generated in this work

MATERIALS AND METHODS

***C. elegans* and bacterial strains.** *C. elegans* strains were maintained on *E. coli* OP50 bacteria on nematode growth media plates, as described [62]. The *C. elegans* strains used in this study were N2 Bristol [62], AU306 *agIs44* [*irg-4::GFP::unc-54-3'UTR; myo-2::mCherry*] [23], RPW248 agIs44 [*irg-4p::GFP, myo-2p::mCherry;fat-6(tm331);fat-7(wa36)*], HA1842 [*fat-7p::GFP*] and all strains listed in Table 4.3. *P. aeruginosa* strains PA14 [31], CF18, PA01, PAK, *ΔgacA P. aeruginosa*, and *P. aeruginosa* transposon mutant library [104] were used in this study.

Gene expression analysis and bioinformatics

Synchronized L1 stage N2 *C. elegans* were grown to the L4 stage and transferred by washing to plates containing OP50, or either wild-type or Δ*gacA P. aeruginosa* lawns. Animals were exposed for 4 hours and subsequently harvested by washing with M9. RNA was isolated using TriReagent (Sigma-Aldrich), column purified (Qiagen), and analyzed by paired-end mRNA-sequencing using the BGISEQ-500 platform (BGIAmericasCorp) with >20 million reads per sample. Raw fastq reads were evaluated by FastQC (version 0.11.5) and clean reads aligned to the *C. elegans* reference genome (WBcel235) and quantified using Kallisto (version 0.45.0) [124]. Differentially expressed genes were identified using Sleuth (version 0.30.0) [125]. Pearson correlation statistical analysis was performed using Prism 9.0. Heat-maps of differentially expressed lipid biosynthesis genes were generated using pheatmap (version 1.0.12). Gene set enrichment analysis of Δ*gacA* RNA-seq was performed using GSEA (version 4.1.0) with a custom gene set database containing all *C. elegans* genes identified as a fatty acid synthesis gene by DAVID Gene Ontology.

Generation of transgenic *C. elegans* strains

To generate tissue specific rescue strains *fat-6, fat-7*, and tissue specific promoters (2kb upstream of start site) were generated by PCR (see Table 4.3 for primers). Each tissue-specific construct was generated using Gibson assembly in pUC19 linearized with XbaI [126]. The plasmid (25 ng/ml), the *myo-3p::mCherry* co-injection marker (15 ng/ml) and pBluescript SK (-) vector (145 ng/ml) were microinjected into RPW248 *agIs44 [Pirg-4::GFP, Pmyo-2::mCherry; fat-6(tm331);fat-7(wa36)]* to generate the strains listed in Table 4.4.

C. elegans Bacterial Infection and Other Assays.

"Slow killing" *P. aeruginosa* pathogenesis assays were performed as previously described [67]. Sample sizes, mean lifespan, and p values for all trials are shown in Table 4.4. The protocol for treatment of animals with 70 μM R24 has also been described [46]. *C. elegans* development assays were performed as previously described [47, 127].

fat-7$_p$::gfp PA14 transposon library screen

A previously described non-redundant PA14 transposon library containing 5,590 unique mutants [104] was used for this study. *C. elegans* encoding the *fat-7*$_p$::*gfp* transgene were L1 synchronized, grown to the L4 stage on *E. coli* OP50 and transferred by washing to the *P. aeruginosa* mutant lawns. Animals were exposed for 24 hours and GFP fluorescence scored by eye. Hits were defined as PA14 mutants that no longer

suppressed *C. elegans fat-7*p::*gfp* and lacked any growth defect, as previously characterized [104].

Microscopy. Nematodes were paralyzed with 10 mM levamisole (Sigma), mounted on agar pads and photographed using a Zeiss AXIO Imager Z2 microscope with a Zeiss Axiocam 506mono camera and Zen 2.3 (Zeiss) software.

Statistical Analyses. *C. elegans* survival was assessed using the Kaplan-Meier method and differences were determined with the log-rank test using OASIS 2 [75]. Other statistical tests, which are indicated in the figure legends, were performed using Prism 7 (GraphPad Software).

Chapter V: Discussion

INTRODUCTION

This body of work demonstrates that metabolism and immunity are linked by the monounsaturated fatty acid (MUFA) oleate in *C. elegans*. As one of the most abundant fatty acids, understanding how oleate affects physiological responses for survival is critical. We have shown that: 1) the MUFA oleate is required for innate immune activation and pathogen defense, 2) *P. aeruginosa* infection alters systemic host metabolism and suppresses MUFA synthesis genes, and 3) Redistribution of oleate from distal tissues to the site of infection provides resistance to pathogen infection. These findings have important implications for understanding the connection between cellular energy stores and immune activation. In addition, it shows how pathogen infection can have consequences on host metabolism.

SYSTEMIC ADAPTATION TO PATHOGEN INFECTION BY THE MONOUNSATURATED FATTY ACID OLEATE

The MUFA oleate is required for innate immune activation and pathogen defense

Our work has identified a requirement for oleate in the *C. elegans* innate immune response. Lack of the stearoyl-CoA desaturase *fat-6* prevented induction of a specific subset of innate immune effectors on our small immunostimulatory molecule R24 (also known as RPW-24). We found that the directly upstream enzyme *elo-2* is also required for this induction. However, the downstream desaturase enzyme *fat-2,* which is required to produce downstream polyunsaturated fatty acids (PUFAs), was not required for immune gene induction. In addition, exogenous supplementation of PUFAs to *fat-*

6(RNAi) animals did not restore immune effector expression, whereas the addition of oleate fully complemented the induction defect of these animals.

Oleate deficiency, achieved by *fat-6(RNAi)* or a mutation in both stearoyl-CoA desaturases, *fat-6* and *fat-7*, also prevented induction of key immune effectors during infection with *P. aeruginosa.* Importantly, we show that *fat-6(tm331);fat-7(wa36)* loss-of-function mutant animals were hypersusceptible to killing by both gram negative and gram positive bacterial pathogens including *P. aeruginosa*, *E. faecalis,* and *S. marcescens,* in a manner dependent on oleate. However, treatment with oleate was unable to provide protection during bacterial infection in wild-type animals. Therefore, oleate is necessary but not sufficient to activate innate immune responses. This indicates a significant and broad role for oleate in immune activation and pathogen defense.

Host metabolism and MUFA synthesis genes are altered during infection with *P. aeruginosa* in a virulence dependent manner

Within this work, we identified novel metabolic changes that occur during infection with *P. aeruginosa*. Within eight hours of *P. aeruginosa* infection, we observed depletion of somatic lipids in wild-type animals. This fat loss was dependent on pathogenic virulence, as animals exposed to *P. aeruginosa gacA* or *rhlR* transposon mutants had normal lipid stores. When animals were treated with *vit-5(RNAi)* prior to pathogen exposure, fat loss was suppressed. This suggests that animals are shuttling lipids to the gonad through vitellogenin proteins which is at least partially responsible for this somatic depletion of fat.

To further characterize this fat loss phenotype, independent of bacterial diet, we utilized a mutant animal that has constitutive activation of the p38 MAPK pathway. Interestingly, animals that harbor a gain-of-function mutation in the upstream MAPKKK component *nsy-1* exhibited accelerated somatic depletion of fat with aging. This phenotype was dependent upon the downstream transcription factor SKN-1. Importantly, animals with a gain-of-function in *skn-1* also exhibit this fat loss at day 2 of adulthood [79]. RNA sequencing of these animals revealed an enrichment of innate immune effector expression at this time point. Together, this suggests that somatic depletion of fat can occur as a consequence of innate immune activation.

To identify additional transcriptional changes that could be involved in this somatic depletion of fat we utilized RNA sequencing of animals on normal *E. coli* diet, infected with *P. aeruginosa*, or infected with a virulence attenuated *gacA* mutant of *P. aeruginosa*. Therefore, we identified genes that are differentially expressed in a virulence-dependent and diet-independent manner. Through gene set enrichment analysis, we observed that fatty acid synthesis genes are suppressed during infection with pathogenic *P. aeruginosa* but not during infection with the *gacA* mutant. Interestingly, we detected a suppression of MUFA, but not PUFA, synthesis genes. Specifically, we found that expression of *fat-7* was reduced upon infection with multiple virulent *P. aeruginosa* strains. We also performed an unbiased screen with a *P. aeruginosa* transposon mutant library and identified a significant overlap between previously published virulence attenuated strains and strains in which infection led to restored *fat-7* expression. This suggests that virulence of *P. aeruginosa* is critical for

suppression of these genes and supports the vital role of the MUFA oleate during pathogen infection.

It has been shown that the MUFAs palmitoleate and oleate can have antibacterial activity against pathogens [128]. Therefore, in addition to being required for defense against pathogen infection, oleate may also play a direct offensive role in the immune response. Indeed, this would provide an evolutionary advantage for pathogens that can suppress synthesis of these fatty acids. However, it is unknown how a pathogen could suppress MUFA synthesis. The bacterial factors associated with the *P. aeruginosa* transposon mutants that have restored *fat-7* expression would be of interest to further investigate. Alternatively, virulence factors may act indirectly to result in MUFA synthesis suppression, perhaps as a consequence of immune activation. Overall, our work shows novel metabolic changes that occur during infection with *P. aeruginosa* with insights to both the consequences of innate immune activation and potential virulence strategies used by this pathogen.

Redistribution of oleate from distal tissues to the site of infection provides resistance to pathogen infection

Our work demonstrates that oleate is a critical fatty acid that acts cell non-autonomously to induce immune responses. We show that rescue of oleate synthesis in a single tissue, by reconstituting *fat-6* and *fat-7* expression under tissue specific promoters in *fat-6(tm331);fat-7(wa36)* mutant animals, was able to restore immune gene induction on R24. Importantly, we were also able to restore defense against *P. aeruginosa* infection by rescuing stearoyl-CoA desaturase activity in tissues distal to the

intestine. The developmental delay of *fat-6(tm331);fat-7(wa36)* mutant animals was also rescued by expression in the intestine, hypodermis, or neurons alone, suggesting that oleate is redistributed among tissues to restore multiple phenotypes.

Nandakumar et al. previously identified that two fatty acids, γ-linoleic acid (GLA) and stearidonic acid (SDA), which are synthesized by the enzyme *fat-3,* are required for the basal expression of immune effectors. These mutants also have neuromuscular defects and stress sensitivities [12]. Our data indicate that oleate and these PUFAs affect immune effector expression and pathogen resistance by different mechanisms. They identified that these PUFAs are not required for innate immune gene induction and act in a cell-autonomous manner. Rescue of *fat-3* in the intestine was able to restore survival during pathogen infection but not the neuromuscular defects. In addition, rescue of *fat-3* in the neurons was unable to restore survival during pathogen infection. This further emphasizes the difference between the role of MUFAs and PUFAs in the *C. elegans* innate immune response.

Future work could help to connect the redistribution and suppression of oleate during infection with virulence dependent somatic depletion of fat. Some of our data suggests that somatic fat is being redistributed to the germline in order to preserve reproductive function. Bagging or matricide is also a common phenotype on *P. aeruginosa* and other pathogens indicating that infection triggers a response that prioritizes offspring under stress conditions [129]. This provides an evolutionary advantage as progeny that enter dauer stage instead of consuming potentially harmful bacteria that surround them would be more likely to survive. Therefore, the hypothesis that lipid resources are shuttled to the gonad via vitellogenin proteins during infection is

well supported. However, it is likely that the depletion of lipid droplets could have multiple functions, such as fatty acid redistribution to cellular membranes or release of antimicrobial peptides stored in lipid droplets as a direct offensive strategy [130]. Indeed, the role of stearoyl-CoA desaturase activity in membrane maintenance suggests this could be a large contributor.

Together, these data implicate a vital role for the MUFA oleate in innate immune responses. This work may help us understand why one person may be more susceptible to certain diseases and ways we can alter these physiological responses. Indeed, the prevalence and ease of dietary fatty acid supplementation would make them an ideal natural treatment in a clinical setting. If increasing nutritional intake of specific fatty acids can alter physiological outcomes, this may help us to develop novel treatment plans in the future.

THE BENEFICIAL ROLES OF THE MONOUNSATURATED FATTY ACID OLEATE ARE DIVERSE AND EVOLUTIONARILY CONSERVED

Oleate has a fundamental and evolutionarily conserved role in innate immune homeostasis

Stearoyl-CoA desaturase (SCD1) activity is conserved from yeast to humans. The significance of oleate in innate immune responses is also shown to be evolutionarily conserved from plants to mice. Mice lacking SCD1 activity were identified in a forward genetic screen looking for animals that were susceptible to infection [128]. These animals, termed *flake* (*flk/flk*), are unable to produce the 16 and 18-carbon MUFAs oleate and palmitoleate, have chronic dermatitis, and reduced sebum

production. These MUFAs were required for the clearance of *Streptococcus pyogenes* and *Staphylococcus aureus* infection in the skin. Importantly, oleate and palmitoleate also had bactericidal activity *in vivo* and *in vitro* against gram-positive pathogens [128]. This demonstrates a conserved benefit of oleate and suggests a potential mechanism for oleate in *C. elegans* pathogen defense.

Interestingly, *Arabidopsis* mutant plants that cannot synthesis oleate have constitutive activation of pathogenesis-related genes and are resistant to multiple pathogens. However, these plants also have stunted growth and develop spontaneous cell death lesions [58, 131]. Oleate also regulated nitric oxide production, which aids in pathogen defense [59]. *Arabidopsis* has six isoforms of SCD1, mice have four isoforms, and humans and *C. elegans* both have two isoforms. This indicates not only the importance of SCD1 activity but the complex evolution of these enzymes through different species. Together, these data show that the benefit of oleate in immune homeostasis is evolutionarily conserved.

Diets rich in monounsaturated fatty acids support several health benefits

Oleate has well known benefits in addition to its role in immune responses. In *C. elegans* under standard laboratory conditions an oleate supplemented diet can extend lifespan by modulating chromatin dynamics [29]. The complexity of this mechanism suggests we may not uncover if this benefit is conserved in mammalian systems. However, many epidemiological studies suggest that dietary MUFAs have beneficial health effects [132].

Dietary oleate has been investigated as a treatment for diabetes. Treatment of rat pancreatic beta cells with oleate enhanced insulin secretion and reversed inflammatory suppression of insulin secretion [133]. Mice gavaged with peanut oil, which contains high levels of oleic acid but not PUFAs, also reduced blood glucose levels in type II diabetic mice [133]. Interestingly, this reduction in blood glucose levels was not observed in a type I diabetic mouse model, suggesting oleate acts to reduce inflammation which increases insulin levels. In an epidemiological study, diabetic patients who ate a high MUFA-diet saw a reduction in body weight, body fat, waist circumference, diastolic blood pressure, and fasting glucose and insulin levels after one year [134]. Together, this indicates a positive role for dietary oleate in helping to control symptoms of diabetes.

High MUFA diets have also been investigated for treatment of heart disease. Appel, *et al.* found that a diet that replaced carbohydrates with unsaturated fat, consisting of mostly MUFAs, lowered blood pressure and triglyceride levels and increased HDL cholesterol [135]. A Mediterranean diet, which is high in MUFAs such as oleate, has also been shown to have numerous health benefits including being protective against cancer and coronary heart disease [136]. Interestingly, the work done in mammals studying the role of the SCD1 enzyme reveals it has different roles in various tissues such as in liver, adipocytes, macrophages, endothelial cells, and myocytes [137]. For example, SCD1 has an anti-inflammatory role in beta-cells but is required for anti-microbial responses in the skin [128, 133]. Overall, the health benefits of a diet high in oleate is well established and our work adds significant support to these observations.

POTENTIAL MECHANISMS OF FATTY ACIDS IN IMMUNE HOMEOSTASIS AND FUTURE DIRECTIONS

Oleate could be involved in the *C. elegans* innate immune response in several ways. As delta-9 fatty acids are incorporated into phospholipids, lack of unsaturated fatty acids in phospholipid bilayers has consequences on cell and organelle membrane integrity and lipid-protein interactions. Loss of stearyl-CoA desaturases triggers activation of ER stress responses as a consequence of disrupted membrane fluidity [31]. In addition, alterations of membrane fluidity have been linked to activation of G protein-coupled receptors [60, 61]. Importantly, stearoyl-CoA desaturates also regulate overall membrane maintenance. RNAi against *fat-6* or *fat-7* had a major impact on turnover rates in *C. elegans* membranes, as the rate of fatty acid replacement per hour was decreased significantly [138]. Together, this indicates the critical role of oleate in maintaining membrane homeostasis for control of stress responses.

Given the critical role for oleate in membranes, the hypothesis that oleate is transported between tissues via membrane dynamics for proper immune signaling, should be further explored. Indeed, cell membrane fluidity is maintained cell non-autonomously through a sensor complex that at least partially requires delta-9 desaturases [61]. This work demonstrated that unsaturated fatty acids can be produced in the hypodermis and spread through cell membranes to achieve systemic membrane homeostasis [61]. Current techniques of radiolabeling fatty acids could help to address the location of oleate during infection to determine whether oleate is being consumed as energy or redistributed to a specific tissue [138].

An RNAi screen of lipid binding and transport proteins was performed in our *fat-6* and *fat-7* tissue specific rescue strains to identify factors that may be required for the cell non-autonomous mechanism but resulted in no significant observations. This could suggest it does not require a specific protein and is transported through membrane dynamics. However, the technical challenge with this screen is that RNAi is usually not as effective in neurons, where such a protein would be required to transport oleate to the intestine. A forward genetic screen in animals that have neuronally rescued oleate synthesis could help to identify factors that would be undetectable by RNAi. In an unbiased forward genetic screen, we may identify proteins that are involved in the transport of oleate or completely novel proteins, such as potential receptor molecules that oleate requires to function cell non-autonomously.

The variety of fatty acids in length and formation gives them the ability to be diverse ligands for NHRs and other proteins, controlling transcriptional output or responding to physiological conditions [139, 140]. Despite the insufficiency of oleate to activate immune responses alone, oleate itself, or incorporated into a complex lipid, may still act as a direct ligand. Yuan, *et al.* used an unbiased approach to identify a ligand that binds directly without altering transcriptional responses [140]. Alternatively, instead of binding directly to a receptor, the redistribution of oleate could be a physiological signal monitored by the host. Indeed, evidence suggests lipophilic signals between the germline and intestine can control lifespan, metabolism, and immune responses [29, 141]. Redistribution of oleate could act as a potential indirect physiological signal for pathogen defense. Somatic depletion of fat during infection partially requires vitellogenin genes indicating that oleate is transported from the

intestine to the germline during infection. An interesting hypothesis is that oleate may be trafficked as an intestine-to-germline signal to activate immune responses and is not merely a consequence of immune activation.

In addition, oleate is critical for proper lipid storage and abundance [37, 121]. The work presented here may suggest how a metazoan animal limits the induction of protective immune defenses to times when the host has accumulated sufficient energy reserves to survive challenge from bacterial pathogens. Lipid droplets and oleate, in *Drosophila* and mice respectively, have also been shown to be directly antimicrobial themselves [128, 130]. Therefore, in *C. elegans,* oleate and lipid droplets could be required for an offensive strategy against pathogen infection.

Fatty acids can also be used as a post-translational modification which can aid in membrane targeting, protein-protein interactions, or signal transduction pathways. Indeed, myristylation of an adaptor protein that participates in Toll-like receptor-4 (TLR4) signaling is required for its membrane localization and subsequent innate immune responses [142]. Although, the attachment of oleate is not common, it can also occur [143]. It is possible that oleate could modify proteins that activate signaling cascades in the *C. elegans* innate immune response.

Lastly, we hope future work will extrapolate these findings to mammalian systems. As discussed above, it seems that in mammalian systems oleate plays distinct roles in each tissue and work has been done to characterize its role in skin and pancreas [128, 133]. However, not much is known about its role in intestinal epithelial cells with regards to microbial interactions and thus would be important to further study. Given the influence of *C. elegans* biology on scientific discoveries and the abundance

and ubiquitous nature of oleate in physiology, this work has substantial significance to science.

Appendix I: The transcription factor T26A8.4 suppresses innate immune activation in *C. elegans*

PREFACE

This project initiated from a screen I performed using *fat-6(tm331);fat-7(wa36);irg-4p::GFP* animals on a transcription factor (TF) library. The hypothesis was that a TF would sense oleate as a measure of cellular energy stores and in low oleate states a TF which lacks its ligand represses immune responses. Thus, lack of this TF would allow immune responses to be activated in the absence of oleate. T26A8.4 was identified but further characterization proved it also increased basal expression in wild-type animals. Thus, the investigation of T26A8.4 diverged from my main project. This is some of the data that was gathered put into the context of a potential manuscript for future use.

ABSTRACT

The co-evolution of our intestinal epithelial cells with bacteria resulted in selection pressure for mechanisms of immune regulation to prevent detrimental inflammatory responses. Transcription factors (TFs) play a large part in tightly monitoring physiological conditions and controlling transcriptional output, for both repressed basal expression and activation upon infection. Using a reverse genetic screen to identify transcriptional suppressors of immune responses in *C. elegans* we identified the zinc finger transcription factor T26A8.4. In its absence, both the basal and inducible expression of specific innate immune genes are increased. This leads to an increase in lifespan during infection. It acts downstream or independently of the known p38 MAPK pathway. The physiological role of this transcription factor may be to aid in recovery

from infection. The exact mechanism of T26A8.4 in the suppression of *C. elegans* innate immune response remains to be determined.

INTRODUCTION

Transcription factors (TFs) bind to specific DNA sequences to control expression of the genome. There are different categories of TFs, such as zinc finger or nuclear hormone receptors (NHR), that can be activators or repressors of gene expression. Some TFs require a ligand to change conformation and exert control over gene levels, while others require phosphorylation. Certain TFs are expressed ubiquitously across tissues to ensure homeostasis and others have specific functions in different organs. The diversity of transcription factors allows for tight control of transcriptional responses in the presence of specific stimuli. In *C. elegans,* many of these TFs are conserved making them an excellent model to uncover functions of unknown TFs or orphan receptors.

As in humans, *C. elegans* require tight transcriptional control of innate immune responses. We have previously shown that the TF NHR-86, a homolog of the human HNF4, is required for transcription of several innate immune effectors. NHR-86 binds directly to the promoters of the immune genes *irg-4* and *irg-5* upon stimulation with an immunostimulatory small molecule [21]. These infection response genes (irg) are induced by *P. aeruginosa* and required for survival during infection. Therefore, NHR-86 controls anti-pathogen responses in C*. elegans*. Thus, activation of TFs is required for maintaining homeostasis when organisms encounter stressful environments but the failure to turn off these transcriptional responses can be detrimental [47, 79] Here, we

show that the zinc finger TF T26A8.4 suppresses the transcription of several innate immune genes and anti-pathogen responses. This seems to be downstream or parallel to the p38 MAPK pathway. The physiological role of this TF may be to help repress innate immune functions during recovery to aid in survival after pathogen infection.

RESULTS

RNAi screen identifies T26A8.4 as a suppressor of specific innate immune genes

To identify TFs that may suppress innate immune responses in *C. elegans* we screened a transcription factor library for genes that suppress immune gene induction. We used an immunostimulatory small molecule called R24 (also called RPW-24) and a GFP-based transcriptional reporter, *irg-4::GFP,* which provides a convenient readout of innate immune activation [21, 23, 46, 144]. The gene *irg-4* (F08G5.6) is transcriptionally upregulated during infection with multiple pathogens and contains a CUB-like domain, which is present in many of the secreted immune effectors in *C. elegans* [7, 21, 43]. Of the approximately 1,200 genes screened, knockdown of 19 transcription factors further increased *irg-4p::GFP* induction on R24 (Table 1). Knockdown of T26A8.4 resulted in a dramatic increase of *irg-4*$_p$*::GFP* and *irg-5*$_p$*::GFP* expression compared to control RNAi on our small molecule R24 (Fig. 1A and 1B). Under basal conditions, on normal *E. coli* diet, or 24 hours after *P. aeruginosa* infection we also observed a significant increase in GFP expression for *irg-4* and *irg-5* with knockdown of T26A8.4 by RNAi compared to control RNAi (Fig. 1C and 1D). Next, we confirmed these transcriptional responses by qRT-PCR and saw significant differences in both *irg-4* and *irg-5* (Fig. 1E). However, *irg-*

1 and *irg-2* were not induced by T26A8.4 RNAi during infection or on *E. coli* (Fig 1E). This suggests that loss of T26A8.4 is inducing selective innate immune genes and not leading to an overall increase of gene expression.

A loss-of-function mutation in T26A8.4 is lethal. To test if loss of this gene initiates toxic effects through organelle stress, we utilized heat shock protein (*hsp)* transcriptional reporters. To study mitochondrial stress, we utilized an *hsp-6*$_p$*::GFP* reporter which is activated by perturbed mitochondrial function, such as loss of the mitochondrial protease *spg-7* [145]. However, *hsp-6* was not increased after knockdown of T26A8.4, despite robust induction by *spg-7(RNAi)* (Fig. 2A). Endoplasmic reticulum (ER) stress, measured by *hsp-4* induction, which is activated by our small molecule R24 among other stressors, was also not activated after loss of T26A8.4 (Fig. 2B). Together, this data suggests that loss of T26A8.4 does not activate innate immune genes as a secondary reaction to mitochondrial or ER stress responses.

Lastly, we confirmed the results from our RNAi experiments in a T26A8.4 mutant. To counteract the lethality of the loss of T26A8.4 we obtained a mutant balancer strain that has an approximately 7% rate of homozygous mutant animals. Animals segregate as GFP positive, which carries the genetic balancer expressing wild-type T26A8.4 gene, or GFP negative which is homozygous for a mutation in T26A8.4. Animals were picked at approximately L4 stage for qRT-PCR. This revealed a significant increase in *irg-4* and *irg-5* expression in the T26A8.4 homozygous mutants (GFP-) compared to GFP+ siblings (Fig. 1F). Together, these data show that T26A8.4 is required to suppress expression of select innate immune genes.

T26A8.4 suppresses anti-pathogen responses

To understand if this increase of innate immune genes provides protection from pathogen infection, we grew animals on T26A8.4 or control RNAi until L4 stage and then picked animals to *P. aeruginosa*. We found a significant increase in lifespan when animals were grown on T26A8.4 RNAi (Fig. 3A and Table 2). Next, we tested if this lifespan extension also occurred in our T26A8.4(gk917) mutant animals. Indeed, GFP- animals homozygous for the T26A8.4 mutation had extended lifespan compared to the GFP+ wild-type animals (Fig. 3B and Table 2). Together this indicates that T26A8.4 suppresses anti-pathogen responses during pathogen infection.

Loss of T26A8.4 activates innate immune genes independent or downstream of the p38 MAPK pathway

Due to the specific transcriptional control of T26A8.4 we sought to identify if this TF functioned upstream of a specific immune pathway. Loss of T26A8.4 significantly increased the immune effectors *irg-4* and *irg-5*, whose basal, or resting, expression is dependent on the p38 MAPK PMK-1 innate immune pathway, but not *irg-1* and *irg-2*, whose transcription are regulated independent of this canonical immune pathway. This suggested we look towards the p38 MAPK PMK-1 pathway. First, we looked at TIR-1, the adaptor protein that is responsible for initiating the phosphorylation cascade which activates the PMK-1. We found that T26A8.4 RNAi treatment in a *tir-1(qd4)* loss-of-function mutant was still able to increase survival during infection with *P. aeruginosa* (Fig. 4A and Table 2). Next, we tested PMK-1 and found that knockdown of T26A8.4 in a *pmk-1(km25)* loss-of-function mutant was also able to increase lifespan during

infection (Fig. 4B and Table 2). Lastly, we looked at the epistasis with a TF that is directly downstream of the p38 MAPK PMK-1 pathway, ATF-7. An *atf-7(qd22 qd130)* loss of function mutant is hypersusceptibility to infection but T26A8.4 RNAi was able to decrease this susceptibility (Fig. 4C and Table 2).

To confirm this lifespan extension was due to increased immune effector induction, we collected wild-type or *tir-1(qd4)* mutant animals grown on control or T26A8.4 RNAi for qRT-PCR. We found that even in the *tir-1(qd4)* mutant animals T26A8.4 RNAi increased expression of *irg-5* under basal conditions and during infection with *P. aeruginosa* (Fig. 4D). T24B8.5 is another p38 MAPK dependent immune effector. Utilizing a GFP transcriptional report for T24B8.5, we found that T26A8.4 RNAi also increases induction of this immune effector (Fig. 4E). An *atf-7(qd22 qd130)* mutant reduces T24B8.5$_p$::GFP expression but treatment with T26A8.4 RNAi further induced GFP expression. This suggests that T26A8.4 acts independent of the p38 MAPK PMK-1 pathway to control innate immune responses in *C. elegans.*

T26A8.4 may be important for recovery from infection

Next, we wanted to understand the physiological role of T26A8.4. We hypothesized that suppression of immune responses must exist to aid in recovery after an animal encounters a pathogen. To test this hypothesis, we exposed control or T26A8.4 RNAi animals to *P. aeruginosa* at L4 stage and transferred to *E. coli* after 10 hours to mimic an initial encounter with pathogen and assess their ability to recover from infection. As seen before, when T26A8.4 animals were exposed to pathogen and then transferred to new *P. aeruginosa* plates they survived longer than control RNAi

animals (Fig. 5 and Table 3). However, when animals were transferred from pathogen to normal *E. coli* food source, they died significantly faster than control RNAi (Fig. 5 and Table 3). Interestingly, Loss of T26A8.4 in uninfected animals on non-pathogenic *E. coli* was detrimental to their overall lifespan (Fig. 5 and Table 3). This supports previous observations that an overactivated immune response is toxic to *C. elegans* causing a decrease in lifespan [47, 122].

CONCLUSIONS

Here we show that the TF T26A8.4 suppresses specific innate immune genes including p38 MAPK targets *irg-4, irg-5*, and T24B8.5 under baseline and inducible conditions. However, T26A8.4 regulates immune responses independently of the p38 MAPK pathway. We confirmed that T26A8.4 mutant animals also have increased lifespan during infection. Lastly, we identified a potential physiological role for T26A8.4 in recovery from pathogen infection. Together, these data suggest that T26A8.4 is a critical TF for *C. elegans* immune homeostasis.

In the wild, *C. elegans* forage for bacteria on rotting fruit. Sometimes they come upon pathogenic bacteria and must respond accordingly. TFs are key regulators to ensure properly controlled immune responses that react quickly when needed but do not activate toxic immune responses unnecessarily, especially once pathogenic bacteria have been avoided. It remains to be determined the exact mechanism by which T26A8.4 controls these anti-pathogen responses. It may be acting directly by binding to the promoters of these genes to suppress transcription. Other research suggests it may be a subunit of the Ccr4-NOT complex which aids in many functions from mRNA

transcription initiation to degradation [146]. Indeed, as a subunit, T26A8.4 may be required to bind to selective mRNA sequences to negatively regulate innate immune transcripts. Alternatively, T26A8.4 may be required to suppress these innate immune genes indirectly by controlling a separate pathway.

Understanding how specific TFs control anti-pathogen responses and immune homeostasis will allow us to extrapolate these findings to mammals for treatment of diseases. Indeed, lack of T26A8.4 increased lifespan and immune gene induction of p38 MAPK mutants during infection. This indicates that manipulation of certain TFs could help immunocompromised individuals mount protective responses. As we address antibiotic resistance and identify other mechanisms that can be used to help fight infections, understanding the role of specific TFs will be an interesting area to investigate. In addition, it is important to identify the molecular causes of aberrant immune activation for developing novel targeted therapies for autoimmune diseases.

FIGURES AND TABLES

Genes that increased *irg-4::GFP* induction on R24

RNAi control
nhr-23
nhr-7
C16A3.4
F28C6.1
zfp-3
T11G6.8
hbl-1
hmg-4
C52B9.2
unc-62
pop-1
C27D6.4
Y65B4BR.5
C52E12.1
lpd-2
gei-17
T26A8.4
bed-2
nhr-8

Reporter induction key
0
1
2
3

Table 1: Results of RNAi Screen. Genes identified in an RNAi screen for transcription factors that suppress the induction of *irg-4*$_p$*::GFP* on R24.

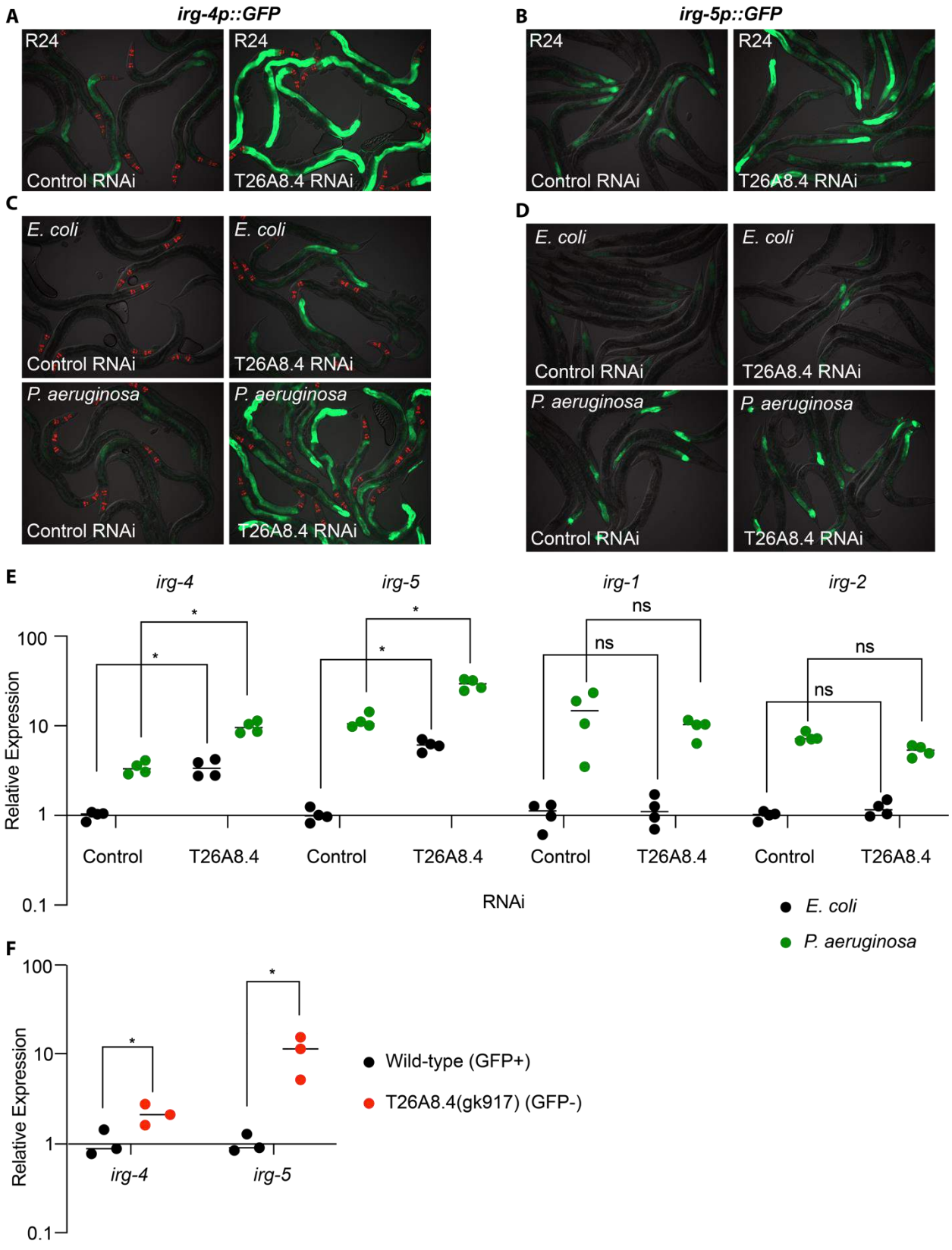

Figure 1: Loss of T26A8.4 increases basal expression and induction of specific

innate immune genes. A. The *C. elegans irg-4p::GFP* immune reporter or **B.** *irg-5p::GFP* immune reporter was exposed to control or T26A8.4 RNAi bacteria. The animals were transferred at the L4 stage to plates containing R24 for approximately 18 hours. Red pharyngeal expression is the *myo-2::mCherry* co-injection marker, which confirms the presence of the transgene. The irg-5p::GFP animals all had a Rol phenotype, which confirms the presence of the transgene. **C.** Animals containing the *irg-4p::GFP* immune reporter or **D.** the irg-5p::GFP immune reporter were grown as described above and exposed to E. coli or P. aeruginosa for approximately 24 hours. **E.** Expression of the indicated immune effectors were determined using qRT-PCR in wild-type animals grown on control or T26A8.4 RNAi bacteria exposed to *P. aeruginosa* or *E. coli* control for six hours. Data are the average of four independent replicates, each normalized to two control genes. Significance was determined by two-way ANOVA, * $p<0.05$. **F.** Expression of *irg-4* and *irg-5* were determined using qRT-PCR in T26A8.4(gk917) animals with a genetic balancer (GFP+) or without (GFP-) at L4 stage. Data are the average of three independent replicates, each normalized to two control genes. Significance was determined by multiple *t*-tests, * $p<0.05$.

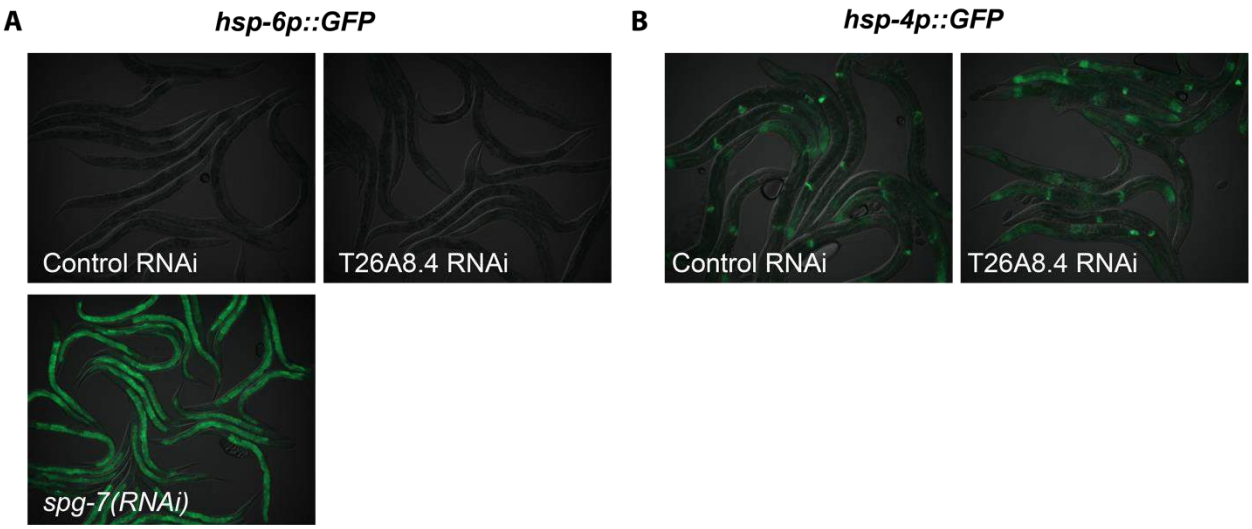

Figure 2: Loss of T26A8.4 does not activate mitochondrial or ER stress. A. The *C. elegans hsp-6p::GFP* immune reporter grown on indicated RNAi until L4 stage. **B.** The *C. elegans hsp-4p::GFP* immune reporter was exposed to control or T26A8.4 RNAi bacteria and imaged at L4 stage.

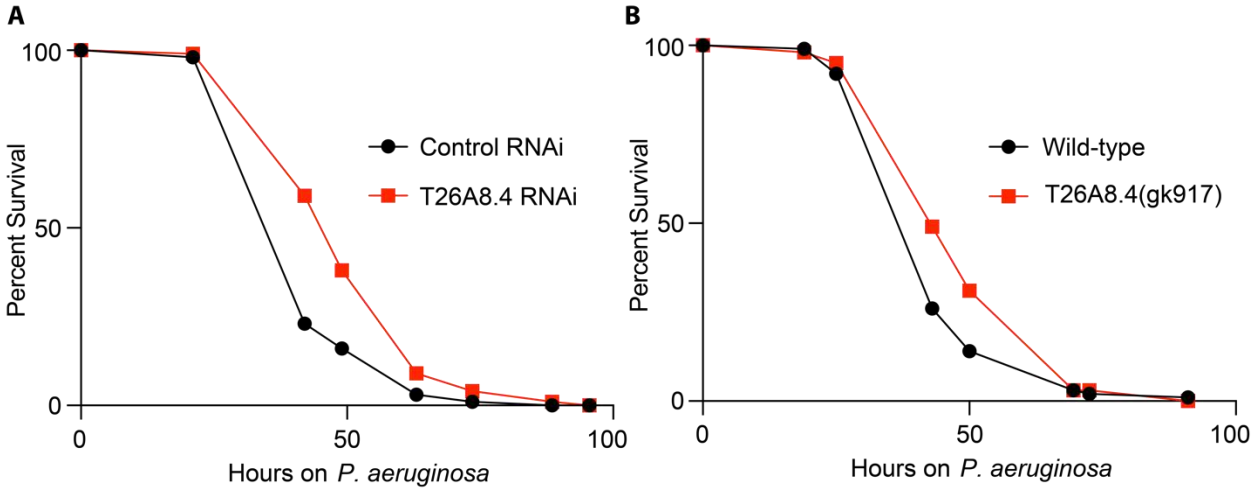

Figure 3: T26A8.4 suppresses anti-pathogen responses. A. *P. aeruginosa* pathogenesis assays of indicated conditions. Animals were transferred at the L4 stage to plates containing *P. aeruginosa*. **A.** Wild-type worms grown on control or T26A8.4

RNAi bacteria. T26A8.4 RNAi is more resistant to killing by *P. aeruginosa* ($p<0.05$). **B.** *P. aeruginosa* pathogenesis assay of T26A8.4(gk914) animals. Wild-type animals are T26A8.4(gk917) animals that carry a genetic balancer (GFP+) with a wild-type copy of T26A8.4. T26A8.4(gk917) (GFP-) is more resistant to killing by *P. aeruginosa* ($p<0.05$). Both A and B data are representative of two trials. Sample sizes, mean lifespan and p values for both trials are shown in Table 2. Significance was determined using Kaplan-Meier survival curves and log-rank tests.

Date	Genotype	RNAi	n	Mean lifespan (hours)		RNAi	n	Mean lifespan (hours)	P value vs. Control RNAi
12.9.19	*irg-4p::GFP*	Control	120	45.74±0.9		T26A8.4	116	52.91±1.2	<0.05
3.9.20	T24B8.5p::GFP	Control	149	48.4±0.82		T26A8.6	142	51.14±1.09	<0.05
p38 MAPK Epistasis									
7.27.20	N2	Control	159	45.69±0.66		T26A8.4	196	56.9±0.95	<0.05
	tir-1(qd4)	Control	126	27.85±0.66		T26A8.4	140	47.38±1.29	<0.05
7.20.20	N2	Control	181	51.07±0.83		T26A8.4	172	58.63±1.10	<0.05
	pmk-1(km25)	Control	153	26.44±0.60		T26A8.4	163	44.29±1.14	<0.05
8.3.20	N2	Control	174	51.49±1.14		T26A8.4	138	54.3±1.25	ns
	atf-7(qd22 qd130)	Control	100	40.78±0.89		T26A8.4	129	46.28±0.96	<0.05
Date	**Genotype**	**RNAi**	**n**	**Mean lifespan (hours)**		**Genotype**	**n**	**Mean lifespan (hours)**	**P value GFP+ vs GFP -**
9.14.20	T26A8.4(gk917) GFP+	NA	207	46.49±0.87		T26A8.4(gk917) GFP-	208	52.12±1.01	<0.05
10.12.20	T26A8.4(gk917) GFP+	NA	165	47.80±1.18		T26A8.4(gk917) GFP-	207	51.76±0.97	<0.05

Table 2: Killing Assay Statistics. Sample sizes, mean lifespan, and p values for all trials of the *C. elegans* pathogenesis assays in Figures 3 and 4.

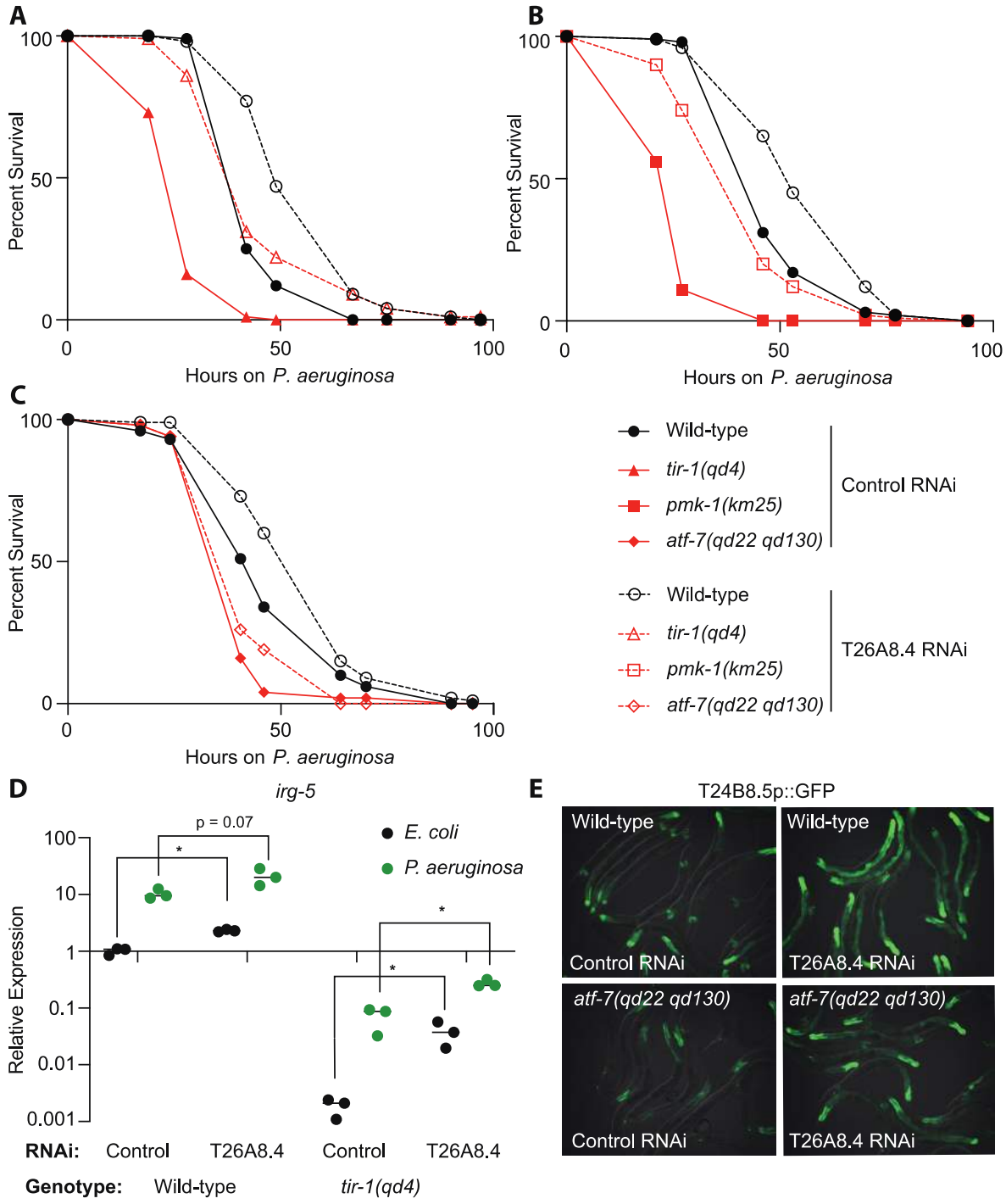

Figure 4: Lack of T26A8.4 induces gene expression in parallel or downstream of the canonical p38 MAPK pathway. A-C. Pilot *P. aeruginosa* pathogenesis assays of wild-type and the indicated mutant worms grown on control or T26A8.4 RNAi are

presented. See Table 2 for sample sizes, mean lifespan and p values. Significance was determined using Kaplan-Meier survival curves and log-rank tests. **D.** Expression of *irg-5* was determined using qRT-PCR in wild-type or *tir-1(qd4)* animals grown on control or T26A8.4 RNAi bacteria exposed to *P. aeruginosa* or *E. coli* control for six hours. Data are the average of three independent replicates, each normalized to two control genes. Significance was determined by two-way ANOVA, * p<0.05. **E.** The T24B8.5p::GFP immune reporter in the indicated genetic background were grown on control or T26A8.4 RNAi and exposed as L4s to *E. coli* or *P. aeruginosa* for approximately 24 hours.

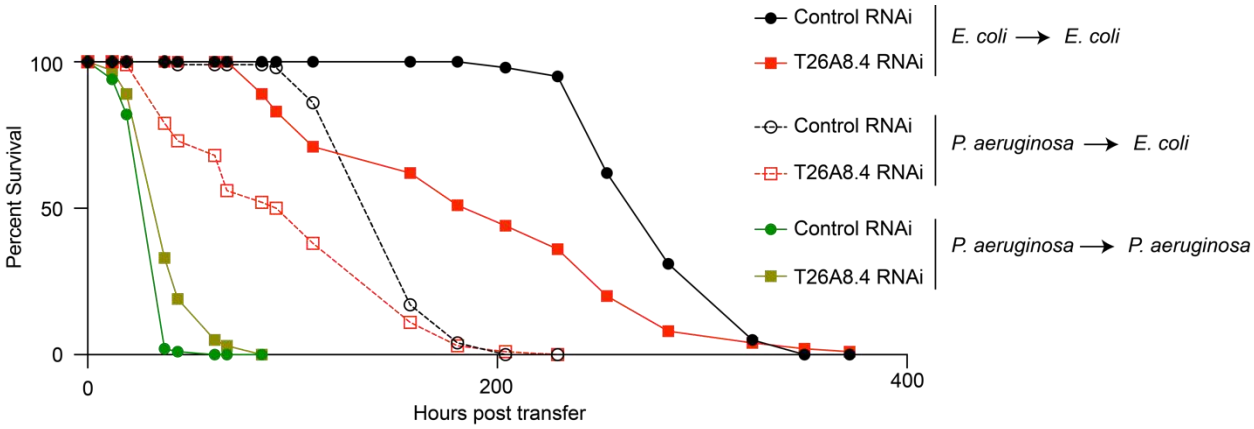

Figure 5: T26A8.4 may be required for recovery from pathogen infection. Animals grown on control or T26A8.4 RNAi were exposed as L4s to *P. aeruginosa* or *E. coli* and transferred to indicated condition after 10 hours (see methods). Data is representative of three trials. Sample sizes, mean lifespan and p values for all trials are shown in Table 3. Significance was determined using Kaplan-Meier survival curves and log-rank tests.

Date	Genotype	RNAi	n	Mean lifespan (hours)		RNAi	n	Mean lifespan (hours)	P value vs. Control RNAi
E. coli --> E. coli									
11.17.20	N2	Control	174	280.38±5.24		T26A8.4	139	225.86±8.38	<0.01
12.7.20	N2	Control	61	284.61±4.34		T26A8.4	90	197.00±8.4	<0.01
12.14.20	N2	Control	106	321.46±5.56		T26A8.4	68	192.25±9.32	<0.01
P. aeruginosa --> E. coli									
11.17.20	N2	Control	155	204.08±5.86		T26A8.4	153	118.27±5.69	<0.01
12.7.20	N2	Control	140	154.89±2.05		T26A8.4	94	103.61±5.68	<0.01
12.14.20	N2	Control	109	181.61±3.25		T26A8.4	43	80.14±6.38	<0.01
P. aeruginosa --> P. aeruginosa									
11.17.20	N2	Control	219	36.62±0.61		T26A8.4	194	40.02±0.96	<0.01
12.7.20	N2	Control	96	34.11±0.88		T26A8.4	63	41.64±1.82	<0.01
12.14.20	N2	Control	158	36.19±0.69		T26A8.4	165	41.71±1.04	<0.01

Table 3: Recovery Assay Statistics. Sample sizes, mean lifespan, and p values for all trials of the *C. elegans* recovery assays in Figure 5.

MATERIALS AND METHODS

***C. elegans* and bacterial strains.** *C. elegans* strains were maintained on *E. coli* OP50 bacteria on nematode growth media plates, as described [62]. The *C. elegans* strains used in this study were N2 Bristol [62], AU306 *agIs43* [*irg-4::GFP::unc-54-3'UTR; myo-2::mCherry*] [23], AY101 *acIs101* [p*DB09.1(irg-5::gfp)*; p*RF4(rol-6(su1006))*] [63], AU78 agls219 [T24B8.5::GFP::unc-54-3' UTR] [147], VC2081 T26A8.4(gk917) IV/nT1 [qIs51], ZD101 *tir-1(qd4)* [147], KU25 *pmk-1(km25)* [100], ZD318 agls219 [T24B8.5::GFP::unc-54-3' UTR];atf-7(qd22 qd130) [44], *hsp-6p::GP, hsp-4p::GFP [148]. P. aeruginosa* strain PA14 [3] was used in this study.

***C. elegans* Bacterial Infection and Other Assays.** "Slow killing" *P. aeruginosa* pathogenesis assays were performed as previously described [67]. The protocol for treatment of animals with 70 μM R24 has also been described [46]. For all assays, L4 stage-matched animals raised from the L1 stage on indicated media were transferred to standard assay plates for the indicated experiment, which were not supplemented with fatty acids. Sample sizes, mean lifespan, and p values for all trials are shown in Table 2 and Table 3. The RNAi screen was performed as previously described [21]. RNAi clones that were used in this study are from the Ahringer [70] or Vidal [71] libraries and were confirmed by sequencing.

***C. elegans* Recovery Assays**

Animals were picked to *P. aeruginosa* or *E. coli* plates with FUDR as described for "slow killing" assays [43]. After 10 hours, animals were washed with M9 three times, and dropped to NGM seeded with *E. coli*. After 1-2 hours, animals were picked to fresh *P. aeruginosa* or *E. coli* "slow killing" plates with FUDR. Animals were scored 1-2 times daily and transferred to fresh plates as needed to prevent contamination. Animals with exploded vulvas or bagging were censored from experiment.

Quantitative RT-PCR (qRT-PCR). The qRT-PCR studies were performed as described previously [23, 46, 47], using previously published primer sequences [7, 23, 36, 46, 47]. All values were normalized against the control gene *snb-1* and *act-3*. Fold change was calculated using the 2 (-DeltaDeltaC(T)) method [149].

Microscopy. Nematodes were paralyzed with 10 mM levamisole (Sigma), mounted on agar pads and photographed using a Zeiss AXIO Imager Z2 microscope with a Zeiss Axiocam 506mono camera and Zen 2.3 (Zeiss) software.

Statistical Analyses. *C. elegans* survival was assessed using the Kaplan-Meier method and differences were determined with the log-rank test using OASIS 2 [75]. Other statistical tests, which are indicated in the figure legends, were performed using Prism 7 (GraphPad Software).

Appendix II: The nuclear hormone receptor NHR-86 controls anti-pathogen responses in *C. elegans*

PREFACE

The work presented in Appendix II was adapted from the published work "The nuclear hormone receptor NHR-86 controls anti-pathogen responses in *C. elegans"* where Nicholas Peterson and Hilary Cheesman are co-first authors, Pengpeng Liu is the third author, I am the fourth author, Kyle Foster, Richa Chhaya, Paola Perrat, Jose Thekkiniath, Qiyuan Yang, and Cole Haynes are the middle authors, and Read Pukkila-Worley is the last author. I was responsible for qPCR experiments in Figure S4, with NHR-86 mutants during *P. aeruginosa* infection. I was also responsible for the initial observation that R24 causes induction of *hsp-4* and that *irg-4* is not activated by ER stressors, such as tunicamycin (Figure S3B and C). Lastly, I quantified the levels of spliced versus total *xbp-1* mRNA by qRT-PCR to further characterize the ER stress response on R24 and the role of NHR-86 in this response (Figure 4C). All other figures and data analysis were performed collaboratively by Nicholas Peterson, Hilary Cheesman, Pengpeng Liu, Kyle Foster, Richa Chhaya, Paula Perrat, Jose Thekkiniath, and Qiyuan Yang.

ABSTRACT

Nuclear hormone receptors (NHRs) are ligand-gated transcription factors that control adaptive host responses following recognition of specific endogenous or exogenous ligands. Although NHRs have expanded dramatically in *C.*

elegans compared to other metazoans, the biological function of only a few of these genes has been characterized in detail. Here, we demonstrate that an NHR can activate an anti-pathogen transcriptional program. Using genetic epistasis experiments, transcriptome profiling analyses and chromatin immunoprecipitation-sequencing, we show that, in the presence of an immunostimulatory small molecule, NHR-86 binds to the promoters of immune effectors to activate their transcription. NHR-86 is not required for resistance to the bacterial pathogen *Pseudomonas aeruginosa* at baseline, but activation of NHR-86 by this compound drives a transcriptional program that provides protection against this pathogen. Interestingly, NHR-86 targets immune effectors whose basal regulation requires the canonical p38 MAPK PMK-1 immune pathway. However, NHR-86 functions independently of PMK-1 and modulates the transcription of these infection response genes directly. These findings characterize a new transcriptional regulator in *C. elegans* that can induce a protective host response towards a bacterial pathogen.

INTRODUCTION

Nuclear hormone receptors (NHRs) are transcription factors that regulate a number of key biological processes following recognition of specific exogenous or endogenous ligands. Interestingly, the genomes of *Caenorhabditis* species contain a large number of NHRs compared to other metazoans [150]. 284 NHRs are present in *C. elegans*, whereas *Drosophila* and humans have only 21 and 48, respectively [151]. The marked expansion of NHRs suggests that these proteins play particularly important roles in nematode physiology [151, 152]; however, only a very small minority of *C.*

elegans NHRs have been characterized in detail [151]. Like other metazoans, *C. elegans* rely on inducible host defense mechanisms during infection with bacterial pathogens [40, 42, 48, 153]. The mechanisms that engage these immune defenses are not completely understood. Considering their roles as intracellular sensors of specific ligands, we hypothesized that NHRs function in innate immune activation in *C. elegans*. However, forward genetic screens did not previously identify an NHR that is necessary for pathogen resistance [44, 100]. We, therefore, designed a genetic screen to determine if an NHR could activate protective immune defenses in *C. elegans*.

Utilizing a potent immunostimulatory small molecule as a chemical probe, we identified NHR-86 and showed that it drives a transcriptional response that protects *C. elegans* from infection with the bacterial pathogen *Pseudomonas aeruginosa*. NHR-86 is a homolog of mammalian hepatocyte nuclear factor 4 (HNF4), an NHR that has been implicated in the pathogenesis of inflammatory bowel disease [154-157]. We show that, in the presence of an immunostimulatory small molecule, NHR-86 induces innate immune defenses by binding to the promoters of immune effectors, in a manner that does not require the canonical p38 MAPK PMK-1 pathway. In this context, PMK-1 sets the basal expression of innate immune response genes, but is dispensable for their induction by NHR-86. These data demonstrate a new mechanism by which immune defenses are engaged to protect the worm and raise the possibility that the expansion of the NHR family in *C. elegans* may have been fueled, at least in part, by the roles of these proteins in the activation of host defense responses.

RESULTS

An RNAi screen identifies a role for the nuclear hormone receptor nhr-86 in the induction of *C. elegans* immune effectors

To determine if an NHR can induce protective immune responses, 258 of the 284 NHR genes in the *C*. *elegans* genome were screened by RNAi using the *C*. *elegans* *Pirg-4*(F08G5.6)::*GFP* transcriptional immune reporter and the immunostimulatory xenobiotic R24 [158]. R24 (also referred to as RPW-24) was originally identified in a screen of 37,214 small molecules for new anti-infective compounds [144]. This molecule robustly activates innate immune defenses and protects nematodes infected with bacterial pathogens [23, 46-48]. For this screen, the *Pirg-4*::*GFP* transcriptional reporter was chosen as a convenient readout of immune activation. IRG-4 (infection response gene-4) contains a CUB-like domain, a group of secreted proteins that are postulated to play a role in host defense [7]. Basal levels of *irg-4* transcription are controlled by the p38 MAPK PMK-1 pathway [7]. This gene is induced during infection by multiple bacterial pathogens, including *P*. *aeruginosa,* and by the small molecule R24 [7, 23, 46, 47, 63, 159-161]. RNAi-mediated knockdown of ten NHRs partially affected the R24-mediated induction of *Pirg-4*::*GFP* by R24 (S1 Table), but only one NHR (*nhr-86*) completely abrogated the upregulation of this immune reporter (Figure 1A).

We confirmed the results of the *nhr-86(RNAi)* experiment using several approaches. The previously characterized null allele *nhr-86(tm2590)*, which contains a 172 bp deletion that removes 33 bp in exon 4 of *nhr-86*, suppressed *Pirg-4*::*GFP* induction by R24 (Fig 1A and 1C). CRISPR-Cas9 was used to generate a clean deletion of *nhr-86 [nhr-86(ums12)]* (Figure 1B). *ums12* is a 5.5 kb deletion that removes

nearly all of the *nhr-86* coding region, which caused a marked reduction in the *nhr-86* transcript (S1A Figure). The *nhr-86(ums12)* mutation fully suppressed the induction of *Pirg-4*::*GFP* by R24 (Figure 1A and 1C).

In addition to *irg-4*, *nhr-86* is required for the R24-dependent transcriptional upregulation of two additional immune effectors that contain CUB-like domains, *irg-5* (F35E12.5) and *irg-6* (C32H11.1) (Figures 1 and S1B). Like *irg-4*, *irg-5* and *irg-6* are induced by several different bacterial pathogens, require the p38 MAPK PMK-1 pathway for their basal transcriptional levels, and are induced in accordance with the virulence potential of the pathogen [7, 23, 63, 159-162]. R24-mediated induction of the *Pirg-5*::*GFP* transgene was abrogated by *nhr-86(RNAi)* and in the *nhr-86(tm2590)* background (Figure 1A). In addition, qRT-PCR of *irg-5* and *irg-6* showed that *nhr-86* loss-of-function mutations suppress induction by R24 (Figures 1C and S1B).

Interestingly, RNAi-mediated knockdown of *irg-4* renders worms hyper-susceptible to killing by *P*. *aeruginosa* [28, 90]. Importantly, *irg-4* knockdown does not shorten the lifespan of nematodes growing on *E*. *coli* OP50, the normal laboratory food source, nor does its knockdown cause susceptibility to other stressors [28, 90]. We confirmed these observations and also found that *irg-5(RNAi)* and *irg-6(RNAi)* animals are more susceptible to killing by *P*. *aeruginosa* (S1C Figure). As with *irg-4(RNAi)*, knockdown of *irg-5* or *irg-6* did not shorten the lifespan of *C. elegans* growing on *E*. *coli* OP50 (S1D Figure). Thus, *nhr-86* drives the induction of at least three innate immune effectors that confer resistance to *P*. *aeruginosa* infection.

nhr-86 **activates the transcription of innate immune response genes**

To define the genes that are dependent on *nhr*-86 for their transcription, we performed mRNA-sequencing. We compared the mRNA expression profiles of wild-type animals and two different *nhr-86* loss-of-function alleles (*tm2590* and *ums12*), each exposed to the immunostimulatory molecule R24 or mock treatment. Exposure to R24 caused the induction of 391 genes, which (as in previous studies) were enriched for innate immune response and xenobiotic detoxification genes [23, 46, 47]. The upregulation of 147 of these genes in the *nhr-86*(*tm2590)* mutants and 205 genes in the *nhr-86(ums12)* mutants were significantly attenuated (Figure 2A). Importantly, the mRNA expression patterns of both *nhr-86* loss-of-function mutants were tightly correlated (Figure 2B) with 142 misregulated genes in common between these two datasets (S2 Table). Analysis of these 142 *nhr-86*-dependent genes revealed a significant enrichment of innate immune genes and those involved in the defense response to bacterial pathogens (Figure 2A and 2C). Included among these *nhr-86*-dependent genes are the representative immune effectors *irg-4*, *irg-5*, *irg-6*, *mul-1*(F49F1.6) and *drd-50*(F49F1.1) (Fig 2A). *mul-1* and *drd-50* are induced during infection with multiple bacterial pathogens, including *P*. *aeruginosa* [7, 23, 63, 159, 161, 162].

To confirm the results of our mRNA-seq data, we used a NanoString codeset to examine the expression of 118 innate immune and stress response genes in biological replicate RNA samples from wild-type and *nhr-86(tm2590)* animals (Figure 2D). From the NanoString codeset, we identified 28 genes induced by R24, 23 of which were pathogen-response genes. Of the 23 pathogen-response genes, we identified 22 that are dependent on *nhr-86* for their induction. The NanoString experiment also confirmed

the observation in the mRNA-seq experiment that *nhr-86* is not required for the induction of all R24-induced genes (Figure 2A and 2D). Interestingly, many of these genes that are upregulated by R24 in a manner independent of *nhr-86* are cytochrome P450s, which are involved in the detoxification of xenobiotics (Figure 2D and S2 Table). Thus, *nhr-86* is required for the upregulation of only a specific subset of the R24-induced genes, a group that is strongly enriched for innate immune effectors (Figure 2C).

Interestingly, examination of the mRNA-seq profiles of *C. elegans* that were not exposed to compound (*i.e.*, normal growth conditions or basal expression) revealed that the expression of 302 genes were significantly lower in the *nhr-86* loss-of-function mutants compared to wild-type animals (>2-fold change, PPEE<0.05) and only 11 of these genes were differentially regulated more than 4-fold (PPEE<0.05). Only 6 of these genes were among the 142 genes that required *nhr-86* for their induction by R24. Comparison of the basal expression of *irg-4*, *irg-5* and *irg-6* in the two *nhr-86* loss-of-function alleles with wild-type animals by qRT-PCR confirmed this observation (Figure 1C and S1B Figure). Thus, while *nhr-86* is necessary for the transcriptional induction of genes and innate immune effectors in particular, it is largely dispensable for their basal regulation.

NHR-86 binds to the promoters of innate immune genes to drive their transcription

To determine the direct targets of NHR-86 during R24 exposure, we performed chromatin immunoprecipitation-sequencing (ChIP-seq). Of the 142 genes that are

induced by R24 in an *nhr-86*-dependent manner, NHR-86 bound to the promoters of 32 of these genes following treatment with R24 compared to control (Figure 3A and S3 Table). All but one of these 32 genes are induced during infection with at least one bacterial pathogen, including 14 genes that are upregulated during infection with *P*. *aeruginosa* (S3 Table). Among the immune effectors whose transcription is directly regulated by NHR-86 are *irg-4* (Figure 3B), *irg-5* (Figure 3C), *mul-1* (Figure 3D), *drd-50* (Figure 3E) and *irg-6* (S3 Table). The ChIP-seq experiment was performed with a strain containing a GFP-tagged NHR-86 protein (NHR-86::GFP) that has been previously characterized [152]. The induction of *irg-4* by R24 was restored in *nhr-86(tm2590)* mutants, which contained this NHR-86::GFP construct (S2A Figure). ChIP followed by qPCR (ChIP-qPCR) was used to confirm that NHR-86 binds to the promoters of innate immune effectors following R24 treatment. Promoter regions associated with *irg-4* (Figure 3B), *irg-5* (Figure 3C), *mul-1* (Figure 3D) and *drd-50* (Figure 3E) were significantly enriched following R24 treatment, but not in samples exposed to the solvent control. In addition, these promoter regions were not enriched in either control or R24-exposed wild-type animals, which do not express NHR-86::GFP that was used to immunoprecipitate promoter fragments. Binding of NHR-86 to the promoters of immune response genes upon R24 treatment was associated with a corresponding increase in mRNA transcript levels of these genes, which was entirely abrogated in both *nhr-86* loss-of-function mutants (Figure 3B–3E). Importantly, a control region within the *irg-5* promoter (Figure 3C) and a random intergenic region on chromosome VI (Figure 3F) were not enriched in the ChIP-qPCR or ChIP-seq experiments. In addition, 110 genes were induced by R24 in an *nhr-86*-dependent

manner, but NHR-86 did not bind to their promoters. Of note, NHR-86 is expressed in the nuclei of *C. elegans* intestinal epithelial cells [152] and promotes the induction of the innate immune effectors *irg-4*::*GFP* and *irg-5*::*GFP* in the intestine (Figure 1A), the tissue that directly interfaces with ingested pathogens.

A motif analysis was performed on the promoters bound by NHR-86::GFP to identify putative regulatory sequences. A single 15 bp sequence was strongly enriched in these promoters (E-value: 1.7e-003, S2C Figure). 15 of the 32 genes whose transcription were directly regulated by NHR-86 in the presence of R24 contain this 15 bp element in their promoters, including *irg-4*, *irg-5* and *mul-1* (S3 Table). However, only 3 of 172 genes that are induced by R24 independent of NHR-86 contain this 15 bp element. These data suggest that this 15 bp sequence may be a potential binding site for NHR-86.

Together, the mRNA-seq and ChIP-seq data demonstrate that, in the presence of an immunostimulatory molecule, NHR-86 engages the promoters of innate immune effector genes to drive their transcription. Under normal growth conditions, *nhr-86* does not bind to the promoters of immune effectors (*e.g.*, *irg-4*, *irg-5*, *mul-1* and *drd-50*) and does not affect their basal expression. These data are the first demonstration of direct immune effector regulation by a nuclear hormone receptor in *C. elegans*.

The immune response induced by *nhr-86* protect a *C. elegans* from P. aeruginosa infection

To determine if *nhr-86* induces a physiologically relevant transcriptional response, we compared the susceptibility of the *nhr-86* loss-of-function mutants

to *P*. *aeruginosa* infection following exposure to R24. R24 protects wild-type *C. elegans* during *P*. *aeruginosa* infection [23, 46, 47]. Consistent with the key role of *nhr-86* in driving the induction of innate immune defenses, *nhr-86* loss-of-function mutants (*tm2590* and *ums12*) significantly suppressed the pathogen-resistance phenotype of R24-exposed wild-type worms (Figure 4A). Together, these data demonstrate that the defense response induced by *nhr-86* promotes host resistance to bacterial infection.

An alternate method of examining the physiological relevance of immune effector induction in *C. elegans* involves studying the effect of induced transcriptional responses on stress in the endoplasmic reticulum (ER). The induction of host immune effectors in *C. elegans* requires compensatory activation of the unfolded protein response (UPR) in the ER, presumably to handle the increase in proteins trafficking through this organelle [163, 164]. Accordingly, R24 exposure caused the induction of *Phsp-4*::*GFP*, a transcriptional reporter for the BiP/GRP78 homolog in *C. elegans*, which indicates UPR activation (Figure 4B). *hsp-4* transcription is regulated by the transcription factor XBP-1, which is activated by the ER-transmembrane protein IRE-1 when unfolded proteins accumulate in the ER. IRE-1 has RNase activity, which upon activation, cleaves *xbp-1* mRNA to change its reading frame and encode the active XBP-1 protein [165]. We found that exposure to R24 increased the active, spliced form of *xbp-1* (Figure 4C). Total *xbp-1* mRNA was also increased following R24 treatment (Figure 4C). Interestingly, knockdown of *nhr-86* suppressed *Phsp-4*::*GFP* induction (Figure 4B) and the accumulation of active *xbp-1* (Figure 4C) following exposure to the xenobiotic R24. In addition, animals deficient in *nsy-1*, the MAPKKK upstream of the p38 MAPK *pmk-1* (Figure 4B), and *pmk-1* (S3A Figure), failed to induce the *Phsp-*

4::*GFP* following exposure to R24. *pmk-1(km25)* mutants abrogated the cleaving of *xbp-1* into its active form (Figure 4C). Thus, R24-mediated immune induction activates the UPR, in a manner dependent on *nhr-86* and the p38 MAP *pmk-1* pathway.

We considered the possibility that R24 is a direct poison of the ER. However, tunicamycin, a potent inducer of ER stress and the UPR, did not activate the immune reporter *Pirg-4*::*GFP* (S3B Figure). In addition, RNAi-mediated knockdown of *nhr-86* did not suppress *Phsp-4*::*GFP* induction by tunicamycin (S3C Figure). Thus, ER stress itself does not lead to the induction of *nhr-86*-dependent innate immune responses, but rather occurs as a consequence of mobilizing this protective host response. These data are consistent with prior reports, which demonstrate that activation of the p38 MAPK *pmk-1* pathway is not dependent on IRE-1/XBP-1 [163, 164]. Together, these data demonstrate that the immune response induced by *nhr-86* following exposure to R24 is a physiologically relevant source of ER stress and provide further support for the conclusion that *nhr-86* activates a pathogen-defense response involving secreted proteins.

In the absence of R24, *C. elegans nhr-86* mutants are not more susceptible to *P. aeruginosa* infection than wild-type animals (Figure 4A). In addition, the induction of the innate immune effectors *irg-5, irg-6* and *irg-1* during *P. aeruginosa* infection is not attenuated in the *nhr-86(ums12)* mutant; however, the induction of *irg-4* is significantly lower (S4 Figure). Given the marked expansion of the NHR family in *C. elegans*, NHRs, or potentially another mechanism, may function redundantly with NHR-86 to activate host defense genes during *P. aeruginosa* infection. It is also possible that *P. aeruginosa* does not produce the ligand sensed by NHR-86.

nhr-86 induces innate immune defenses independent of the p38 MAPK *pmk-1*

The immunostimulatory molecule R24 upregulates innate immune effectors whose basal expression requires the p38 MAPK *pmk*-1 [46], a key signaling mediator in a pathway that is critically important for host defense against bacterial pathogens [7, 100]. To determine if *nhr-86* and *pmk-1* function in the same or distinct pathways in the transcriptional modulation of innate immune effector genes, we compared gene expression (Figures 5A and S5A) and pathogen resistance (Figure 5B) phenotypes of the *pmk-1(km25)* and *nhr-86(tm2590)* single mutants with the *pmk-1(km25); nhr-86(tm2590)* double mutant. We previously observed that R24 can extend the lifespan of *pmk-1(km25)* mutant animals that are infected with *P*. *aeruginosa* [[46] and Figure 5B]. In addition, we found that *pmk-1* is dispensable for the induction of a group of innate immune effectors, including *irg-4*, *irg-5*, *mul-1* and *drd-50* [[46], see also Figures 5A and S5A]. However, because the basal level of expression of these four effectors is decreased in the *pmk-1(km25)* mutant, the absolute level of immune effector expression following exposure to R24 is markedly lower compared to controls (Figures 5A and S5A). The deficiency in the basal regulation of immune effectors in the *pmk-1(km25)* mutant contributes to the enhanced susceptibility of this mutant to *P*. *aeruginosa* infection in both naive and R24-treated animals [7, 100] (Figure 5B). These data indicate that R24 drives the induction of a protective immune response independent of *pmk-1*. Consistent with this observation, exposure to R24 does not cause an increase in the percentage of active (phosphorylated) PMK-1 relative to total PMK-1 in wild-type or *nhr-86(ums12)* animals (Figure 5C and 5D).

The susceptibility of the *pmk-1(km25); nhr-86(tm2590)* double mutant to *P*. *aeruginosa* infection in the absence of R24 is identical to the *pmk-1(km25)* mutant, further suggesting that NHR-86 functions in an R24-dependent manner (Figure 5B). Importantly, the *nhr-86(tm2590)* allele suppressed the R24-mediated enhanced longevity in the *pmk-1(km25)* background (Figure 5B). Accordingly, the basal expression of *irg-4*, *irg-5*, *mul-1*, *drd-50* and *irg-6* is reduced in the *pmk-1(km25); nhr-86(tm2590)* double mutant to the same level as the *pmk-1(km25)* mutant (Figures 5A and S5A). Importantly, the R24-mediated induction of these immune effectors in the *pmk-1(km25)* background is blocked by the *nhr-86(tm2590)* mutation (Figures 5A and S5A).

Of note, the induction of at least two cytochrome P450 xenobiotic detoxification genes by R24 is not dependent on either *nhr-86* or *pmk-1* (S5B Figure). These data further support that *nhr-86* is required for only a specific subset of the R24-induced genes (Figure 2).

In summary, these genetic epistasis experiments support the model that, upon activation, NHR-86 traffics to the promoters of immune effectors to mount a protective immune response in a manner independent of the p38 MAPK *pmk-1* pathway (Figure 6). In this context, a principal role of the p38 MAPK *pmk-1* is to ensure basal resistance to pathogens by controlling the tonic expression of innate immune effectors, such as *irg-4*, *irg-5*, *mul-1* and *drd-50*.

DISCUSSION

This study extends the known functions of *C. elegans* NHRs to include the activation of anti-pathogen transcriptional responses. Following treatment with an immunostimulatory small molecule, NHR-86 directly activates innate immune effector transcription in a manner that promotes resistance to bacterial infection. ChIP-seq and mRNA-seq revealed an enrichment for innate immune effectors among the transcriptional targets of NHR-86, including at least three genes, *irg-4*, *irg-5* and *irg-6*, that are each required for normal resistance to *P*. *aeruginosa* infection. Consistent with this model, the induction of protective immune defenses by NHR-86 occurs independently of the p38 MAPK *pmk-1*. In addition, in the absence of an immunostimulatory molecule, NHR-86 is not required for the basal regulation and is not at the promoters of immune effectors. Arda *et al*. proposed that NHRs, and NHR-86 in particular, organize modular gene regulatory networks to facilitate the rapid coordination of adaptive responses to intracellular ligands [152]. Our data show that an anti-pathogen transcriptional response is one such adaptive response.

We previously demonstrated that a conserved component of the Mediator transcriptional regulatory complex, MDT-15/MED15, links detoxification and innate immune defenses in *C. elegans* [23]. The Mediator complex is conserved from yeasts to humans and regulates transcription by physically interacting with both transcriptional regulators and RNA polymerase II [166, 167]. Individual mediator subunits, particularly those like MDT-15, which are in the tail region of the complex, dictate the physical interactions with transcriptional regulators and play important roles in modulating specific transcriptional outputs [52, 166-168]. Like *nhr-86*, *mdt-15* is required for the induction of immune effectors whose basal expression is dependent on the p38 MAPK

PMK-1 pathway [23]. In addition, MDT-15 functions downstream of the PMK-1 cascade to control the expression of immune effectors [23]. Notably, a subset of the immune effectors in *mdt-15*-deficient animals, including *irg-4*, *irg-5*, and *drd-50* have reduced basal levels of expression [as in *pmk-1(km25)* mutants] and cannot be induced by the small molecule R24 (as in *nhr-86* loss-of-function mutants). Importantly, NHR-86 is known to physically interact with MDT-15 [152]. Thus, we hypothesize that MDT-15 and NHR-86 function together to drive the transcription of immune response genes, such as *irg-4*, *irg-5* and *drd-50*.

The ligand that activates NHR-86 is not known. Indeed, it is possible that R24 or a metabolite derived from this compound is an activating ligand of NHR-86. However, it is important to note that not all R24-induced genes are dependent on *nhr-86* for their upregulation. Alternatively, NHR-86 may detect a host-derived ligand that is associated with the toxic effects of R24 on nematode cells. R24 induces xenobiotic detoxification genes and shortens the lifespan of nematodes growing in standard laboratory conditions [46]. *C. elegans* activates immune defenses following toxin-mediated disruption of cellular homeostasis [41]. Thus, NHR-86 may function as part of a similar cellular surveillance mechanism, although this is not known. Notably, *nhr-86* loss-of-function mutants are not more susceptible to *P*. *aeruginosa* infection at baseline. While *nhr-86* is required for the induction of the immune effectors *irg-5* and *irg-6* by the immunostimulatory xenobiotic R24, it is dispensable for their induction during *P*. *aeruginosa* infection. Thus, it is possible that *P*. *aeruginosa* infection does not produce a ligand that is sensed by NHR-86 or there are redundant mechanisms engaged to activate *C. elegans* defenses during pseudomonal infection. In either case,

our data demonstrate that a *C. elegans* NHR can drive a protective transcriptional response towards a bacterial pathogen. These findings raise the possibility that NHRs provide a facile and evolutionarily adaptable mechanism to activate protective immune defenses in response to diverse ligands.

FIGURES

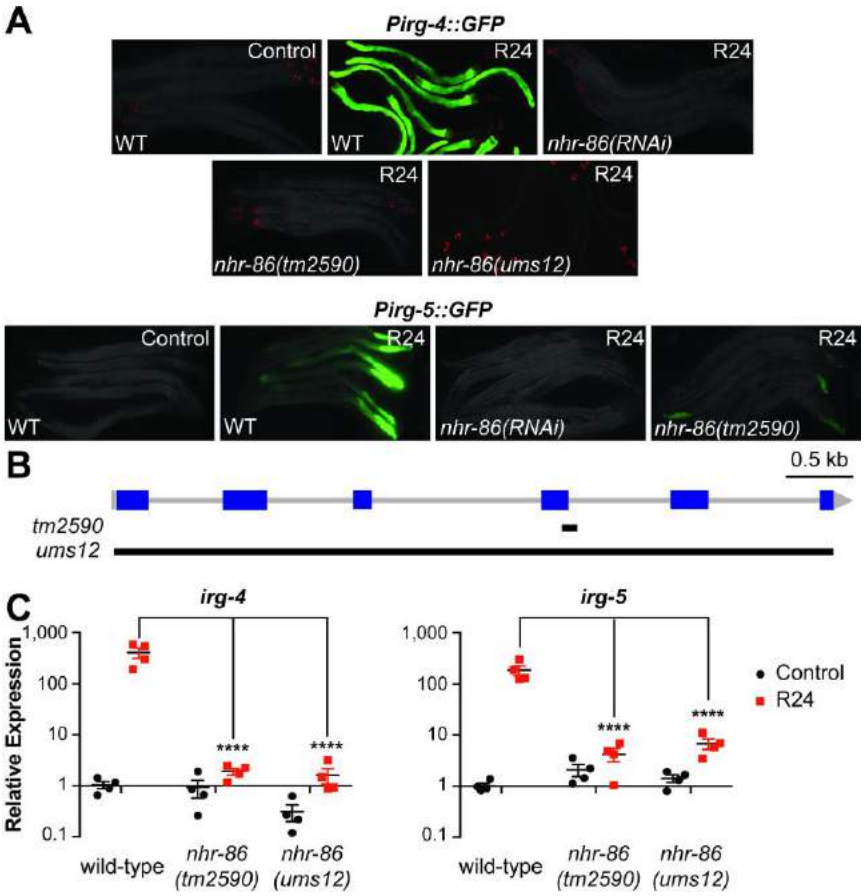

Figure 1. An RNAi screen identifies a role for the nuclear hormone receptor *nhr-86* in the induction of *C. elegans* immune effectors. (A) *C. elegans* carrying either the *Pirg-4*(F08G5.6)::*GFP* or the *Pirg-5*(F35E12.5)::*GFP* immune reporter of the indicated genotypes were transferred at the L4 stage to media supplemented with either R24 or the solvent control (1% DMSO) for approximately 18 hours. Red pharyngeal

expression is the *Pmyo-2*::*mCherry* co-injection marker, which confirms the presence of the *Pirg-4*::*GFP* transgene. Presence of the *Pirg-5*::*GFP* transgene was confirmed by assaying for the Rol phenotype. Photographs were acquired using the same imaging conditions for each immune reporter. **(B)** Model of the *nhr-86* gene. Blue squares are exons. Black lines show the locations of the deletions in each of the *nhr-86* mutants. **(C)** The expression of the *C*. *elegans* immune effector genes *irg-4*, *irg-5* and *irg-6* (C32H11.1) were analyzed by qRT-PCR in wild-type animals and in two different *nhr-86* loss-of-function mutants (*tm2590* and *ums12*), each exposed to either R24 or control for approximately 18 hours. Data for *irg-6* is shown in S1B Fig. Data are the average of four independent replicates, each normalized to a control gene with error bars representing SEM. Data are presented as the value relative to the average expression from all replicates of the indicated gene in the baseline condition (wild-type animals exposed to control). The difference in induction of *irg-4*, *irg-5* and *irg-6* by R24 in wild-type animals compared to each of the two *nhr-86* mutant strains is significant (**** $p<0.0001$ by 2-way ANOVA with Bonferroni multiple comparisons test).

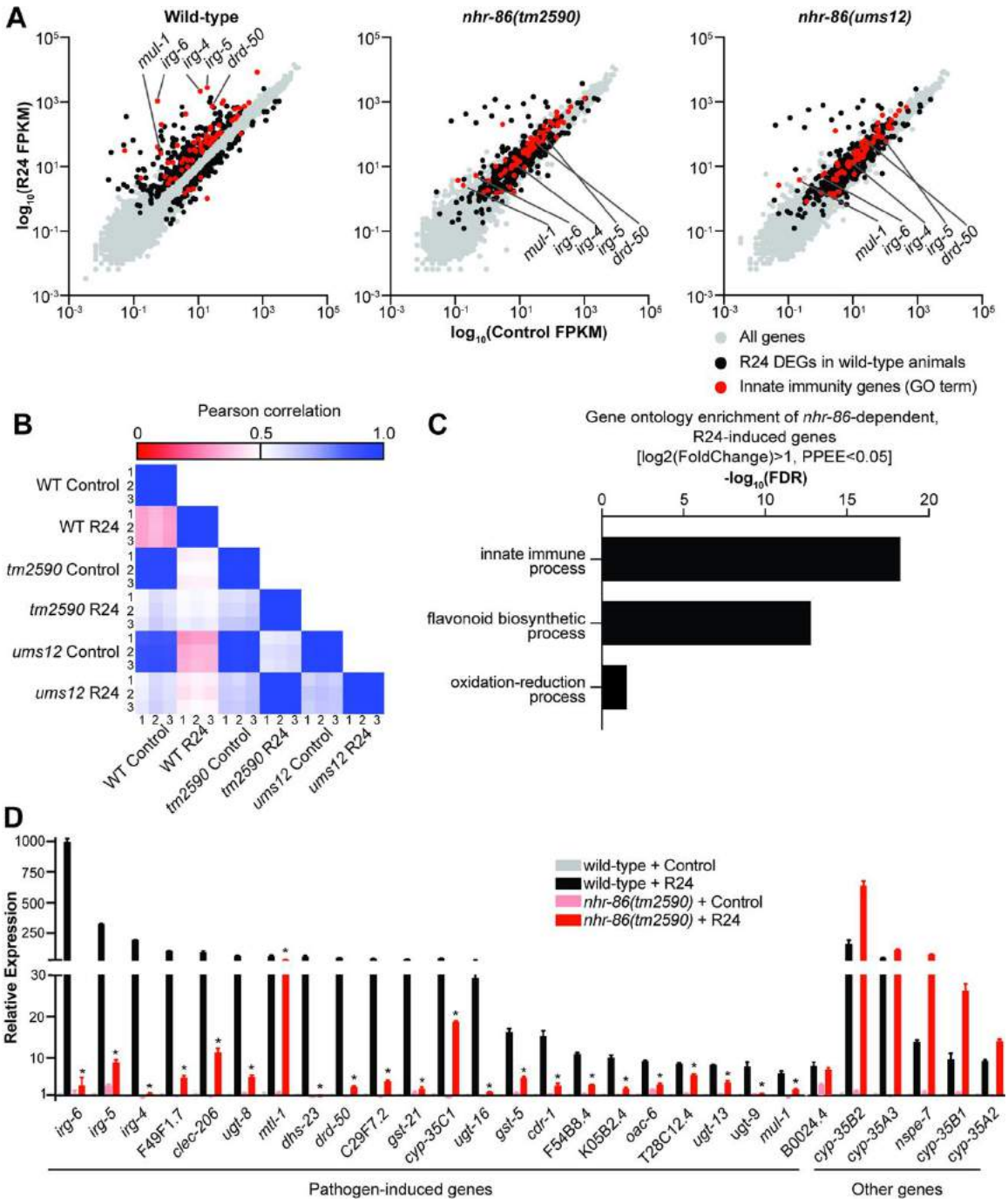

Figure 2. *nhr-86* activates the transcription of innate immune response genes.

(A) All data from the mRNA-seq experiment are presented on scatter plots. Genes that were differentially regulated upon R24 treatment in wild-type animals are shown in black

(Fold change> 2, PPEE<0.05). These same genes are also highlighted in black in the *nhr-86(tm2590)* and *nhr-86(ums12)* scatter plots. Genes involved in innate immunity by Gene Ontology (GO) term are highlighted in red. **(B)** Pearson correlation coefficients are presented for all samples in the mRNA-seq experiment. **(C)** Gene ontology enrichment of the *nhr-86*-dependent, R24-induced genes identified in the mRNA-seq experiment are shown. **(D)** Results of NanoString nCounter gene expression analysis for 118 *C. elegans* genes performed on wild-type and *nhr-86(tm2590)* animals exposed to either R24 or control. The 28 genes that were induced 5-fold or greater in wild-type animals by R24 are presented. Data are the average of three replicates, each of which was normalized to three control genes, with error bars representing standard deviation and are presented as the value relative to the average expression from the replicates of the indicated gene in the baseline condition (wild-type animals exposed to control). * p<0.05 by student's t-test for the comparison of the R24-induced conditions.

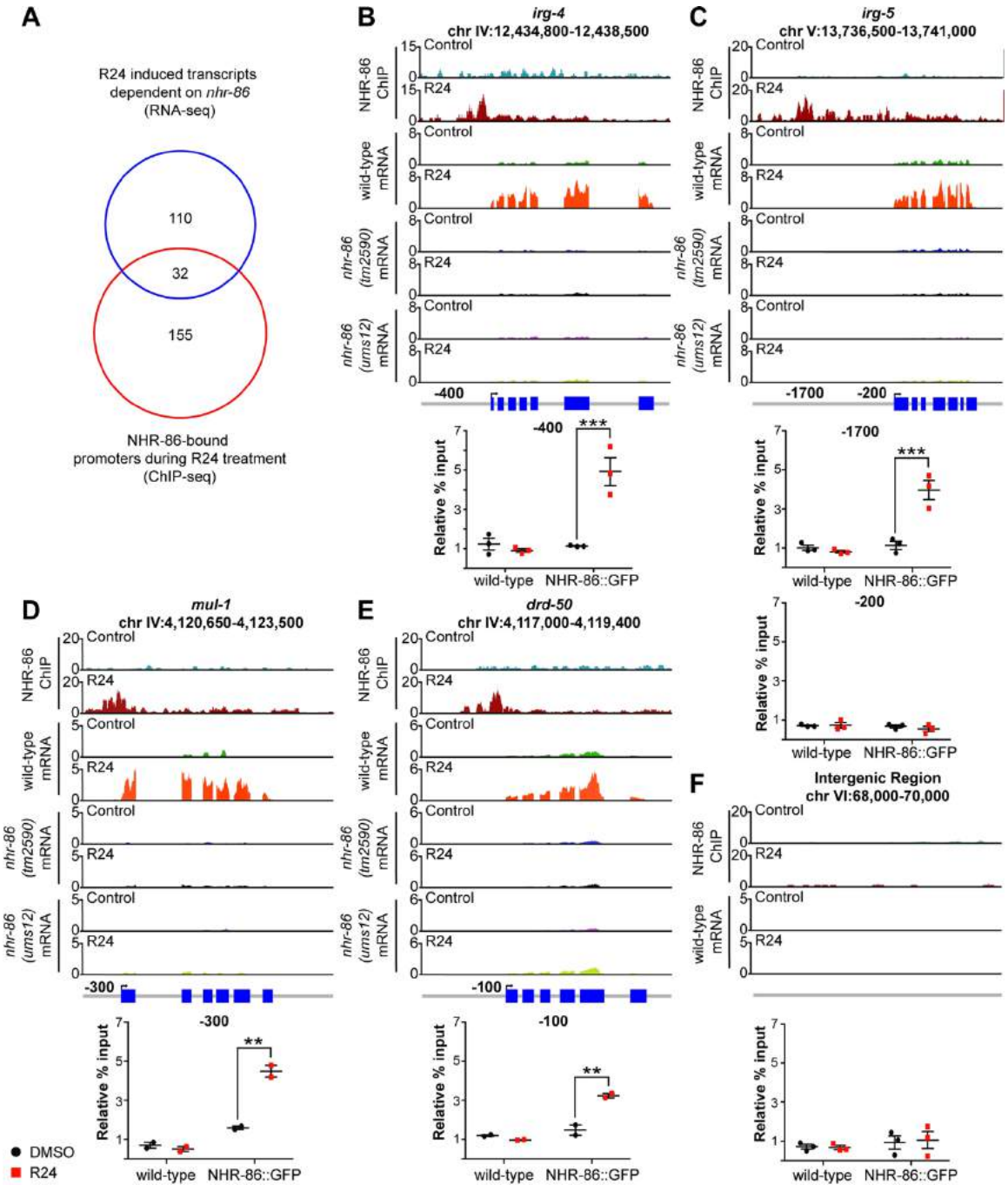

Figure 3. NHR-86 binds to the promoters of innate immune genes to drive their transcription. (A) Venn diagram showing the number of *nhr-86*-dependent, R24-induced genes in the mRNA-seq experiment, the genes whose promoters were bound by NHR-86 following R24 treatment in the ChIP-seq experiment, and the overlap between these datasets. The overlap between these datasets is significantly more than

is expected by chance alone (1.1 gene overlap expected by chance, hypergeometric p-value = $2x10^{-39}$). ChIP-seq profiles, mRNA-seq profiles and confirmatory ChIP-PCR are presented for the representative immune effectors *irg-4* **(B),** *irg-5* **(C),** *mul-1* (F49F1.6) **(D)** and *drd-50* (F49F1.1) **(E)** in animals of the indicated genotype exposed to R24 or the control. The y-axis is the number of reads (log_2). A gene model shows the location of the exons (blue) of the indicated genes. ChIP was performed with an anti-GFP antibody in *C. elegans* wild-type and transgenic NHR-86::GFP animals. Final set of peaks were called if the difference in intensity values of samples had a significance level of p-value < 0.025 (see S3 Table) for the indicated comparison. In the ChIP-PCR data, the percent input for each condition was normalized to the abundance of a random intergenic region of chromosome four. ** p<0.01 and *** p<0.001 by 2-way ANOVA with Bonferroni multiple comparisons test for the indicated comparison. A region 200 bp upstream of *irg-5* **(C)** and a random intergenic region on chromosome six **(F)** were not enriched by control or R24 treatment. Each data point in the ChIP-qPCR data is from an independent biological replicate.

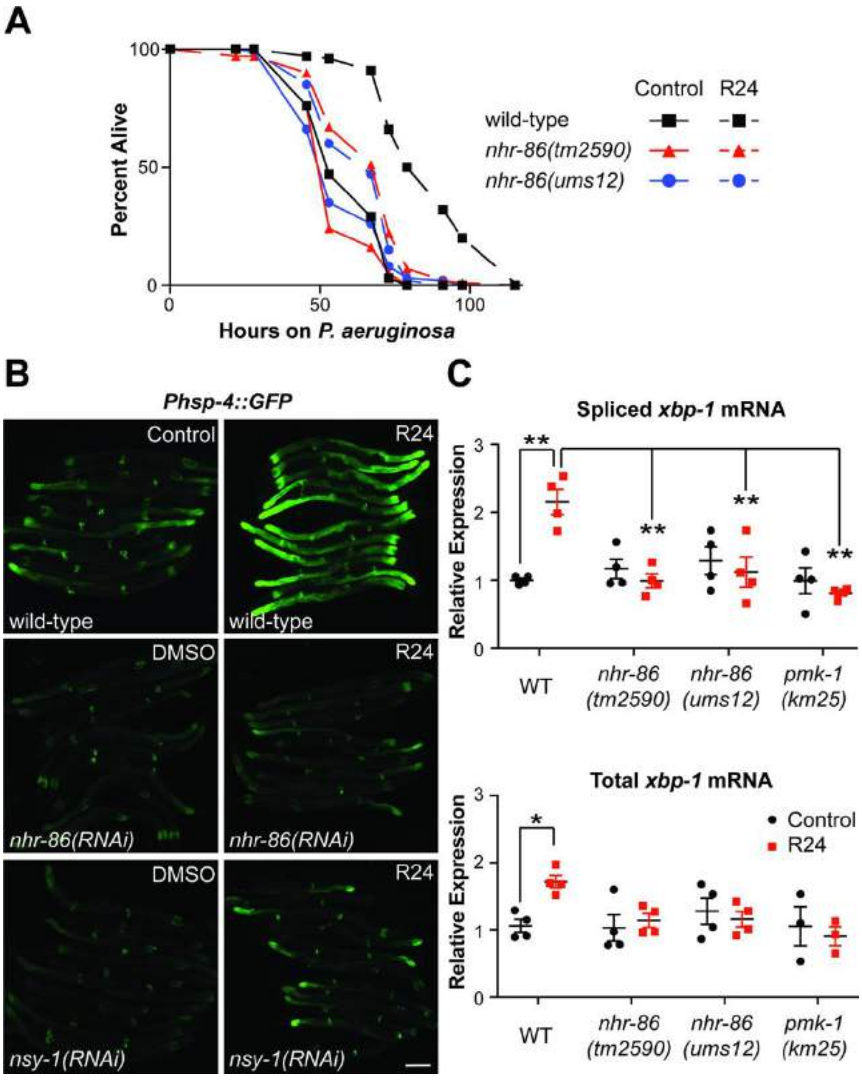

Figure 4. The immune response induced by *nhr-86* protects *C. elegans* from *P. aeruginosa* infection.

(A) *P. aeruginosa* infection assays of *C. elegans* wild-type, *nhr-86(tm2590)* and *nhr-86(ums12)* treated with R24 or 1% DMSO (control) are shown. The difference in susceptibility to *P. aeruginosa* between R24-exposed wild-type and each of the mutant animals is significant ($p<0.001$ by the log-rank test). Data are representative of three

trials. Sample sizes, mean lifespan, % lifespan extension conferred by R24 treatment in each background and p values for all trials are shown in S4A Table. Significance was determined using Kaplan-Meier survival curves and log-rank tests. **(B)** *C. elegans* carrying the *Phsp-4*::*GFP* reporter were exposed to the indicated RNAi bacteria and transferred at the L4 stage to media supplemented with either R24 or control for approximately 18 hours. Scale bar equals 100 μm. **(C)** qRT-PCR was used to measure the spliced (active) and total *xbp-1* mRNA in animals of the indicated genotype exposed to R24 or control. Comparisons were calculated using 2-way ANOVA with Bonferroni multiple comparisons test and * $p<0.05$ and ** $p<0.0001$. Data are the average of four independent replicates, each normalized to a control gene with error bars representing SEM. Data are presented as the value relative to the average expression from all replicates of the indicated gene in the baseline condition (wild-type animals exposed to control).

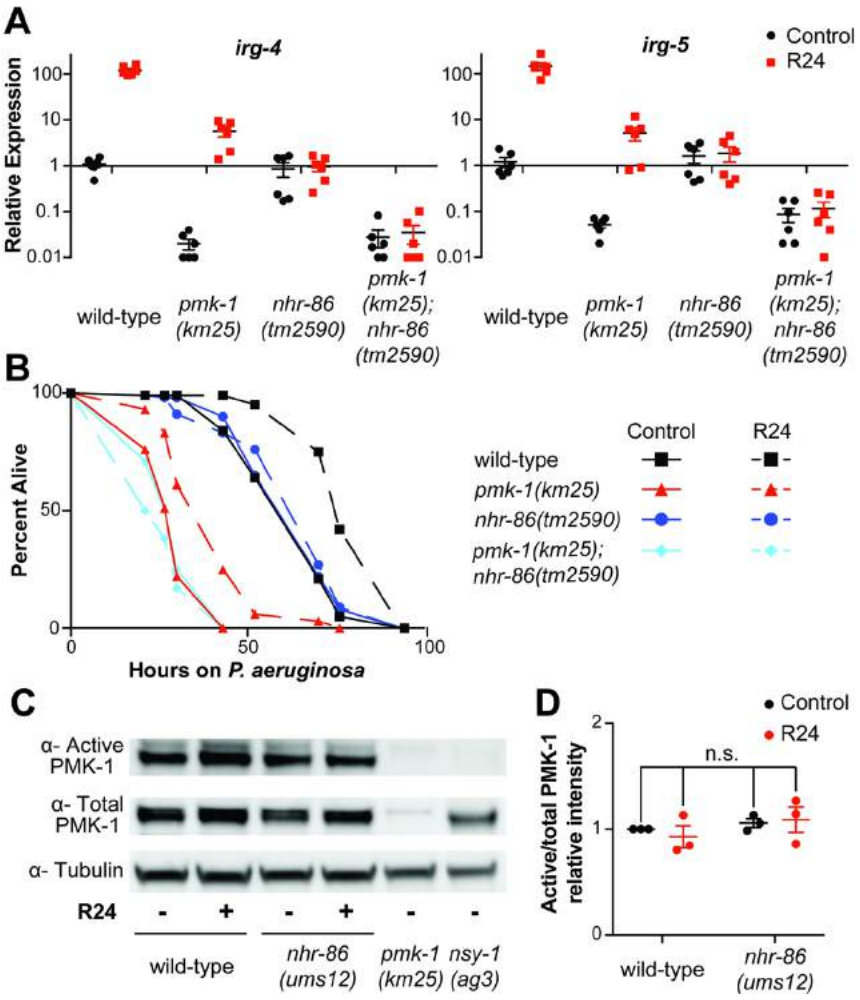

Figure 5. *nhr-86* induces innate immune defenses independent of the p38 MAPK *pmk-1*.

(A) The expression of the *C. elegans* immune effector genes *irg-4*, *irg-5*, *drd-50*, *mul-1* and *irg-6* were analyzed by qRT-PCR in wild-type animals, *pmk-1(km25)*, *nhr-86(tm2590)*, and *pmk-1(km25); nhr-86(tm2590)* double mutants, each exposed to either R24 or the control for approximately 18 hours. Data for *drd-50*, *mul-1* and *irg-6* are shown in S5A Figure. Data are the average of six independent replicates, each normalized to a control gene with error bars representing SEM. Data are presented as the value relative to the average expression from all replicates of the indicated gene in the baseline condition (wild-type animals exposed to control). The difference in

induction of *irg-4*, *irg-5*, *drd-50*, *mul-1* and *irg-6* by R24 in wild-type animals compared to each of the mutant strains is significant ($p<0.0001$ by 2-way ANOVA with Bonferroni multiple comparisons test). There is no significant difference between the expression of these genes in *pmk-1(km25)* animals exposed to control compared to either condition in the *pmk-1(km25); nhr-86(tm2590)*. **(B)** *P. aeruginosa* infection assays of *C. elegans* wild-type, *pmk-1(km25)*, *nhr-86(tm2590)*, and *pmk-1(km25); nhr-86(tm2590)*, each exposed to control or R24, are shown. The difference in susceptibility to *P. aeruginosa* between control and R24-exposed wild-type and *pmk-1(km25)* animals is significant ($p<0.001$). There is no significant difference between control and R24-exposed *nhr-86(tm2590)* and *pmk-1(km25); nhr-86(tm2590)* animals. Data are representative of three trials. Sample sizes, mean lifespan, % lifespan extension conferred by R24 treatment in each background and p values for all trials are shown in S4B Table. Significance was determined using Kaplan-Meier survival curves and log-rank tests. **(C)** Immunoblot analysis of lysates from L4 stage animals of the indicated genotype using antibodies that recognize the doubly phosphorylated TGY motif of PMK-1 (α-Active PMK-1), the total PMK-1 protein (α-Total PMK-1) and tubulin (α-Tubulin). The total PMK-1 antibody detects total, but not active (phosphorylated) PMK-1. **(D)** The relative intensity of active PMK-1 and total PMK-1 was quantified from three biological replicates and is expressed as the average ratio of active to total PMK-1, relative to wild-type control. Error bars report SEM. There is no significant difference (n.s.) between these conditions (2-way ANOVA with Bonferroni multiple comparisons test).

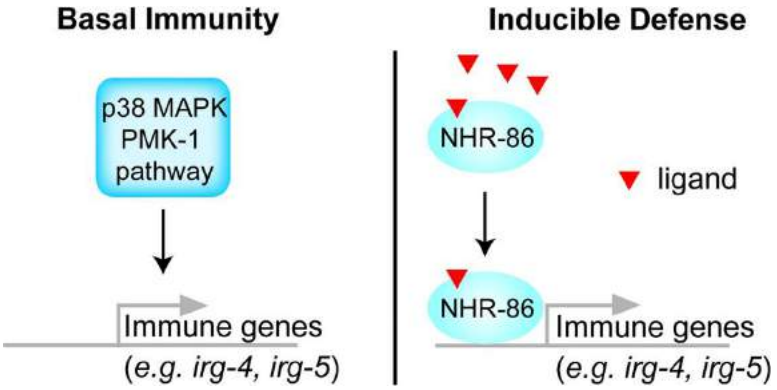

Figure 6. Model of NHR-86-mediated immune regulation in *C. elegans***.** The basal expression of immune effectors such as *irg-4***,** *irg-5***,** *mul-1* and *drd-50* are ensured by p38 MAPK PMK-1. Activated NHR-86 traffics to the promoters of these and other immune effectors to drive their induction and provide protection from bacterial infection.

SUPPLEMENTAL FIGURES

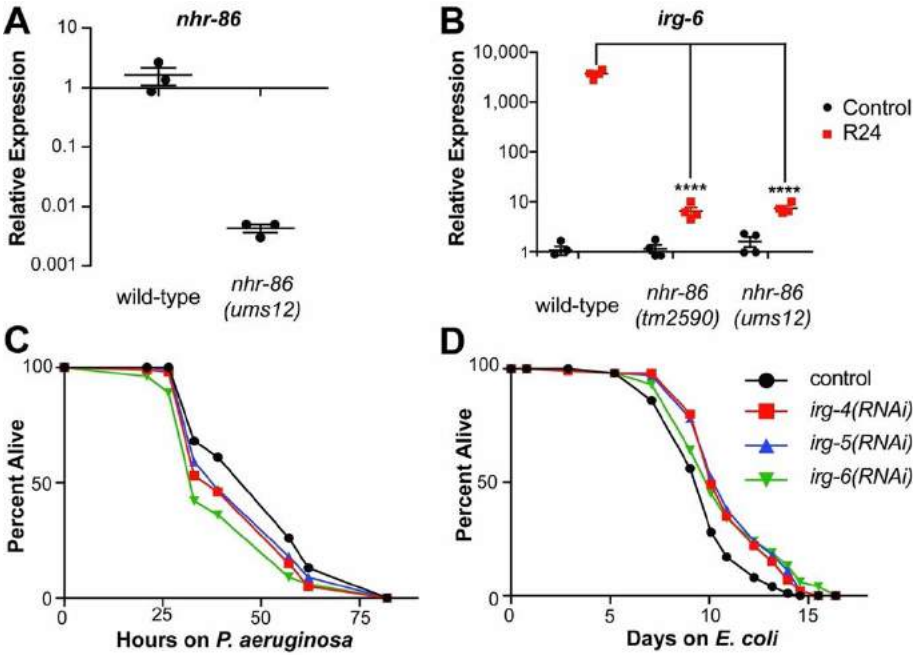

S1 Fig: An RNAi screen identifies a role for the nuclear hormone receptor *nhr-86* in the induction of *C. elegans* immune effectors.

(A) qRT-PCR data of *nhr-86* mRNA in the *nhr-86(ums12)* mutant. **(B)** qRT-PCR data of *irg-6* as described in Fig 1. In A and B, data are the average of three or four independent replicates, respectively, each normalized to a control gene with error bars representing SEM. Data are presented as the value relative to the average expression from all replicates of the indicated gene in the baseline condition (wild-type animals exposed to control). **(C)** *P. aeruginosa* pathogenesis assay and **(D)** lifespan on *E. coli* OP50 of animals exposed to the indicated RNAi bacteria. Data are representative of three trials. Sample sizes, mean lifespan and p values for all trials are shown in S4C and S4D Table. Significance was determined using Kaplan-Meier survival curves and log-rank tests.

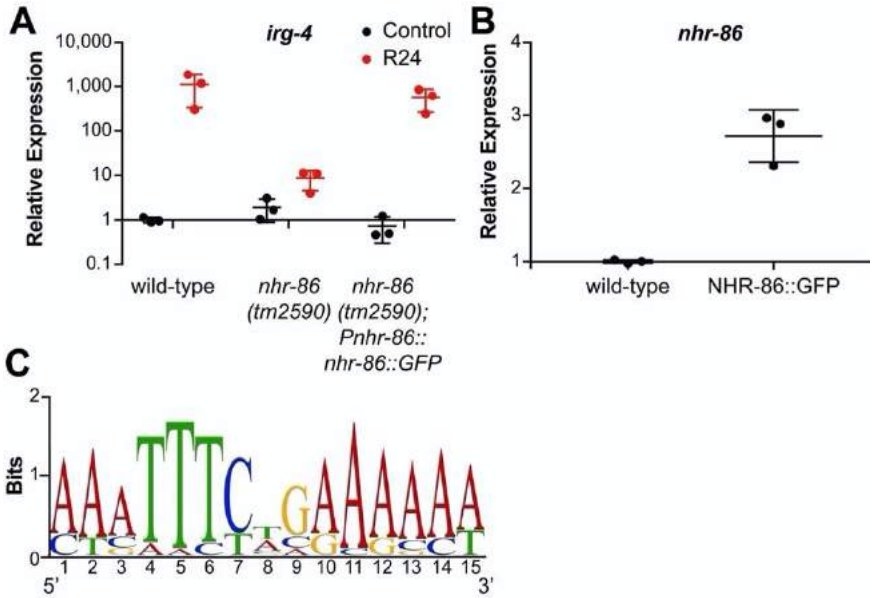

S2 Fig: NHR-86 binds to the promoters of innate immune genes to drive their transcription.

qRT-PCR was used to measure **(A)** *irg-4* and **(B)** *nhr-86* in animals of the indicated genotypes. Data are the average of three independent replicates, each normalized to a control gene with error bars representing SEM. Data are presented as the value relative to the average expression from all replicates of the indicated gene in the baseline condition (wild-type animals exposed to control in A and wild-type in B). **(C)** The 15-bp sequence that was enriched in the promoters that were bound by NHR-86::GFP.

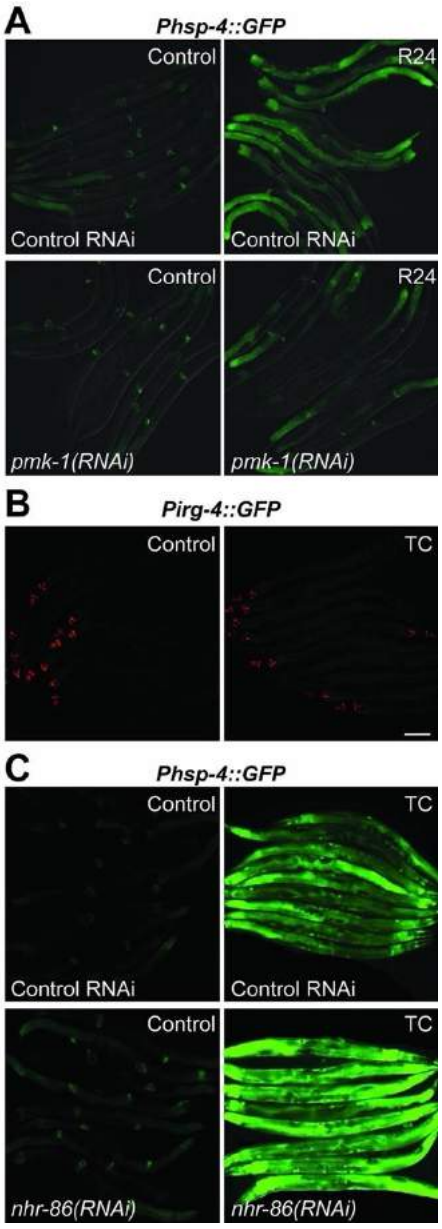

S3 Fig: The immune response induced by *nhr-86* protects *C. elegans* against *P. aeruginosa* infection.

(A) *Phsp-4*::*GFP*, **(B)** *Pirg-4*::*GFP* and **(C)** *Phsp-4*::*GFP* animals were exposed to the indicated RNAi conditions and treated with DMSO (control) or 10 μg/mL tunicamycin

(TC) overnight at 20°C and photographed. Red expression in *Pirg-4*::*GFP* animals is the *Pmyo-2*::*mCherry* co-injection marker. Scale bar equals 100 μm.

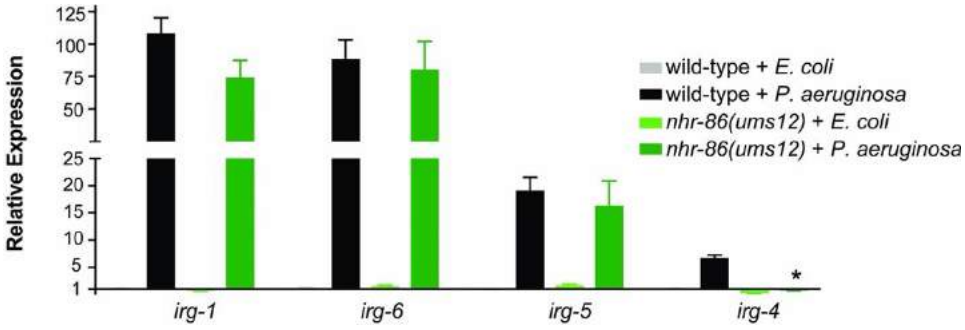

S4 Fig: *nhr-86(ums12)* does not abrogate the induction of *irg-1*, *irg-5* or *irg-6* during *P. aeruginosa* infection

qRT-PCR data of *irg-1*, *irg-4*, *irg-5* and *irg-6* in wild-type or *nhr-86(ums12)* animals exposed to *E. coli* or *P. aeruginosa* for 6 hours. * equals $p<0.05$ for the difference in expression of the indicated gene between wild-type and *nhr-86(ums12)* in the *P. aeruginosa*-exposed condition. All other differences were not significant. Data are presented relative to uninfected wild-type animals.

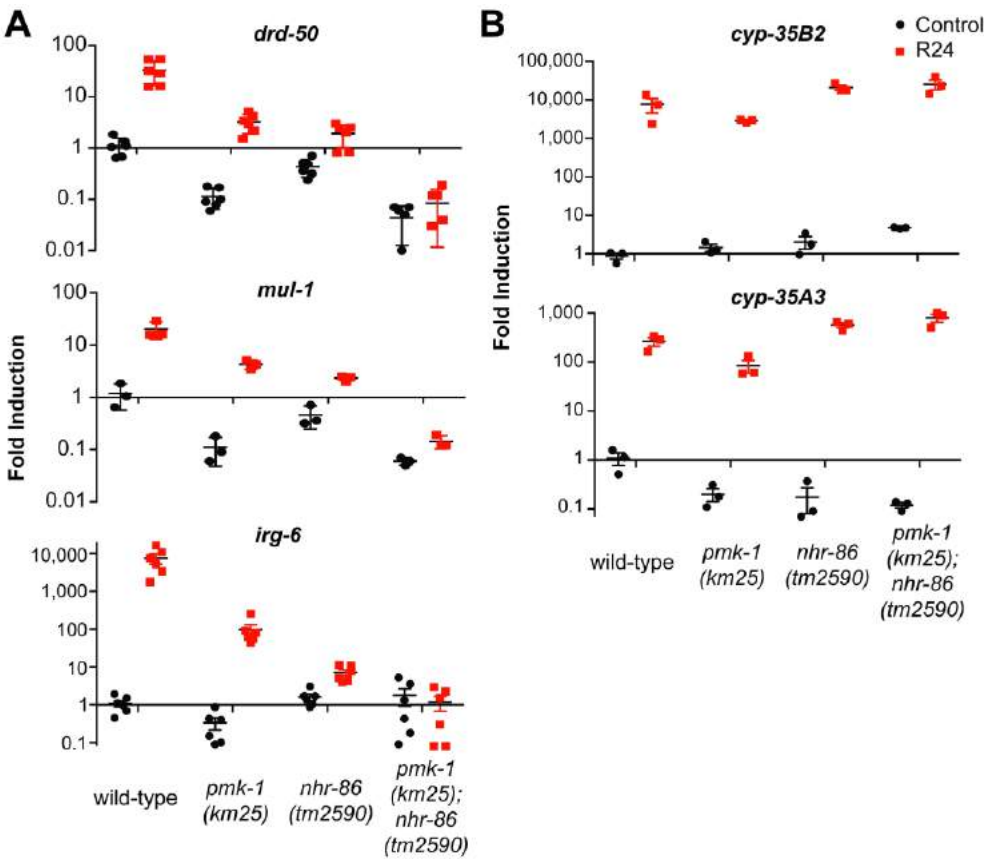

S5 Fig: *nhr-86* induces innate immune defenses independent of the p38 MAPK *pmk-1*.

qRT-PCR data of *drd-50*, *mul-1 and irg-6* **(A),** and *cyp-35B2* and *cyp-35A3* **(B)** as described in Fig 5A.

TABLES

Supplemental tables referenced in this manuscript can be found by following the included links to the publisher's website.

Table S1: Genes identified in an RNAi screen for NHRs that control the induction of *Pirg-4*::GFP by R24.

https://doi.org/10.1371/journal.pgen.1007935.s006

Table S2: *nhr-86*-dependent genes from the mRNA-seq experiment.

https://doi.org/10.1371/journal.pgen.1007935.s007

Table S3: ChIP-seq data showing the promoters that were bound by NHR-86.

https://doi.org/10.1371/journal.pgen.1007935.s008

Table S4: Sample sizes, mean lifespan, % lifespan extension conferred by R24 treatment in each background and p values for the *C. elegans* pathogenesis and lifespan assays.

(A) Data for Fig 4A. **(B)** Data for Fig 5B. **(C)** Data for S1C Fig. **(D)** Data for S1D Fig.

https://doi.org/10.1371/journal.pgen.1007935.s009

Table S5: Primer sequences that were designed for this study.

https://doi.org/10.1371/journal.pgen.1007935.s010

MATERIALS AND METHODS

C. elegans and bacterial strains

C. elegans strains were maintained on standard nematode growth media plates with *E*. *coli* OP50 as a food source, as described [62]. The previously published *C. elegans* strains used in this study were: N2 Bristol [62], KU25 *pmk-1(km25)* [100], AU306 *agIs44* [P*irg-4*::*GFP*::*unc-54-3'UTR;Pmyo-2*::*mCherry*], AY101 *acIs101* [p*DB09.1(Pirg-5*::*gfp)*; p*RF4(rol-6(su1006))]* [63], SJ405 *zcIs4 (Phsp-4*::*gfp)* [148], VL491 *nhr-86(tm2590)* [152], and VL648 *unc-119(ed3)*; *wwIs22 [Pnhr-86*::*nhr-*

86ORF::*GFP unc-119(+)*] [152]. The strains developed in this study were: RPW137 *nhr-86(ums12)*, RPW119 *pmk-1(km25);nhr-86(tm2590)*, RPW99 *nhr-86(tm2590); agIs44*, RPW106 *nhr-86(tm2590)*; *acIs101*, and RPW165 *nhr-86(ums12); agIs44*. *Pseudomonas aeruginosa* strain PA14 was used for all studies [169].

C. elegans strain construction

CRISPR/Cas9 was used to generate *nhr-86(ums12)* as described [170]. Target sequences were selected on exons 1 and 6 of *nhr-86*. Forward and reverse oligonucleotides were designed to contain the target sequence and overhangs compatible with *Bsa*I sites in plasmid pPP13, a modified version of pRB1017 [170, 171]. Forward and reverse oligonucleotides were annealed and ligated into pPP13 cut with *Bsa*I to create the gRNA plasmids. Plasmids were confirmed by sequencing. A DNA mixture of pDD162 (50 ng/L), the gRNA plasmids (25 ng/L each), pJA58 (50 ng/L) and the ssODN repair template for *dpy-10(cn64)* (20 ng/L) was prepared in injection buffer (20 mM potassium phosphate, 3 mM potassium citrate, 2% PEG, pH 7.5) and injected into N2 worms. Mutations in the *dpy-10* gene were used as a CRISPR co-conversion marker. The F1 progeny were screened for Rol and Dpy phenotypes 3–4 days after injection and then for deletions in the *nhr-86* coding region using PCR. The *nhr-86(ums12)* mutant contains a 5539 bp deletion that spans from 17 bp upstream of the ATG to 30 bp before the stop codon with an insertion of 6 bp at the breakpoint. Primer sequences used for genotyping are listed in S5 Table.

Feeding RNAi screen

A previously described library containing RNAi clones corresponding to 258 of the 284 NHRs in the *C. elegans* genome was used for this study [158]. These genes were screened for their ability to abrogate the induction of *agIs44* by 70 μM R24, as described [23].

C. elegans bacterial infection and other assays

"Slow killing" *P*. *aeruginosa* infection experiments were performed as previously described [47, 67]. In all of these assays, the final concentration of DMSO was 1% and 70 μM R24 was used. Wild-type is either N2 or *agIs44*. All pathogenesis and lifespan assays are representative of three biological replicates. Sample sizes, mean lifespan, % lifespan extension conferred by R24 treatment in each background (where applicable) and p values for all trials are shown in S4 Table.

mRNA-seq, NanoString ncounter gene expression analyses and qRT-PCR

Synchronized, L1 stage, hermaphrodites *C. elegans* of the indicated genotypes were grown to the L4/ young adult stage, transferred to assay plates, and incubated at 20°C overnight. 70 μM R24 or solvent control (DMSO, 1% final concentration) assay plates were prepared as described [23, 46, 47]. RNA was isolated using TriReagent (Sigma-Aldrich), purified on a column (Qiagen), and analyzed by mRNA-seq using the BGISEQ-500 platform (BGI Americas Corp). mRNA-seq data analysis was performed by BGI Americas Corp. Biological replicate RNA samples were analyzed using NanoString nCounter Gene Expression Analysis (NanoString Technologies) with a "codeset" designed by NanoString that contained probes for 118 *C. elegans* genes. The codeset has been described previously [23, 47]. Probe hybridization, data acquisition

and analysis were performed according to instructions from NanoString with each RNA sample normalized to the control genes *snb-1*, *ama-1* and *act-1*. For the qRT-PCR studies, RNA was reverse transcribed to cDNA using the RETROscript Kit (Life Technologies) and analyzed using a CFX1000 machine (Bio-Rad). The sequences of primers that were designed for this study are presented in S5 Table. Other primers were previously published [7, 52, 55, 164]. All values were normalized against the control gene *snb-1*. Fold change was calculated using the Pfaffl method [72].

Immunoblot analyses

C. elegans were prepared as described above to ensure that stage-matched, hermaphrodite animals at the young L4 larval stage were studied in each condition. Protein lysates were prepared as previously described [23] and probed with a 1:1000 dilution of an antibody that recognizes the doubly-phosphorylated TGY motif of PMK-1 (Promega Corporation). Monoclonal anti-α-tubulin antibody was used at a dilution of 1:1,000 (Sigma-Aldrich). A polyclonal antibody against the total PMK-1 protein was raised using the peptide DFQKNVAFADEEEDEEKMES (PMK-1 amino acids 358 to 377) in a rabbit (Thermo Scientific Pierce Custom Antibody Services) and used at a dilution of 1:1000. We confirmed that the total PMK-1 antibody detects total, but not active (phosphorylated) PMK-1 (Figure 5C). Horseradish peroxidase (HRP)-conjugated anti-rabbit (Cell Signaling Technology) and anti-mouse IgG secondary antibodies (Abcam) were diluted 1:10,000 and used to detect the primary antibodies following the addition of ECL reagents (Thermo Fisher Scientific, Inc.), which were visualized using a BioRad ChemiDoc MP Imaging System. The band intensities were quantified using BioRad Image Lab software version 5.2.1, and the ratio of active phosphorylated PMK-1

to total PMK-1 was calculated with all samples normalized to the ratio of wild-type control animals.

ChIP-qPCR, ChIP-seq and bioinformatics

Chromatin immunoprecipitation was performed with a strain containing a GFP-tagged NHR-86 protein (NHR-86::GFP) that has been previously characterized [152]. *nhr-86* transcript levels are 2.7-fold elevated in the NHR-86::GFP strain compared to wild-type (S2B Figure). ChIP was performed as previously described [172, 173] with modifications. Briefly, L4 synchronized, hermaphrodite *C. elegans* (wild-type and transgenic NHR-86::GFP animals) were exposed to “slow killing” plates [67], containing either DMSO (1%) or 70 μM R24 for approximately 18 hours. Animals were then collected and washed with 4°C M9 and phosphate-buffered saline to remove bacteria. Cross-linking of protein and DNA was performed in 2% formaldehyde for 30 minutes at room temperature. Cross-linking was quenched with 100 mM glycine, animals were washed in M9, resuspended in lysis buffer (50 mM Hepes–KOH pH 7.5, 300 mM NaCl, 1 mM EDTA, 1% (v/v) Triton X-100, 0.1% (w/v) sodium deoxycholate, 0.5% (v/v) N-Lauroylsarcosine, and protease inhibitors) and lysed with a Teflon homogenizer. Lysates were then sonicated using a Bioruptor UCD-200 for 10 cycles (30 s on, 30 s off) to obtain 500–1000 bp DNA fragments. Sonicated lysates (2 mg) were pre-cleared with protein G Dynabeads (Invitrogen), 10% of lysate removed for input, and incubated with 5 μg anti-GFP antibody (Roche) overnight. Immune complexes were collected with protein G Dynabeads, washed, and eluted from beads. Cross-links were reversed at 65°C overnight and DNA fragments were purified with PCR purification columns (Qiagen). qPCR was performed on input and immunoprecipitated samples using

primers designed around the transcription start site. All ChIP data are presented as percent input normalized to a random intragenic region on chromosome four. Primer sequences are available in S5 Table.

ChIP-seq was performed by BGI Americas Corp. The raw sequencing data were first clipped for adaptor sequences and then mapped to the *C. elegans* genome (ce10, UC Santa Cruz) by the Burrows-Wheeler Aligner algorithm (BWA MEM, BWA version 0.7.15). The output SAM files were processed and sorted with the Picard tools. The output mapping files (BAM files) were filtered with SAMtools to remove any read that had a mapping quality less than 10 (SAMtools view–b–q 10 input.bam > output.bam). Peaks were determined using MACS version 2.1 with the no-model parameter. The final set of peaks were called if the difference in intensity values of samples had a significance level of p-value < 0.025.

To identify candidate motifs for NHR-86 binding, ChIP peaks that were located in promoter regions of genes were examined using the MEME motif analysis platform [Parameters: minw = 8, maxw = 25, in two modes (zoops & anr), significance threshold (E-value > = 1e-01), http://meme.sdsc.edu]. A background model is used by MEME to calculate the log likelihood ratio and statistical significance of the motif. We set the following requirements: the most significant motif should exist in 50% of input sequences, and the genes containing the motif should have the largest overlap between ChIP-Seq and RNA-seq datasets. A single 15 bp motif was identified that met these criteria (E-value: 1.7e-003, S2C Figure). 66 sites of 101 input sequences had this motif, including 15 of the 32 genes that overlapped in the ChIP-Seq and RNA-seq datasets.

Microscopy

Nematodes were mounted onto agar pads, paralyzed with 10 mM levamisole (Sigma) and photographed using a Zeiss AXIO Imager Z2 microscope with a Zeiss Axiocam 506mono camera and Zen 2.3 (Zeiss) software.

Statistical analyses

Differences in survival of *C. elegans* in the *P*. *aeruginosa* pathogenesis assays were determined with the log-rank test using OASIS 2 as previously described [75]. Data from one experiment that is representative of the replicates is shown. Other statistical tests, indicated in the Figure legends, were performed using Prism 7 (GraphPad Software).

References

1. McGhee, J.D., *The C. elegans intestine.* WormBook, 2007: p. 1-36.
2. Kenyon, C., et al., *A C. elegans mutant that lives twice as long as wild type.* Nature, 1993. **366**(6454): p. 461-4.
3. Henderson, S.T. and T.E. Johnson, *daf-16 integrates developmental and environmental inputs to mediate aging in the nematode Caenorhabditis elegans.* Current Biology, 2001. **11**(24): p. 1975-1980.
4. Murphy, C.T., et al., *Genes that act downstream of DAF-16 to influence the lifespan of Caenorhabditis elegans.* Nature, 2003. **424**(6946): p. 277-83.
5. Garsin, D.A., et al., *Long-lived C. elegans daf-2 mutants are resistant to bacterial pathogens.* Science, 2003. **300**(5627): p. 1921.
6. Wolkow, C.A., et al., *Regulation of C. elegans life-span by insulinlike signaling in the nervous system.* Science, 2000. **290**(5489): p. 147-50.
7. Troemel, E.R., et al., *p38 MAPK regulates expression of immune response genes and contributes to longevity in C. elegans.* PLoS Genet, 2006. **2**(11): p. e183.
8. Evans, E.A., T. Kawli, and M.W. Tan, *Pseudomonas aeruginosa suppresses host immunity by activating the DAF-2 insulin-like signaling pathway in Caenorhabditis elegans.* PLoS Pathog, 2008. **4**(10): p. e1000175.
9. Dowen, R.H., *CEH-60/PBX and UNC-62/MEIS Coordinate a Metabolic Switch that Supports Reproduction in C. elegans.* Dev Cell, 2019. **49**(2): p. 235-250 e7.
10. Amrit, F.R.G., et al., *The longevity-promoting factor, TCER-1, widely represses stress resistance and innate immunity.* Nat Commun, 2019. **10**(1): p. 3042.
11. Wu, Z., et al., *Dietary Restriction Extends Lifespan through Metabolic Regulation of Innate Immunity.* Cell Metab, 2019. **29**(5): p. 1192-1205 e8.
12. Nandakumar, M. and M.W. Tan, *Gamma-Linolenic and Stearidonic Acids Are Required for Basal Immunity in Caenorhabditis elegans through Their Effects on p38 MAP Kinase Activity.* PLoS Genet, 2008. **4**(11): p. e1000273.
13. Ding, W., et al., *s-Adenosylmethionine Levels Govern Innate Immunity through Distinct Methylation-Dependent Pathways.* Cell Metab, 2015. **22**(4): p. 633-45.
14. Walker, Amy K., et al., *A Conserved SREBP-1/Phosphatidylcholine Feedback Circuit Regulates Lipogenesis in Metazoans.* Cell, 2011. **147**(4): p. 840-852.
15. Deng, P., et al., *Mitochondrial UPR repression during Pseudomonas aeruginosa infection requires the bZIP protein ZIP-3.* Proc Natl Acad Sci U S A, 2019. **116**(13): p. 6146-6151.
16. Nargund, A.M., et al., *Mitochondrial import efficiency of ATFS-1 regulates mitochondrial UPR activation.* Science, 2012. **337**(6094): p. 587-90.
17. Pellegrino, M.W., et al., *Mitochondrial UPR-regulated innate immunity provides resistance to pathogen infection.* Nature, 2014. **516**(7531): p. 414-7.
18. Liu, Y., et al., *Caenorhabditis elegans pathways that surveil and defend mitochondria.* Nature, 2014. **508**(7496): p. 406-10.
19. Mao, K., et al., *Mitochondrial Dysfunction in C. elegans Activates Mitochondrial Relocalization and Nuclear Hormone Receptor-Dependent Detoxification Genes.* Cell Metab, 2019. **29**(5): p. 1182-1191 e4.

20. Kirienko, N.V., F.M. Ausubel, and G. Ruvkun, *Mitophagy confers resistance to siderophore-mediated killing by Pseudomonas aeruginosa.* Proc Natl Acad Sci U S A, 2015. **112**(6): p. 1821-6.
21. Peterson, N.D., et al., *The nuclear hormone receptor NHR-86 controls anti-pathogen responses in C. elegans.* PLoS Genet, 2019. **15**(1): p. e1007935.
22. Sim, S. and M.L. Hibberd, *Caenorhabditis elegans susceptibility to gut Enterococcus faecalis infection is associated with fat metabolism and epithelial junction integrity.* BMC Microbiol, 2016. **16**: p. 6.
23. Pukkila-Worley, R., et al., *The evolutionarily conserved mediator subunit MDT-15/MED15 links protective innate immune responses and xenobiotic detoxification.* PLoS Pathog, 2014. **10**(5): p. e1004143.
24. Magner, Daniel B., et al., *The NHR-8 Nuclear Receptor Regulates Cholesterol and Bile Acid Homeostasis in C. elegans.* Cell Metabolism, 2013. **18**(2): p. 212-224.
25. Otarigho, B. and A. Aballay, *Cholesterol Regulates Innate Immunity via Nuclear Hormone Receptor NHR-8.* iScience, 2020. **23**(5): p. 101068.
26. Rajan, M., et al., *NHR-14 loss of function couples intestinal iron uptake with innate immunity in C. elegans through PQM-1 signaling.* Elife, 2019. **8**.
27. Watts, J.L. and J. Browse, *Genetic dissection of polyunsaturated fatty acid synthesis in Caenorhabditis elegans.* Proceedings of the National Academy of Sciences, 2002. **99**(9): p. 5854-5859.
28. Nandakumar, M. and M.-W. Tan, *Gamma-Linolenic and Stearidonic Acids Are Required for Basal Immunity in Caenorhabditis elegans through Their Effects on p38 MAP Kinase Activity.* PLOS Genetics, 2008. **4**(11): p. e1000273.
29. Han, S., et al., *Mono-unsaturated fatty acids link H3K4me3 modifiers to C. elegans lifespan.* Nature, 2017. **544**(7649): p. 185-190.
30. Hansen, M., T. Flatt, and H. Aguilaniu, *Reproduction, fat metabolism, and life span: what is the connection?* Cell Metab, 2013. **17**(1): p. 10-9.
31. Hou, N.S., et al., *Activation of the endoplasmic reticulum unfolded protein response by lipid disequilibrium without disturbed proteostasis in vivo.* Proc Natl Acad Sci U S A, 2014. **111**(22): p. E2271-80.
32. Miller, M., et al., *Triglycerides and cardiovascular disease: a scientific statement from the American Heart Association.* Circulation, 2011. **123**(20): p. 2292-333.
33. Watts, J.L. and J. Browse, *A palmitoyl-CoA-specific delta9 fatty acid desaturase from Caenorhabditis elegans.* Biochem Biophys Res Commun, 2000. **272**(1): p. 263-9.
34. Watts, J.L. and J. Browse, *Genetic dissection of polyunsaturated fatty acid synthesis in Caenorhabditis elegans.* Proc Natl Acad Sci U S A, 2002. **99**(9): p. 5854-9.
35. Watts, J.L., et al., *Deficiencies in C20 polyunsaturated fatty acids cause behavioral and developmental defects in Caenorhabditis elegans fat-3 mutants.* Genetics, 2003. **163**(2): p. 581-9.
36. Brock, T.J., J. Browse, and J.L. Watts, *Genetic regulation of unsaturated fatty acid composition in C. elegans.* PLoS Genet, 2006. **2**(7): p. e108.
37. Brock, T.J., J. Browse, and J.L. Watts, *Fatty acid desaturation and the regulation of adiposity in Caenorhabditis elegans.* Genetics, 2007. **176**(2): p. 865-75.

38. Shi, X., et al., *A Caenorhabditis elegans model for ether lipid biosynthesis and function.* J Lipid Res, 2016. **57**(2): p. 265-75.
39. Kim, D.H. and J.J. Ewbank, *Signaling in the innate immune response.* WormBook, 2018. **2018**: p. 1-35.
40. Cohen, L.B. and E.R. Troemel, *Microbial pathogenesis and host defense in the nematode C. elegans.* Curr Opin Microbiol, 2015. **23**: p. 94-101.
41. Pukkila-Worley, R., *Surveillance Immunity: An Emerging Paradigm of Innate Defense Activation in Caenorhabditis elegans.* PLoS Pathog, 2016. **12**(9): p. e1005795.
42. Pukkila-Worley, R. and F.M. Ausubel, *Immune defense mechanisms in the Caenorhabditis elegans intestinal epithelium.* Curr Opin Immunol, 2012. **24**(1): p. 3-9.
43. Shapira, M., et al., *A conserved role for a GATA transcription factor in regulating epithelial innate immune responses.* Proc Natl Acad Sci USA, 2006. **103**(38): p. 14086-91.
44. Shivers, R.P., et al., *Phosphorylation of the conserved transcription factor ATF-7 by PMK-1 p38 MAPK regulates innate immunity in Caenorhabditis elegans.* PLoS Genet, 2010. **6**(4): p. e1000892.
45. Kim, D.H., et al., *A conserved p38 MAP kinase pathway in Caenorhabditis elegans innate immunity.* Science, 2002. **297**(5581): p. 623-6.
46. Pukkila-Worley, R., et al., *Stimulation of host immune defenses by a small molecule protects C. elegans from bacterial infection.* PLoS Genet, 2012. **8**(6): p. e1002733.
47. Cheesman, H.K., et al., *Aberrant Activation of p38 MAP Kinase-Dependent Innate Immune Responses Is Toxic to Caenorhabditis elegans.* G3 (Bethesda), 2016. **6**(3): p. 541-9.
48. Peterson, N.D. and R. Pukkila-Worley, *Caenorhabditis elegans in high-throughput screens for anti-infective compounds.* Curr Opin Immunol, 2018. **54**: p. 59-65.
49. Ding, W., et al., *Stress-responsive and metabolic gene regulation are altered in low S-adenosylmethionine.* PLoS Genet, 2018. **14**(11): p. e1007812.
50. Taubert, S., et al., *A Mediator subunit, MDT-15, integrates regulation of fatty acid metabolism by NHR-49-dependent and -independent pathways in C. elegans.* Genes Dev, 2006. **20**(9): p. 1137-49.
51. Goh, G.Y., et al., *The conserved Mediator subunit MDT-15 is required for oxidative stress responses in Caenorhabditis elegans.* Aging Cell, 2014. **13**(1): p. 70-9.
52. Taubert, S., et al., *The Mediator subunit MDT-15 confers metabolic adaptation to ingested material.* PLoS Genet, 2008. **4**(2): p. e1000021.
53. Van Gilst, M.R., et al., *Nuclear hormone receptor NHR-49 controls fat consumption and fatty acid composition in C. elegans.* PLoS Biol, 2005. **3**(2): p. e53.
54. Goudeau, J., et al., *Fatty acid desaturation links germ cell loss to longevity through NHR-80/HNF4 in C. elegans.* PLoS Biol, 2011. **9**(3): p. e1000599.
55. Estes, K.A., et al., *bZIP transcription factor zip-2 mediates an early response to Pseudomonas aeruginosa infection in Caenorhabditis elegans.* Proc Natl Acad Sci U S A, 2010. **107**(5): p. 2153-8.

56. Liberati, N.T., et al., *Requirement for a conserved Toll/interleukin-1 resistance domain protein in the Caenorhabditis elegans immune response.* Proc Natl Acad Sci USA, 2004. **101**(17): p. 6593-8.
57. Couillault, C., et al., *TLR-independent control of innate immunity in Caenorhabditis elegans by the TIR domain adaptor protein TIR-1, an ortholog of human SARM.* Nat. Immunol., 2004. **5**(5): p. 488-94.
58. Kachroo, A. and P. Kachroo, *Fatty Acid-derived signals in plant defense.* Annu Rev Phytopathol, 2009. **47**: p. 153-76.
59. Mandal, M.K., et al., *Oleic acid-dependent modulation of NITRIC OXIDE ASSOCIATED1 protein levels regulates nitric oxide-mediated defense signaling in Arabidopsis.* Plant Cell, 2012. **24**(4): p. 1654-74.
60. Yang, Q., et al., *Influence of the membrane lipid structure on signal processing via G protein-coupled receptors.* Mol Pharmacol, 2005. **68**(1): p. 210-7.
61. Bodhicharla, R., et al., *Membrane Fluidity Is Regulated Cell Nonautonomously by Caenorhabditis elegans PAQR-2 and Its Mammalian Homolog AdipoR2.* Genetics, 2018. **210**(1): p. 189-201.
62. Brenner, S., *The genetics of Caenorhabditis elegans.* Genetics, 1974. **77**(1): p. 71-94.
63. Bolz, D.D., J.L. Tenor, and A. Aballay, *A conserved PMK-1/p38 MAPK is required in caenorhabditis elegans tissue-specific immune response to Yersinia pestis infection.* J Biol Chem, 2010. **285**(14): p. 10832-40.
64. Garsin, D.A., et al., *A simple model host for identifying Gram-positive virulence factors.* Proc Natl Acad Sci USA, 2001. **98**(19): p. 10892-7.
65. Flyg, C., K. Kenne, and H.G. Boman, *Insect pathogenic properties of Serratia marcescens: phage-resistant mutants with a decreased resistance to Cecropia immunity and a decreased virulence to Drosophila.* J Gen Microbiol, 1980. **120**(1): p. 173-81.
66. Deline, M.L., T.L. Vrablik, and J.L. Watts, *Dietary supplementation of polyunsaturated fatty acids in Caenorhabditis elegans.* J Vis Exp, 2013. **81**: p. e50879.
67. Tan, M.W., S. Mahajan-Miklos, and F.M. Ausubel, *Killing of Caenorhabditis elegans by Pseudomonas aeruginosa used to model mammalian bacterial pathogenesis.* Proc Natl Acad Sci USA, 1999. **96**(2): p. 715-20.
68. Yuen, G.J. and F.M. Ausubel, *Both live and dead Enterococci activate Caenorhabditis elegans host defense via immune and stress pathways.* Virulence, 2018. **9**(1): p. 683-699.
69. Pujol, N., et al., *A reverse genetic analysis of components of the Toll signaling pathway in Caenorhabditis elegans.* Curr Biol, 2001. **11**(11): p. 809-21.
70. Kamath, R.S. and J. Ahringer, *Genome-wide RNAi screening in Caenorhabditis elegans.* Methods, 2003. **30**(4): p. 313-21.
71. Rual, J.F., et al., *Toward improving Caenorhabditis elegans phenome mapping with an ORFeome-based RNAi library.* Genome Res, 2004. **14**(10B): p. 2162-8.
72. Pfaffl, M.W., *A new mathematical model for relative quantification in real-time RT-PCR.* Nucleic Acids Res, 2001. **29**(9): p. e45.
73. Soukas, A.A., et al., *Rictor/TORC2 regulates fat metabolism, feeding, growth, and life span in Caenorhabditis elegans.* Genes Dev, 2009. **23**(4): p. 496-511.

74. Pino, E.C., et al., *Biochemical and high throughput microscopic assessment of fat mass in Caenorhabditis elegans.* J Vis Exp, 2013. **73**: p. e50180.
75. Han, S.K., et al., *OASIS 2: online application for survival analysis 2 with features for the analysis of maximal lifespan and healthspan in aging research.* Oncotarget, 2016. **7**(35): p. 56147-56152.
76. Sykiotis, G.P. and D. Bohmann, *Stress-activated cap'n'collar transcription factors in aging and human disease.* Sci Signal, 2010. **3**(112): p. re3.
77. Papp, D., P. Csermely, and C. Sőti, *A role for SKN-1/Nrf in pathogen resistance and immunosenescence in Caenorhabditis elegans.* PLoS Pathog, 2012. **8**(4): p. e1002673.
78. Hoeven, R., et al., *Ce-Duox1/BLI-3 generated reactive oxygen species trigger protective SKN-1 activity via p38 MAPK signaling during infection in C. elegans.* PLoS Pathog, 2011. **7**(12): p. e1002453.
79. Lynn, D.A., et al., *Omega-3 and -6 fatty acids allocate somatic and germline lipids to ensure fitness during nutrient and oxidative stress in Caenorhabditis elegans.* Proc Natl Acad Sci U S A, 2015. **112**(50): p. 15378-83.
80. Pang, S. and S.P. Curran, *Adaptive capacity to bacterial diet modulates aging in C. elegans.* Cell Metab, 2014. **19**(2): p. 221-31.
81. Wang, X.J., et al., *Nrf2 enhances resistance of cancer cells to chemotherapeutic drugs, the dark side of Nrf2.* Carcinogenesis, 2008. **29**(6): p. 1235-43.
82. Lo, J.Y., B.N. Spatola, and S.P. Curran, *WDR23 regulates NRF2 independently of KEAP1.* PLoS Genet, 2017. **13**(4): p. e1006762.
83. Paek, J., et al., *Mitochondrial SKN-1/Nrf mediates a conserved starvation response.* Cell Metab, 2012. **16**(4): p. 526-37.
84. Blackwell, T.K., et al., *SKN-1/Nrf, stress responses, and aging in Caenorhabditis elegans.* Free Radic Biol Med, 2015. **88**(Pt B): p. 290-301.
85. Oliveira, R.P., et al., *Condition-adapted stress and longevity gene regulation by Caenorhabditis elegans SKN-1/Nrf.* Aging Cell, 2009. **8**(5): p. 524-41.
86. Pang, S., et al., *SKN-1 and Nrf2 couples proline catabolism with lipid metabolism during nutrient deprivation.* Nat Commun, 2014. **5**: p. 5048.
87. Black, J.C., C. Van Rechem, and J.R. Whetstine, *Histone lysine methylation dynamics: establishment, regulation, and biological impact.* Mol Cell, 2012. **48**(4): p. 491-507.
88. Prasad, T.K., et al., *Evidence for Chilling-Induced Oxidative Stress in Maize Seedlings and a Regulatory Role for Hydrogen Peroxide.* Plant Cell, 1994. **6**(1): p. 65-74.
89. Liu, F., et al., *The cAMP-PKA pathway-mediated fat mobilization is required for cold tolerance in C. elegans.* Sci Rep, 2017. **7**(1): p. 638.
90. Shapira, M., et al., *A conserved role for a GATA transcription factor in regulating epithelial innate immune responses.* Proc Natl Acad Sci U S A, 2006. **103**(38): p. 14086-91.
91. Irazoqui, J.E., et al., *Distinct pathogenesis and host responses during infection of C. elegans by P. aeruginosa and S. aureus.* PLoS Pathog, 2010. **6**(7): p. e1000982.

92. Przybysz, A.J., et al., *Increased age reduces DAF-16 and SKN-1 signaling and the hormetic response of Caenorhabditis elegans to the xenobiotic juglone.* Mech Ageing Dev, 2009. **130**(6): p. 357-69.
93. Li, X., et al., *Specific SKN-1/Nrf stress responses to perturbations in translation elongation and proteasome activity.* PLoS Genet, 2011. **7**(6): p. e1002119.
94. Ewald, C.Y., et al., *NADPH oxidase-mediated redox signaling promotes oxidative stress resistance and longevity through memo-1 in C. elegans.* Elife, 2017. **6**.
95. Steinbaugh, M.J., et al., *Lipid-mediated regulation of SKN-1/Nrf in response to germ cell absence.* Elife, 2015. **4**.
96. Tullet, J.M., et al., *Direct inhibition of the longevity-promoting factor SKN-1 by insulin-like signaling in C. elegans.* Cell, 2008. **132**(6): p. 1025-38.
97. Garigan, D., et al., *Genetic analysis of tissue aging in Caenorhabditis elegans: a role for heat-shock factor and bacterial proliferation.* Genetics, 2002. **161**(3): p. 1101-12.
98. Portal-Celhay, C., E.R. Bradley, and M.J. Blaser, *Control of intestinal bacterial proliferation in regulation of lifespan in Caenorhabditis elegans.* BMC Microbiol, 2012. **12**: p. 49.
99. Shivers, R.P., M.J. Youngman, and D.H. Kim, *Transcriptional responses to pathogens in Caenorhabditis elegans.* Curr Opin Microbiol, 2008. **11**(3): p. 251-6.
100. Kim, D.H., et al., *A conserved p38 MAP kinase pathway in Caenorhabditis elegans innate immunity.* Science, 2002. **297**(5581): p. 623-626.
101. Inoue, H., et al., *The C. elegans p38 MAPK pathway regulates nuclear localization of the transcription factor SKN-1 in oxidative stress response.* Genes Dev, 2005. **19**(19): p. 2278-83.
102. Cezairliyan, B., et al., *Identification of Pseudomonas aeruginosa phenazines that kill Caenorhabditis elegans.* PLoS Pathog, 2013. **9**(1): p. e1003101.
103. Mahajan-Miklos, S., et al., *Molecular mechanisms of bacterial virulence elucidated using a Pseudomonas aeruginosa-Caenorhabditis elegans pathogenesis model.* Cell, 1999. **96**(1): p. 47-56.
104. Feinbaum, R.L., et al., *Genome-wide identification of Pseudomonas aeruginosa virulence-related genes using a Caenorhabditis elegans infection model.* PLoS Pathog, 2012. **8**(7): p. e1002813.
105. Head, B.P., A.O. Olaitan, and A. Aballay, *Role of GATA transcription factor ELT-2 and p38 MAPK PMK-1 in recovery from acute P. aeruginosa infection in C. elegans.* Virulence, 2017. **8**(3): p. 261-274.
106. Darby, C., *Interactions with microbial pathogens.* WormBook, 2005: p. 1-15.
107. Escorcia, W., et al., *Quantification of Lipid Abundance and Evaluation of Lipid Distribution in Caenorhabditis elegans by Nile Red and Oil Red O Staining.* J Vis Exp, 2018(133).
108. Pino, E.C., et al., *Biochemical and high throughput microscopic assessment of fat mass in Caenorhabditis elegans.* J Vis Exp, 2013(73).
109. Anderson, S.M., et al., *The fatty acid oleate is required for innate immune activation and pathogen defense in Caenorhabditis elegans.* PLoS Pathog, 2019. **15**(6): p. e1007893.

110. Sandstrom, A., et al., *Functional degradation: A mechanism of NLRP1 inflammasome activation by diverse pathogen enzymes.* Science, 2019. **364**(6435).
111. McEwan, D.L., N.V. Kirienko, and F.M. Ausubel, *Host translational inhibition by Pseudomonas aeruginosa Exotoxin A Triggers an immune response in Caenorhabditis elegans.* Cell Host Microbe, 2012. **11**(4): p. 364-74.
112. Pavri, R., et al., *Histone H2B monoubiquitination functions cooperatively with FACT to regulate elongation by RNA polymerase II.* Cell, 2006. **125**(4): p. 703-17.
113. Cruz, C., et al., *Tri-methylation of histone H3 lysine 4 facilitates gene expression in ageing cells.* Elife, 2018. **7**.
114. Orphanides, G. and D. Reinberg, *RNA polymerase II elongation through chromatin.* Nature, 2000. **407**(6803): p. 471-5.
115. Wang, S., K. Fisher, and G.B. Poulin, *Lineage specific trimethylation of H3 on lysine 4 during C. elegans early embryogenesis.* Dev Biol, 2011. **355**(2): p. 227-38.
116. Kitzler, J.W., H. Minakami, and I. Fridovich, *Effects of paraquat on Escherichia coli: differences between B and K-12 strains.* J Bacteriol, 1990. **172**(2): p. 686-90.
117. Pradhan, A., et al., *The C-Box Region of MAF1 Regulates Transcriptional Activity and Protein Stability.* J Mol Biol, 2017. **429**(2): p. 192-207.
118. Khanna, A., D.L. Johnson, and S.P. Curran, *Physiological roles for mafr-1 in reproduction and lipid homeostasis.* Cell Rep, 2014. **9**(6): p. 2180-91.
119. Dalton, H.M. and S.P. Curran, *Hypodermal responses to protein synthesis inhibition induce systemic developmental arrest and AMPK-dependent survival in Caenorhabditis elegans.* PLoS Genet, 2018. **14**(7): p. e1007520.
120. Tan, M.W., et al., *Pseudomonas aeruginosa killing of Caenorhabditis elegans used to identify P. aeruginosa virulence factors.* Proc Natl Acad Sci U S A, 1999. **96**(5): p. 2408-13.
121. Shi, X., et al., *Regulation of lipid droplet size and phospholipid composition by stearoyl-CoA desaturase.* J Lipid Res, 2013. **54**(9): p. 2504-14.
122. Nhan, J.D., et al., *Redirection of SKN-1 abates the negative metabolic outcomes of a perceived pathogen infection.* Proc Natl Acad Sci U S A, 2019. **116**(44): p. 22322-22330.
123. Vasquez-Rifo, A., et al., *The Pseudomonas aeruginosa accessory genome elements influence virulence towards Caenorhabditis elegans.* Genome Biol, 2019. **20**(1): p. 270.
124. Bray, N.L., et al., *Near-optimal probabilistic RNA-seq quantification.* Nat Biotechnol, 2016. **34**(5): p. 525-7.
125. Pimentel, H., et al., *Differential analysis of RNA-seq incorporating quantification uncertainty.* Nat Methods, 2017. **14**(7): p. 687-690.
126. Gibson, D.G., et al., *Enzymatic assembly of DNA molecules up to several hundred kilobases.* Nat Methods, 2009. **6**(5): p. 343-5.
127. Foster, K.J., et al., *Innate Immunity in the C. elegans Intestine Is Programmed by a Neuronal Regulator of AWC Olfactory Neuron Development.* Cell Reports, 2020. **31**(1): p. 107478.

128. Georgel, P., et al., *A toll-like receptor 2-responsive lipid effector pathway protects mammals against skin infections with gram-positive bacteria.* Infect Immun, 2005. **73**(8): p. 4512-21.
129. Mosser, T., I. Matic, and M. Leroy, *Bacterium-induced internal egg hatching frequency is predictive of life span in Caenorhabditis elegans populations.* Appl Environ Microbiol, 2011. **77**(22): p. 8189-92.
130. Anand, P., et al., *A novel role for lipid droplets in the organismal antibacterial response.* Elife, 2012. **1**: p. e00003.
131. Kachroo, A., et al., *An oleic acid-mediated pathway induces constitutive defense signaling and enhanced resistance to multiple pathogens in soybean.* Mol Plant Microbe Interact, 2008. **21**(5): p. 564-75.
132. Kuna, A. and P. Achinna, *Mono unsaturated fatty acids for CVD and diabetes: A healthy choice.* International Journal of Nutrition, Pharmacology, Neurological Diseases, 2013. **3**(3): p. 236-248.
133. Vassiliou, E.K., et al., *Oleic acid and peanut oil high in oleic acid reverse the inhibitory effect of insulin production of the inflammatory cytokine TNF-alpha both in vitro and in vivo systems.* Lipids Health Dis, 2009. **8**: p. 25.
134. Brehm, B.J., et al., *One-year comparison of a high-monounsaturated fat diet with a high-carbohydrate diet in type 2 diabetes.* Diabetes Care, 2009. **32**(2): p. 215-20.
135. Appel, L.J., et al., *Effects of protein, monounsaturated fat, and carbohydrate intake on blood pressure and serum lipids: results of the OmniHeart randomized trial.* Jama, 2005. **294**(19): p. 2455-64.
136. Tosti, V., B. Bertozzi, and L. Fontana, *Health Benefits of the Mediterranean Diet: Metabolic and Molecular Mechanisms.* J Gerontol A Biol Sci Med Sci, 2018. **73**(3): p. 318-326.
137. Liu, X., M.S. Strable, and J.M. Ntambi, *Stearoyl CoA desaturase 1: role in cellular inflammation and stress.* Adv Nutr, 2011. **2**(1): p. 15-22.
138. Dancy, B.C., et al., *13C- and 15N-Labeling Strategies Combined with Mass Spectrometry Comprehensively Quantify Phospholipid Dynamics in C. elegans.* PLoS One, 2015. **10**(11): p. e0141850.
139. Briscoe, C.P., et al., *The orphan G protein-coupled receptor GPR40 is activated by medium and long chain fatty acids.* J Biol Chem, 2003. **278**(13): p. 11303-11.
140. Yuan, X., et al., *Identification of an endogenous ligand bound to a native orphan nuclear receptor.* PLoS One, 2009. **4**(5): p. e5609.
141. Berman, J.R. and C. Kenyon, *Germ-cell loss extends C. elegans life span through regulation of DAF-16 by kri-1 and lipophilic-hormone signaling.* Cell, 2006. **124**(5): p. 1055-68.
142. Rowe, D.C., et al., *The myristoylation of TRIF-related adaptor molecule is essential for Toll-like receptor 4 signal transduction.* Proc Natl Acad Sci U S A, 2006. **103**(16): p. 6299-304.
143. DeMar, J.C., Jr. and R.E. Anderson, *Identification and quantitation of the fatty acids composing the CoA ester pool of bovine retina, heart, and liver.* J Biol Chem, 1997. **272**(50): p. 31362-8.
144. Moy, T.I., et al., *High-throughput screen for novel antimicrobials using a whole animal infection model.* ACS Chem Biol, 2009. **4**(7): p. 527-33.

145. Yoneda, T., et al., *Compartment-specific perturbation of protein handling activates genes encoding mitochondrial chaperones.* J Cell Sci, 2004. **117**(Pt 18): p. 4055-66.
146. Simonis, N., et al., *Empirically controlled mapping of the Caenorhabditis elegans protein-protein interactome network.* Nat Methods, 2009. **6**(1): p. 47-54.
147. Shivers, R.P., et al., *Tissue-specific activities of an immune signaling module regulate physiological responses to pathogenic and nutritional bacteria in C. elegans.* Cell Host Microbe, 2009. **6**(4): p. 321-30.
148. Calfon, M., et al., *IRE1 couples endoplasmic reticulum load to secretory capacity by processing the XBP-1 mRNA.* Nature, 2002. **415**(6867): p. 92-6.
149. Schmittgen, T.D. and K.J. Livak, *Analyzing real-time PCR data by the comparative C(T) method.* Nat Protoc, 2008. **3**(6): p. 1101-8.
150. Sluder, A.E., et al., *The nuclear receptor superfamily has undergone extensive proliferation and diversification in nematodes.* Genome Res, 1999. **9**(2): p. 103-20.
151. Taubert, S., J.D. Ward, and K.R. Yamamoto, *Nuclear hormone receptors in nematodes: evolution and function.* Mol Cell Endocrinol, 2011. **334**(1-2): p. 49-55.
152. Arda, H.E., et al., *Functional modularity of nuclear hormone receptors in a Caenorhabditis elegans metabolic gene regulatory network.* Mol Syst Biol, 2010. **6**: p. 367.
153. Ewbank, J.J. and N. Pujol, *Local and long-range activation of innate immunity by infection and damage in C. elegans.* Curr Opin Immunol, 2016. **38**: p. 1-7.
154. Ahn, S.H., et al., *Hepatocyte nuclear factor 4alpha in the intestinal epithelial cells protects against inflammatory bowel disease.* Inflamm Bowel Dis, 2008. **14**(7): p. 908-20.
155. Barrett, J.C., et al., *Genome-wide association study of ulcerative colitis identifies three new susceptibility loci, including the HNF4A region.* Nat Genet, 2009. **41**(12): p. 1330-4.
156. van Sommeren, S., et al., *HNF4α and CDH1 are associated with ulcerative colitis in a Dutch cohort.* Inflamm Bowel Dis, 2011. **17**(8): p. 1714-8.
157. Marcil, V., et al., *Association between genetic variants in the HNF4A gene and childhood-onset Crohn's disease.* Genes Immun, 2012. **13**(7): p. 556-65.
158. MacNeil, L.T., et al., *Transcription Factor Activity Mapping of a Tissue-Specific in vivo Gene Regulatory Network.* Cell Syst, 2015. **1**(2): p. 152-162.
159. Engelmann, I., et al., *A comprehensive analysis of gene expression changes provoked by bacterial and fungal infection in C. elegans.* PLoS One, 2011. **6**(5): p. e19055.
160. Lee, S.H., et al., *Burkholderia pseudomallei suppresses Caenorhabditis elegans immunity by specific degradation of a GATA transcription factor.* Proc Natl Acad Sci U S A, 2013. **110**(37): p. 15067-72.
161. Wong, D., et al., *Genome-wide investigation reveals pathogen-specific and shared signatures in the response of Caenorhabditis elegans to infection.* Genome Biol, 2007. **8**(9): p. R194.
162. Gravato-Nobre, M.J., et al., *Multiple genes affect sensitivity of Caenorhabditis elegans to the bacterial pathogen Microbacterium nematophilum.* Genetics, 2005. **171**(3): p. 1033-45.

163. Richardson, C.E., S. Kinkel, and D.H. Kim, *Physiological IRE-1-XBP-1 and PEK-1 signaling in Caenorhabditis elegans larval development and immunity.* PLoS Genet, 2011. **7**(11): p. e1002391.
164. Richardson, C.E., T. Kooistra, and D.H. Kim, *An essential role for XBP-1 in host protection against immune activation in C. elegans.* Nature, 2010. **463**(7284): p. 1092-5.
165. Ron, D. and P. Walter, *Signal integration in the endoplasmic reticulum unfolded protein response.* Nat Rev Mol Cell Biol, 2007. **8**(7): p. 519-29.
166. Conaway, R.C. and J.W. Conaway, *Function and regulation of the Mediator complex.* Curr Opin Genet Dev, 2011. **21**(2): p. 225-30.
167. Malik, S. and R.G. Roeder, *The metazoan Mediator co-activator complex as an integrative hub for transcriptional regulation.* Nat Rev Genet, 2010. **11**(11): p. 761-72.
168. Taubert, S., et al., *A Mediator subunit, MDT-15, integrates regulation of fatty acid metabolism by NHR-49-dependent and-independent pathways in C. elegans.* Genes & development, 2006. **20**(9): p. 1137-1149.
169. Rahme, L.G., et al., *Common virulence factors for bacterial pathogenicity in plants and animals.* Science, 1995. **268**(5219): p. 1899-902.
170. Arribere, J.A., et al., *Efficient marker-free recovery of custom genetic modifications with CRISPR/Cas9 in Caenorhabditis elegans.* Genetics, 2014. **198**(3): p. 837-46.
171. Ward, J.D., *Rapid and precise engineering of the Caenorhabditis elegans genome with lethal mutation co-conversion and inactivation of NHEJ repair.* Genetics, 2015. **199**(2): p. 363-77.
172. Ercan, S., et al., *X chromosome repression by localization of the C. elegans dosage compensation machinery to sites of transcription initiation.* Nat Genet, 2007. **39**(3): p. 403-8.
173. Nargund, A.M., et al., *Mitochondrial and nuclear accumulation of the transcription factor ATFS-1 promotes OXPHOS recovery during the UPR(mt).* Mol Cell, 2015. **58**(1): p. 123-33.